Complexity

Cyber Physical Control

Lead Guest Editor: Peter Galambos
Guest Editors: Imre J. Rudas, Lixian Zhang, and Shun-Feng Su

Cyber-Physical Control

Complexity

Cyber-Physical Control

Lead Guest Editor: Péter Galambos
Guest Editors: Imre J. Rudas, Lixian Zhang, and Shun-Feng Su

Editorial Board

Contents

Hindawi
Complexity
Volume 2018, Article ID 9834608, 2 pages
https://doi.org/10.1155/2018/9834608

Editorial
Cyber-Physical Control

Péter Galambos,[1] **Imre J. Rudas**,[2] **Lixian Zhang**,[3] **and Shun-Feng Su**[4]

[1]*Antal Bejczy Center for Intelligent Robotics, Óbuda University, Bécsi út 96/b, Budapest H-1034, Hungary*
[2]*University Research and Innovation Center, Óbuda University, Bécsi út 96/b, Budapest H-1034, Hungary*
[3]*School of Astronautics, Harbin Institute of Technology, P.O. Box 3015, Yikuang Street 2, Nangang District, Harbin 150080, China*
[4]*National Taiwan University of Science and Technology, Taipei 106, Taiwan*

Correspondence should be addressed to Péter Galambos; peter.galambos@irob.uni-obuda.hu

Received 5 June 2018; Accepted 5 June 2018; Published 3 September 2018

It has recently become evident that the so-called enabling technologies in various fields are reaching a level of maturity that allows us to build large-scale intelligent production systems, bionic devices, or even autonomously controlled infrastructures never seen before. Such enabling technologies are high-speed computing, large bandwidth and low-latency telecommunications, data storage, sensor and actuator technologies, precise mechatronic devices (robotics), efficient learning algorithms and knowledge representations, and computational neurosciences to name a few. All of these advances in combination with modern control theory are automatically leading to new complex solutions and change a given field disruptively. These systems over a certain scale of complexity are often referred to as cyber-physical systems (CPS).

Cyber-physical control (CPC) as a multidisciplinary research field investigates existing methodologies in the context of regulating CPSs at different levels from sensing and actuation to system-level orchestration.

In this special issue, we have invited research teams and experts of various supporting disciplines to contribute with recent original research and review articles to help to uncover the indirect impact of novel mathematical methods, computing technologies, and other research results to the conceptual framework of CPC.

After the careful selection and review process, six articles were selected, representing the most critical aspects of the broad CPS horizon:

H. Khan et al. provided a study that applies the achievements of modern control theory for physiological problems, namely, the type 1 diabetes mellitus, contributing this way to the global research efforts on the artificial pancreas. Authors applied the so-called receding horizon controller that were designed via nonlinear programming using the generalized reduced gradient method. Simulated performance test scenarios with different disturbance patterns show promising results.

J. Kuti and P. Galambos's work contributes to the mathematical apparatus of polytopic system modeling and control synthesis supporting the cyber-physical control concepts in a generic problem-independent level. The proposed affine tensor product model transformation is a powerful methodology applicable for quasi-linear parameter varying systems covering a wide range of real-world engineering applications. The affine TP model is introduced as a unique intermediate representation of qLPV systems, bringing significant benefits in complexity reduction and enclosing polytope generation and convex optimization-based controller design.

The paper of J. Zhang et al. investigates the cluster-delay synchronization in directed networks governed by an intermittent control approach. The study presents proof of the viability of synchronization of oscillators in intra- and intercluster cases. Besides the theoretical study, the paper comprises a benchmark study comparing the proposed structure to other controllers in the literature. Numerical examples are also provided to underpin the practical usefulness of the proposed schemes. This study underpins the importance of networked control systems within the scope of CPC.

Aligned to the previous papers, the short article of P. Li et al. investigates the input-to-state stability of nonlinear switched systems. The proposed approach relaxes the stability condition via eliminating the necessity of the negativeness of the derivative of the Lyapunov function. Since a wide range of industrial control systems is implemented as switched system, the practical significance of such theoretical results is outstanding.

The last two papers of the issue deal with the higher level, practical information technology of CPC applications, and Industry 4.0. R. Lovas et al. propose a unified and scalable cloud-based back-end platform that is specially designed for large-scale sensor networks. The novel framework exploits the synergy of existing functional blocks resulting in a cutting-edge solution with relatively low entry barriers for most of the recently emerging industrial applications. This study represents very well the close relationship of CPC to the latest achievements of cloud computing technologies.

Finally, U. H. Govindarajan et al.'s study reviews the literature and the patents related to the immersive technologies (VR, AR, BMI, BCI, etc.) in the context of Industry 4.0. The analysis considers 197 publications and 2672 patents through 10 years in the period 2007–2016. These resources have been analyzed via text mining and probabilistic analysis resulting in different analytics and conclusions including a domain ontology, technology specifications, patent statistics, and a technology function matrix (TFM). This study clearly shows the crucial role of advanced human-machine interfaces in complex cyber-physical systems.

Each paper of the issue represents a specific field of systems and control science with a clear relationship to cyber-physical systems. At first sight, the topics are quite different, but the collection reveals a broader context that connects all of them.

As the editors of this special issue, we hope that the heavily theoretical systems and control science and the application-oriented R&D can coevolve in a fruitful synergy leading to disruption in the new age of cyber-physical control.

Peter Galambos
Imre J. Rudas
Lixian Zhang
Shun-Feng Su

Hindawi
Complexity
Volume 2018, Article ID 8281079, 16 pages
https://doi.org/10.1155/2018/8281079

Research Article

Orchestrated Platform for Cyber-Physical Systems

Róbert Lovas, Attila Farkas, Attila Csaba Marosi, Sándor Ács, József Kovács, Ádám Szalóki, and Botond Kádár

Institute for Computer Science and Control, Hungarian Academy of Sciences (MTA SZTAKI), P.O. Box 63, Budapest 1518, Hungary

Correspondence should be addressed to Róbert Lovas; lovas.robert@sztaki.mta.hu

Received 24 November 2017; Revised 21 March 2018; Accepted 19 April 2018; Published 5 July 2018

Academic Editor: Shun-Feng Su

One of the main driving forces in the era of cyber-physical systems (CPSs) is the introduction of massive sensor networks (or nowadays various Internet of things solutions as well) into manufacturing processes, connected cars, precision agriculture, and so on. Therefore, large amounts of sensor data have to be ingested at the server side in order to generate and make the "twin digital model" or virtual factory of the existing physical processes for (among others) predictive simulation and scheduling purposes usable. In this paper, we focus on our ultimate goal, a novel software container-based approach with cloud agnostic orchestration facilities that enable the system operators in the industry to create and manage scalable, virtual IT platforms on-demand for these two typical major pillars of CPS: (1) server-side (i.e., back-end) framework for sensor networks and (2) configurable simulation tool for predicting the behavior of manufacturing systems. The paper discusses the scalability of the applied discrete-event simulation tool and the layered back-end framework starting from simple virtual machine-level to sophisticated multilevel autoscaling use case scenario. The presented achievements and evaluations leverage on (among others) the synergy of the existing EasySim simulator, our new CQueue software container manager, the continuously developed Occopus cloud orchestrator tool, and the latest version of the evolving MiCADO framework for integrating such tools into a unified platform.

1. Introduction

As indicated in [1], we are the witnesses of a parallel but strongly interinfluencing development in computer and manufacturing sciences including the related rapid technology evolution. The achievements of computer and ICT research efforts were directly applied in manufacturing hardware, control systems, and software. Moreover, the complexity and challenges generated in the field of manufacturing continuously influenced the developments in computer science and ICT. In line with the latest research and development trends, big data-related tools (see Section 2), such as predictive analytics and simulations, have been contributing to the increasingly wider range of sectors, including manufacturing, agriculture, healthcare, and other services. In many of those cases, cloud computing serves as an elastic and efficient paradigm for implementing sensor data ingestion and simulation back-ends. With the emerging lightweight software container technologies (see Section 2), the feasible approaches and design options for such platforms have been significantly enriched for cyber-physical systems (CPSs).

CPSs, relying on such latest and foreseeable further developments of (i) computer science, (ii) information and communication technologies, and (iii) manufacturing science and technology, may lead to the 4th Industrial Revolution, frequently noted as Industry 4.0 [1]. In our paper, we present the evolution of our ultimate goal, an *orchestrated platform* for Industry 4.0, realized first within the Docker@SZTAKI project (see Section 3), which is responsible for collecting (among others) sensor data and enables sophisticated simulations using the data. The different versions, namely, the cloud VM-based and the software containerized variants, provide the three key requested features, that is, highly scalable, vendor-independent (cloud provider/technology agnostic), and open-source facilities that help protect the sensitive factory data by using, for example, in-house cloud or servers at the company premises but, at the same time, allow

accessing public cloud services seamlessly when it becomes necessary (e.g., in the case of peek/unpredictable load or for high-availability functionalities). Therefore, they formed a robust and adaptive framework for further pilot application areas, for example, connected cars and precision farming (see Section 5), as the presented evaluation illustrates, for example, the elasticity and other parameters of the current implementation that has been ported under MiCADO (see Section 4.2).

As a vital part of our back-end platform, the main goal of the presented *orchestrated platform* (see Section 3.1) is to reliably receive and store incoming sensor data (including images) from multiple arrays of configured sensors that are deployed in the factory, on the trucks, and so on. One of the most crucial requirements concerning such back-ends is the capability to scale as the number of sensors and the volume of incoming data grow rapidly. It can be achieved by the appropriate architecture, solid fundamental building blocks, and exhaustive testing. Another important goal of the sensor data back-end is to serve the collected data for analytical purposes, for example, to feed the simulators with initial data or to compare the already collected data with the simulation results.

As another fundamental component of the orchestrated back-end platform, a *discrete-event simulation* (DES) kernel is utilized to forecast the behavior of a manufacturing system, denoted as EasySim hereafter (see Section 3.2). Specific details about the simulation kernel are provided in [2]; here, we just provide some highlights of EasySim. The simulation kernel is an implementation of the classical simulation modeling approach called discrete-event simulation (DES) and developed earlier in MTA SZTAKI. In a nutshell, the DES approach utilizes a mathematical/logical model of a physical system that portrays state changes at precise points in a simulated time horizon. Both the nature of the state changes and the time at which the change occurs mandate precise description. DES models are mainly flow models tracking the flow of entities through the factory. The tracking is done using times at which the various events occur and are sequentially ordered according to their occurrence time. In the modeling phase, the task of a modeler is to determine the state variables that capture the behavior of the system, the events that can change the values of those variables and the logic associated with each event. Executing the logic associated with each event in a time-ordered sequence produces a simulation of the system. As each event occurs and expires, it is removed from the sequence called an event list, and the next event is activated. This continues until all the events have occurred or an earlier-defined time window limit is achieved. Statistics are gathered throughout the simulation and reported with performance measures. Later in the paper, we provide the simulation scenarios, where the EasySim kernel is applied (see Section 4.1), but the main focus will be on the scenario generation and the evaluation of the simulation runs, which, contrary to the initial desktop environment, will run in parallel on the orchestrated back-end platform. With the parallelization support of this back-end platform, we are able to significantly speed up the evaluation of different scenarios which earlier run only sequentially in desktop environments. Additionally, it is important to mention that other simulation engines, even third-party, off-the-shelf simulation software, would have been suitable to model the scenarios presented in Section 3.2. EasySim was selected because of performance reasons.

2. Related Work

In this section, we discuss popular approaches, methods, and already-available services related to our ultimate goals and particularly addressed high-level features: (i) multilevel autoscaling in the cloud involving VMs and containers, (ii) cloud technology/provider agnostic mechanisms including high portability, and (iii) generic open-source implementation, which together enable the efficient deployment and operation of the wide range of CPS services.

Regarding cloud technologies, already, several authors underlined the fact that cloud computing is playing a significant role in realizing cyber-physical systems [3–5].

Amazon Web Services (AWS), Microsoft Azure, and Google Cloud may be considered the three dominant forces in public cloud computing, and all the three provide their own IoT [6] platform and services [7–9]. These are generic, hosted platforms and not available as an on-premise private solution. There are several proposals available for data processing that are aimed at providing a generic architecture rather than one that fits a single-use case [10–12]; thus, these can be exploited not just for strict big data scenarios.

The FIWARE big data architecture [13] was created within the FIWARE (Core Platform of the Future Internet) project as one of many generic enablers (GEs). A GE represents a functional building unit. A GE implementation supports a given set of functions over a set of APIs and interoperable interfaces that conform to the open specifications given for that GE [14]. The big data GE architecture expands the basic Apache Hadoop one. The Master Node has all management software and acts as a front-end for the users. Infinity is the permanent storage cluster (based on HDFS). Computing clusters have a lifecycle: they are created, they are used for computation, and, finally, they are removed. All data must be uploaded to Infinity beforehand. Data can be uploaded to and retrieved from Infinity via WebHDFS [15] or Cosmos CLI (a command line interface to WebHDFS). The big data GE specifies the use of SQL-like analytic tools like Hive, Impala [16], or Shark. Although the GE is based on Hadoop [17], it proposes several alternatives: (i) the Cassandra [18] File System can be used instead of HDFS, (ii) a distributed NoSQL database like HBase can be installed on top of HDFS, and (iii) use, for example, Cascading [19] as an extension or replacement.

DICE [20] is an EU Horizon 2020 research project that is aimed at providing a methodology and framework for developing data-intensive applications. It offers a framework consisting of an Eclipse-based IDE and tools and supports Apache Spark [21], Storm [22], Hadoop (MapReduce), Cassandra, and MongoDB [23]. By using its methodology, it allows the architecture enhancement, agile delivery, and testing for batch and stream processing applications.

Building on application containers and orchestration (e.g., via Docker [24] or Kubernetes [25]), serverless computing is an execution model for cloud computing where the cloud provider manages dynamically the underlaying machine resources. The pricing model is based on the actual resources consumed during execution (e.g., CPU execution time, memory, and network). All major public cloud providers support this model, for example, AWS Lambda, Google Cloud Functions, or Azure Functions. There are several open-source implementations like OpenLambda [26], OpenFaaS [27] (Open Function as a Service), Kubeless [28], Funktion, Iron Functions, and Fission.

Terraform [29] is an open-source tool for building, managing, and versioning virtual infrastructures in public or private cloud environments. Terraform allows defining whole virtual infrastructures via a configuration template. This can contain low-level information like machine types, storage, or network configuration but also high-level components like SaaS services or DNS entries. Based on the configuration, Terraform creates an execution plan and a resource graph to build the defined infrastructure. Topology and Orchestration Specification for Cloud Applications (TOSCA) [30, 31] is a standard language by OASIS [32] for describing collections or topologies of services, their relationships, components, and so on. It is similar to Amazon CloudFormation, OpenStack Heat, and Terraform. It is aimed at being an open standard that provides a superset of features (and grammar).

Regarding the representation and sharing industrial data in distributed systems, several initiatives exist. The National Institute of Standards and Technology (NIST) initiated the Smart Manufacturing Systems (SMS) Test Bed [33] in which data is collected from the manufacturing lab using the MTConnect (link is external) standard. That data is aggregated and published internally and externally of NIST via web services. Other initiative from General Electric is Predix [34], a huge platform enabling the collection and analysis of product- and asset-related data in order to improve and optimize operations. The SMS Test Bed is a source from where data can be retrieved and analyzed, but the Test Bed itself does not include solvers or simulators. Predix with its own multiple layers is designed for collection and analytics and includes tools for analysis, but building models which are later applied in the decision support here is also always necessary and at the same time almost the most difficult part. How to build these models is still not clear from the available sources of Predix. In our solution, to be presented in the simulation scenario, the model in question is built as discrete-event simulation with a tool developed earlier in an earlier project at MTA SZTAKI. This model is built automatically based on the Core Manufacturing Simulation Data (CMSD) standard, specifically designed for manufacturing simulation studies.

3. Docker@SZTAKI Project

The main motivation behind the Docker@SZTAKI project was to elaborate and demonstrate a Docker software container-based platform that can be formed on demand in a highly portable way, that is, according to the complexity and the actual needs of the CPS application in various IT environments. The supported environments (see Figure 1) include even the user's laptop, or the on-premise servers of the institute, and also a wide range of private/public/community clouds, for example, the Hungarian academic federated community cloud, the MTA Cloud (based on OpenStack middleware), or the public Amazon Web Services (AWS) cloud.

The Docker@SZTAKI platform (see Figure 1) consist of a private repository of Docker images, for example, the EasySim simulator (see Section 3.2), the various components of the presented sensor data back-end, and further auxiliary tools, such as the CQueue manager (see Section 3.2) or the Occopus [35] cloud orchestrator. CQueue plays a crucial role when the push model of the Docker Swarm clustering mechanism cannot be applied, and the pull model is more suitable for the application (e.g., in the case of EasySim). The Occopus cloud orchestrator is responsible for creating and managing the required VMs in the selected clouds when the Docker@SZTAKI user needs extra or 24/7 available IT capacities for their applications.

The platform has been used for demonstrating two major pillars of the CPS components: sensor data back-end and DES simulation.

3.1. Orchestrated Back-End Framework for CPS. The goal of the framework is to reliably receive and store incoming sensor data (including images) from arrays of configured sensors and scale the number of sensors as needed. The framework also includes complementary user and administrative applications and connected analytics. In this section, we are going to detail the evolution of the framework in three iterations. Sensor data is usually generated by small microcontroller-based devices where usually raw data is from an arbitrary number of different instruments. Measurements are taken periodically and, thus, it generates a large number of small packets. Storing a large volume of this kind of data requires a tailored infrastructure with the capability to scale out (horizontally) as the volume of data grows.

3.1.1. Virtual Machine-Based Architecture. The architecture follows a three-tier layout as depicted in Figure 2. Each component of each tier can be deployed on a separate node. This allows easy scaling of the appropriate tiers.

The delivery tier (shown in Figure 2) accepts incoming sensor data and forwards it to one of the data collector application instances in the aggregation tier. The forwarding decision is made in two steps. First, based on a round-robin algorithm, a high-availability proxy and load balancer (based on HAProxy [36]) are selected. The proxy, in turn, will select an application server with the lowest load and forward the request to that one. A data collector instance in the aggregation tier (shown in Figure 2) will decode the received data and store them in the database tier (shown in Figure 2). Besides the data collector, other functionalities are also available and work similarly. Database services are provided by the Cassandra or MongoDB [23] database cluster, besides RDBMS-like MySQL. Cassandra is a decentralized structured

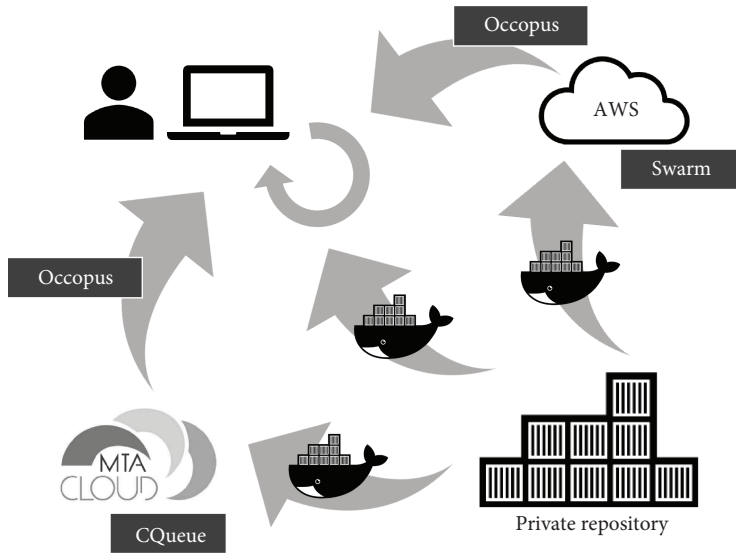

Figure 1: Docker@SZTAKI: main components with their typical usage scenarios.

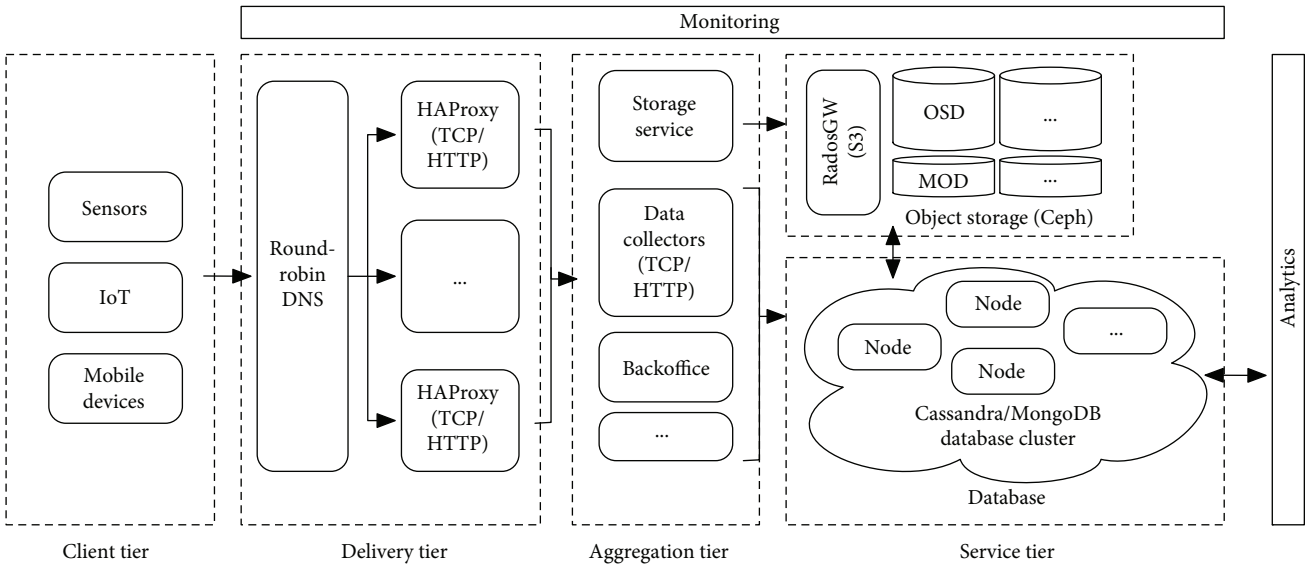

Figure 2: General architecture of the framework.

storage system that is well suited for storing time-series data like sensor data. As the volume of incoming data changes, Cassandra allows dynamically adding or removing new nodes to the database.

Data submission is initiated by the client tier resolving the DNS endpoint of a given service. The DNS endpoint may contain one or more load balancer address; in turn, they distribute the load between the available receiver instances. Using round-robin DNS techniques, it is possible to scale the number of load balancer nodes. It is a well-known simple method for load sharing, fault tolerance, and load distribution for making multiple redundant service hosts available. Next, HAProxy servers are responsible for balancing the load across multiple application servers (e.g., data collectors) after through the round-robin DNS the client contacts one. HAProxy also continuously monitors the health and performance of the application servers connected.

A data receiver application and connected components are depicted in Figure 3. It consists of the following: Chef is used as a deployment orchestrator for bootstrapping new nodes for the different tiers. The data processing component and Cassandra connector are implemented using the Flask web framework and Python. The sensor metadata decoder is responsible for interpreting the incoming data and passing it to the Cassandra connector. The Cassandra connector is used to store the decoded metadata in the database cluster. uWSGI [37] is used as a WSGI [38] application server, and, finally, Nginx [39] is connected to the wire protocol of uWSGI to achieve a high-performance WSGI-based web front-end.

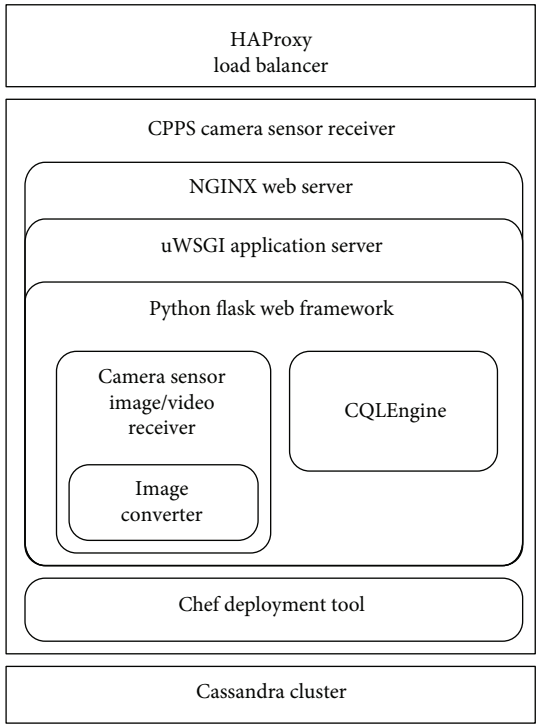

Figure 3: Architecture of a web-based data collector application for sensor image data.

3.1.2. Container-Based Architecture. The original data collector framework is based on virtual machines, and the components are run on separate nodes. This architecture is ideal to scale out or scale in the components based on the application utilization. On the other hand, this separation might have a negative effect on the resource utilization. To achieve better resource utilization, we have created the Docker version of the data collector infrastructure with smaller granularity. With the Docker container technology [24], the components of the architecture can be separated into containers; therefore, we can run more than one collector component on one particular virtual machine. The Docker version of the collector provides more efficient resource utilization than the virtual machine-based solution.

To create the Docker-based version, we built container images from each of the infrastructure components. We extended the application with a new configuration file which can be customized through the environment variables on the container start. This configuration is performed by the Docker entry point script at the start (this is the main configuration method in the Docker ecosystem). For the Cassandra Docker version, the official Cassandra image was selected from the Docker Hub but we applied some modifications; the official entry point script was extended to support the automatic Cassandra cluster creation at the start time on a Docker Swarm cluster. With these images, we created a Docker compose file to provide a simple container orchestration method. With the compose file, the main part of the collector infrastructure can be deployed by the service operator on one machine or on a Swarm cluster as a Docker stack, and the containers can be easily configured through the compose file with various environment variables.

The service operator can deploy the data collector framework as a Docker stack from the described Docker compose file on a cluster managed by Docker Swarm. Another important feature of Docker Swarm is the provided overlay network between the Swarm nodes for the containers. In this network, the containers can access each other like they are on one virtual machine. Furthermore, Swarm provides an ingress routing mesh on this network. With the routing mesh, the Swarm services can expose their ports on the virtual machines so they can be reached on every Swarm node from outside of the cluster. With that feature, Swarm provides an external load balancer between the application containers within a Docker service. Therefore, we decided to replace the HAProxy in the data collector infrastructure with the above-described routing mesh facility of Swarm. The resulting architecture is demonstrated in Figure 4. Prometheus [40] is used for monitoring the infrastructure with agents deployed on the nodes.

The infrastructure is deployed and managed by the Occopus [35] cloud orchestrating tool. Occopus is open-source software providing features to orchestrate, configure, and manage virtual infrastructures. It allows describing virtual infrastructures in a cloud agnostic way. We created the necessary description files to build and maintain the collector framework. As an additional benefit, the number of Swarm workers in the framework can be automatically scaled based on their CPU load.

3.1.3. Extended Architecture. In the next iteration of the data collector, we improved the data storage layer and separated the functions of the data collector layer to improve the disadvantages of the framework. In the first version, all metadata about the sensors and the measured data are stored in the Cassandra database. This is not an optimal database schema to store related data in a NoSQL database; therefore, we separated the stored data into two databases. The information and the corresponding metadata of the sensors are stored in an SQL database, and measurement data will be stored in a NoSQL database or distributed file system. Originally, data collectors served multiple purposes: receiving, processing, and storing the data in a database. These functions have been separated into distinct components. These streaming components push data to a streaming component, and dedicated processors store the data for further analytics or process them in-stream. This greatly reduces the stress on the data collector and furthers the architecture. The extended collector architecture is demonstrated in Figure 5.

3.2. EasySim Discrete-Event Simulation for CPS

3.2.1. CQueue and Its Pull Execution Model for Tasks. Since Docker does not provide a pull model for task execution (Swarm uses a push execution model), the new CQueue framework provides a lightweight queue service for processing tasks via application containers. The framework consists of four main components (see Figure 6): (i) one or more

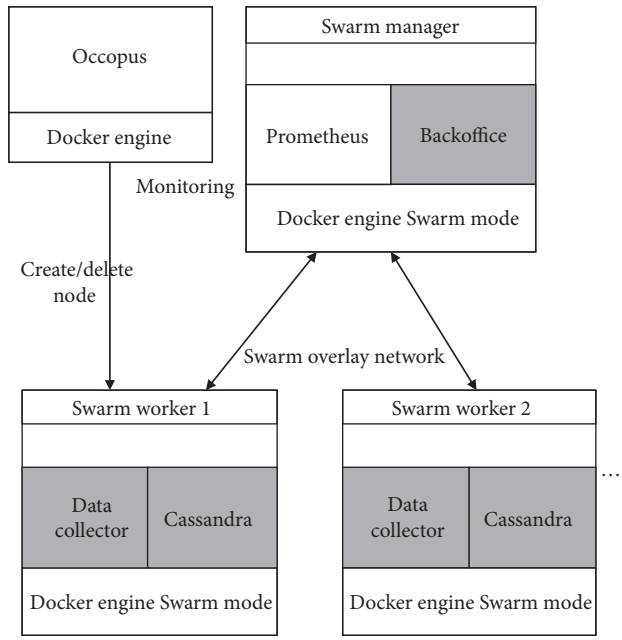

Figure 4: Container-based architecture of the sensor data back-end framework with VM-level autoscaling.

CQueue server, which acts as a front-end and receives the container-based task requests; (ii) a queue server which schedules the task requests for workers; (iii) CQueue workers that pull tasks from the queue server; and (iv) a key-value store that stores the state and the output of the finished tasks. Currently, queuing is handled by RabbitMQ, and Redis is used as the key-value store. The front-end server and the worker components are written in Golang, and they have a shared code base. All of the components are running inside Docker containers and can be scaled based on their utilization. The design goals of the framework are to use standard interfaces and components to create generic job processing middleware.

The framework is built for executing Docker container-based tasks with their specific inputs. Also, environment variables and other input parameters can be specified for each container. CQueue uses a unique ID to identify the pushed tasks, and the user has to specify it. The ID, the application container, and the inputs of the task must be specified in the standard JSON (JavaScript Object Notation) format. The CQueue server receives the tasks via a REST-like API. After this step, the server transforms the JSON-formatted tasks to standard AMQP (Advanced Message Queuing Protocol) messages and pushes them to the queue server. The workers pull the registered tasks from the queue server via the same AMQP protocol and execute them. One worker processes one task at a time. After the task is completed, the workers send a notification to the queue server, and this task will be removed from the queue. The worker continuously updates the status (*registered*, *running*, *finished*, or *failed*) of the task with the task's ID in the key-value store. When the task is finished or failed, the worker stores the *stdout* and *stderr* of the task in the key-value store as well. The status of a task and the result can be queried from the key-value store through the CQueue server. The output of the task is not processed; it is stored in the key-value store in its original format.

3.2.2. Architecture from the Simulation Point of View. Figure 7 illustrates the overall architecture of the system from a simulation experiment point of view. The graphical user interface, denoted by GUI in Figure 7, is the place where the configuration of an experiment with different parameters can be defined. The Experiment Manager then forwards the complete setup of the simulation and initiates the parallelized simulation runs accordingly. The main database is given by the DB symbol in the bottom of the figure, storing both the structural input of the simulation and the parameters of the simulation instances, and, later, after the simulation runs are terminated, all the outputs are streamed by the simulation runs. To better understand the process within this structure, the following section gives the details of the modules introduced above.

3.2.3. Standardized Database. Concerning the implementation of the persistence layer, MySQL has been selected to store all the necessary back-end information.

Regarding the standardization of manufacturing and logistic systems, there are different standards approved and offered by different organizations; the most known one is ISA 95, provided by the International Society of Automation [41]. Having a comparison on the base of applicability, finally, we selected the standard for Core Manufacturing Simulation Data (CMSD) [42] in order to have a standardized system with reusable components. In this way, we applied standard data formats for representing certain structures of the system related to the simulation module, namely, the SISO-STD-008-2010; the standard for Core Manufacturing Simulation Data (SISO CMSD) provided by SISO (http://www.sisostds.org, visited 2017-11-01) is applied in the research.

This standard addresses interoperability between simulation systems and other manufacturing applications. As such, it inherently includes the most relevant and simulation-related data for the simulation of manufacturing systems. The CMSD model is a standard representation for core manufacturing simulation data, providing neutral structures for the efficient exchange of manufacturing data in a simulation environment. These neutral data structures are applied to support the integration of simulation software with other manufacturing applications.

The CMSD standard has several packages, but not all of them are necessary in this application. Just as an example, the layout package was not used, as in our scenario the focus of the experiment which is the layout is not relevant. The standard itself is described as a UML model; furthermore, there are XML and representations in different programming languages. Within the context of the research, the back-end database was designed and implemented with an implementation of the CMSD standard in a relational database format, based on the initial UML version, forming the main data storage of different simulation forecasting

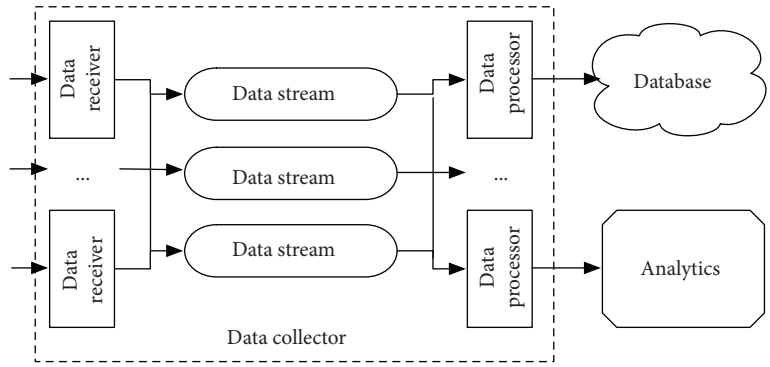

Figure 5: Data collectors in the extended sensor data back-end architecture.

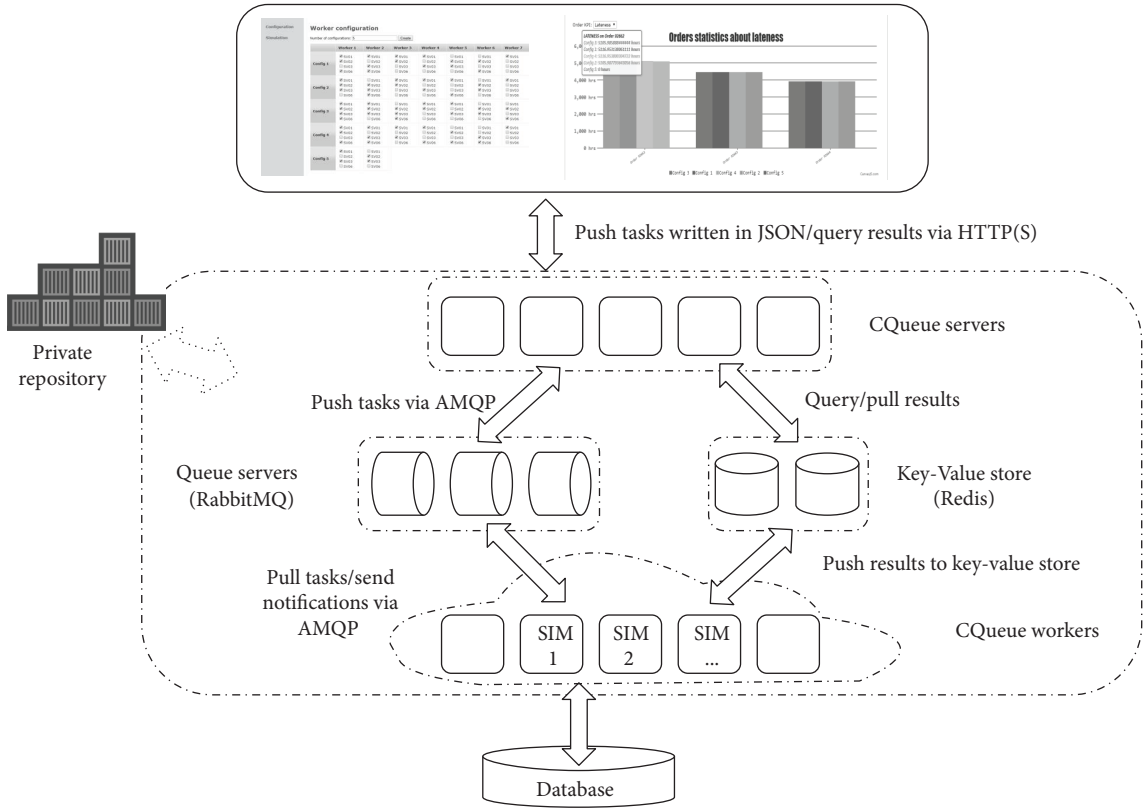

Figure 6: CQueue architecture in the context of simulation.

scenarios. All the data about the resources, the entities or workpieces traveling in the manufacturing system, the routings, the sequence of operations, the control logic, and the manufacturing orders to be completed are all stored in the database according to the CMSD specification. One of the nonfunctional requirements for selecting this solution, namely, the direct implementation of SQL database tables and relations, was the speed of building and updating simulation models instantly.

According to the nature of the data stored in the MySQL database, two types of tables can be distinguished. On the one hand, the implementation of the CMSD standard provides the information related to simulation. On the other hand, there are tables, which store specific information necessary for the application itself in this new environment.

3.2.4. Data Access Layer. Both the higher-level GUI that is responsible for setting up the input parameters and visualizing the results of simulation scenarios and the Docker Container Manager (currently CQueue) are connected to the main database with a data access layer (DAL) (see Figure 7).

The correspondence, the bidirectional match between classes in the system and data in the database, is assured by the data access layer which is implemented with the Entity Framework. This allows a higher level of abstraction when dealing with data and supports the creation and maintenance of data-oriented applications with less code than in traditional applications. The objects linked to relational data are defined just like normal objects and decorated with attributes to identify how properties correspond to columns in the database tables.

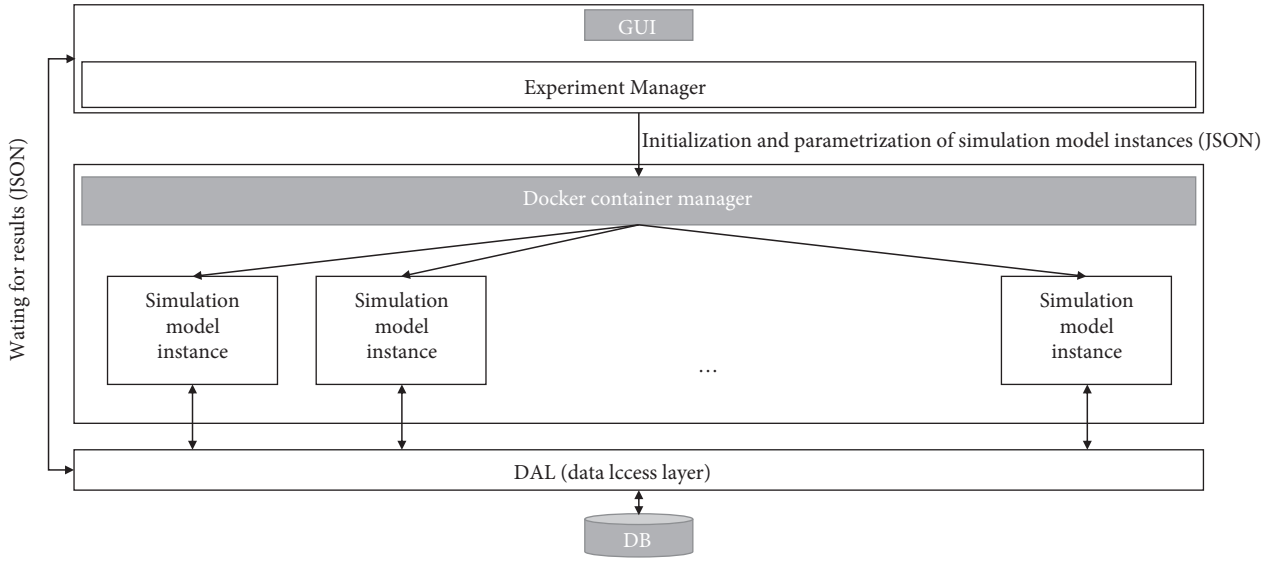

Figure 7: Web application architecture for simulation management/visualization (extended by the Docker Container Manager).

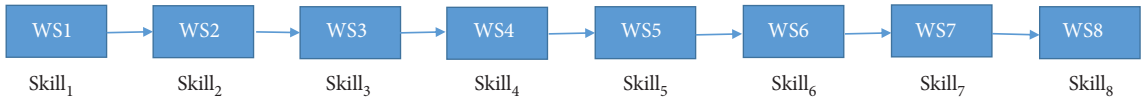

Figure 8: The layout of the flow-shop system.

4. Evaluation of CPS Use Cases

4.1. EasySim: The Modeled System and Its Simulation Experiments. As mentioned in the introductory part, the reason for using EasySim instead of any other existing DES tools is the difference in performance. EasySim is a simulation kernel providing only the core functionality of a DES tool. No graphical user interface had been developed for it, and we believe that one the most promising data structures had been selected to represent the event list because its properties (size, the speed of accessing its content) can highly influence the speed of the simulation. Furthermore, EasySim had been developed for building a DES model in the most direct way with programming. The overall intention to develop EasySim in such way was to achieve fast simulation runs, and because EasySim is our own implementation, we could be sure that the integration with the other tools in this paper would be in the most convenient way. Again, it is true that the simulation model presented below would have been implemented in any other simulation software. EasySim was selected because of its flexibility to be integrated in the back-end platform.

Regarding the simulation model, it implements a production line which contains eight workstations connected to each other in a linear way, called a flow-shop line. The modeled production line is part of a real manufacturing factory, and operation times were given for each workstation provided by the factory. Additionally, the model implements some kind of stochastic behavior such as failure of workstations which can be optionally used in the simulation. This capability of stochastic behavior has been realized by integrating a mathematical software package during the development of EasySim which ensures proper random number handling and different mathematical functions to approximate reality as much as it is possible. The operations on each workstation are different and may require the presence of one or more human workers who perform the manufacturing of the assembly task at the given station. As in a real production system, the workers are also different; for each specific task at a workstation, a worker needs to have a specific skill. Moreover, the operators are assigned to specific shifts meaning that shift by shift we can have different teams, grouping different workers with different skills. As Figure 8 illustrates, it is a linear, acyclic production line which contains eight workstations (WS1, WS2, etc.). Below each workstation, there is a required skill name which indicates that a worker can operate on the workstation only if the worker has the specific skill. A worker can have multiple different skills meaning that he can operate on different workstations. An evident solution is to have one worker for each workstation with the required skills of course, but in reality, factories have less workers available to allocate them, so the task is to find an optimal worker set which is able to carry the order out with a minimal number of workers.

The task of the planner is to find the right configuration of workers for each specific shift. Naturally, the problem can be formulated as a formalized mathematical problem, but as the nature of the operation times is stochastic (i.e., each operation varies and follows a distribution; additionally, failures may occur unexpectedly at each workstation), the

Table 1: The layout of the flow-shop system.

	$Skill_1$	$Skill_2$	$Skill_3$	$Skill_4$	$Skill_5$	$Skill_6$	$Skill_7$	$Skill_8$
$Worker_1$	1	0	0	1	0	1	0	0
$Worker_2$	0	0	0	0	1	0	1	1
$Worker_3$	0	1	1	1	0	1	0	0

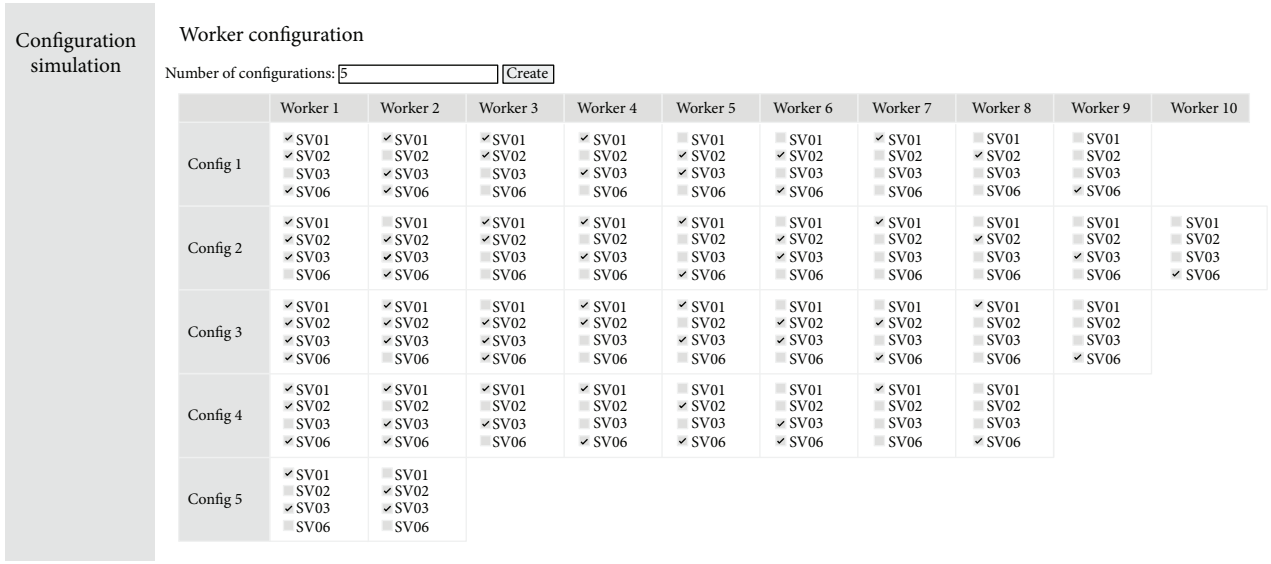

Figure 9: User interface for parameterizing workers' skills and teams.

usage of a discrete-event simulation tool is more adequate to model the line in question. To provide input, control the run of the simulation model, and visualize the results of the simulation scenarios, a web application was developed and integrated with the orchestrated back-end platform described earlier. This is presented in the upper part of Figure 7 and includes the Experiment Manager and the GUI for visualization. The visualized functionality of the EasySim DES kernel introduced at the beginning of the paper is available through this web application, and some examples of the GUI of the system is presented in the figures of the following section.

4.1.1. Parametrization of the System. There are two main input sets for each simulation experiment. First, the model should be fed with production orders which are recorded giving the order IDs, due dates, and product quantities. All other data describing the products, their routing, and the operation times are given in advance and stored in the database. The second input, which is specific to the model, is the matrix of workers and their skills.

In the example presented in Table 1, $Worker_1$ can work on WS1, WS4, and WS6 workstations but cannot work on WS2, WS3, WS5, WS7, and WS8 workstations. A worker can have multiple different skills, so considering the example before, a worker can operate both on WS2 and on WS3 only if he has the $Skill_2$ and $Skill_3$ skills.

Figure 9 shows how the parametrization of the worker's skills can be completed with the help of the high-level GUI. As you can see, there are ten different workers provided as columns in the matrix while in each configuration—which will run in parallel on the orchestrated back-end platform—separate skill patterns can be defined for each worker. These are denoted by the names of the workstations, e.g. SV01 and SV02.

4.1.2. Execution of Simulation Runs and the GUI. Having the input parameter set, the simulation model instances are built dynamically for each configuration and the simulation runs start in parallel. One simulation run includes one worker configuration (a row with a Config *X* label on the figure of the worker configuration) with the selected orders. These instantiated simulations as configurations are detached from the GUI, and they are handled on the orchestrated back-end platform as separate workers. When a simulation run is completed (i.e., the worker with its simulation finishes), the output statistics are saved into the database for each configuration. After the successful execution of each worker, the Docker Container Manager notifies the GUI about the completion of the simulation run, and when all the running configurations were completed, the GUI can visualize the simulation results. Figure 10 provides the statistics about the utilization of the workers in configuration number 3. The blue part in the top region of the figure illustrates the percentage the operator was idle while the green part indicates the time where the operator was working. With the orders completed in this configuration, we can see that by

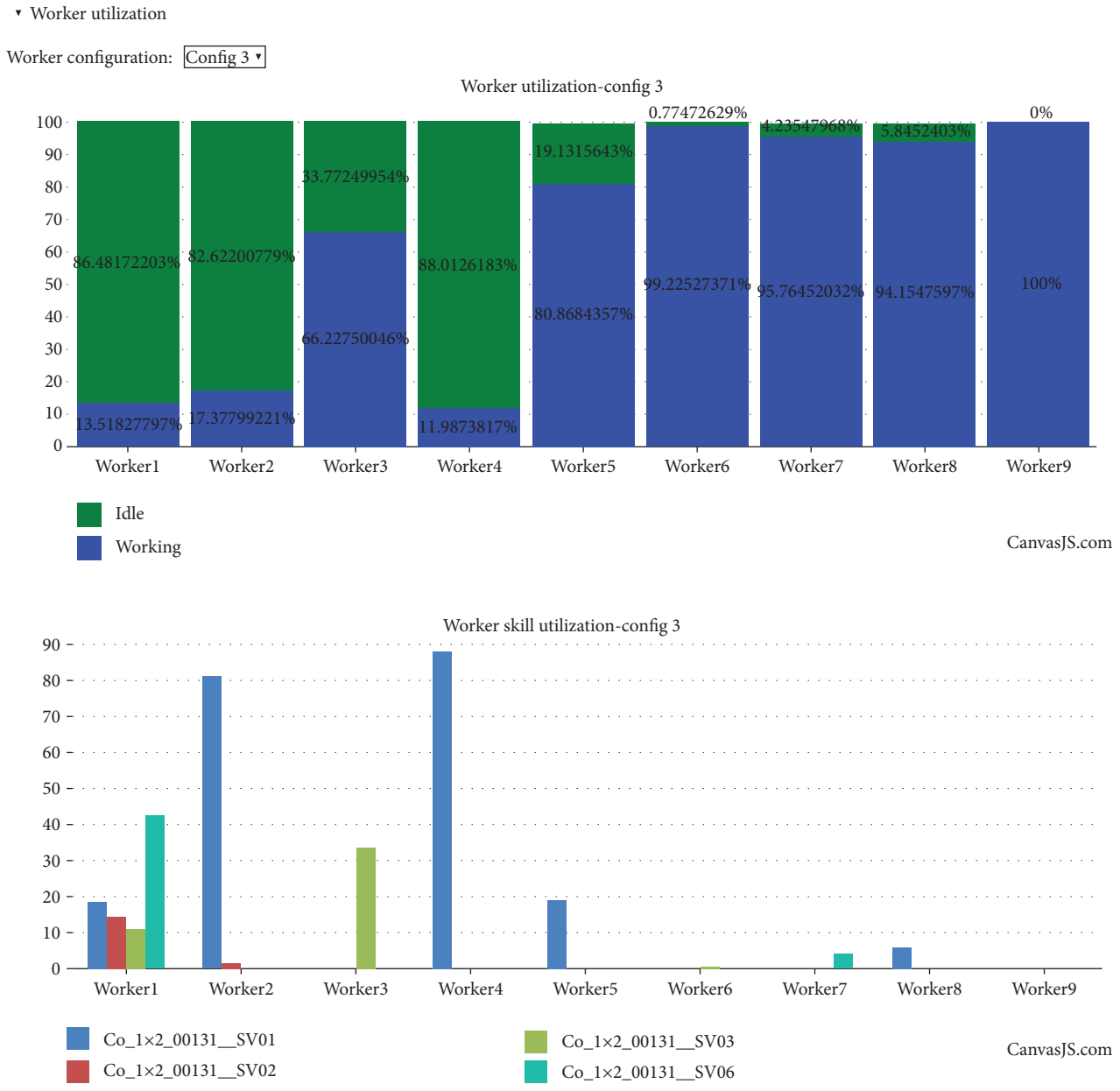

Figure 10: Chart representing the utilization of workers in a configuration.

applying seven operators, we will have a very underutilized environment. Figure 11 gives an overview of how the 3 distinct orders behaved in the system, mainly meaning that there were no significant differences between the five different configurations. As the main focus of the paper is the orchestrated back-end, we additionally included some explanatory charts, but many additional key performance indicators can be visualized within the GUI. Some of them visualize aggregated measures while others specific resource, buffer, or worker-related measures.

4.2. Sensor Data Back-End Experiments: Multilevel Autoscaling in MiCADO. The developed sensor data back-end has been successfully migrated under the MiCADO [43] (Microservices-based Cloud Application-level Dynamic Orchestrator) framework that attempts to unify and also to extend the previously described tools including Occopus and CQueue in a long term. It allowed us to evaluate the sensor data back-end in a more fine-grained way using multi-level scaling, that is, not only at the VM level but also at the container level. This approach utilized the two control loops of MiCADO that led to the presented results.

4.2.1. MiCADO from a Scalability Point of View. MiCADO [43] (developed by the EU H2020 COLA [44] project) is a framework performing the execution of compound microservice-based infrastructure on cloud resources. Beyond the execution, the most important functionality of MiCADO is the automatic scaling on two levels. The microservice-level autoscaling deals with keeping the optimal number of

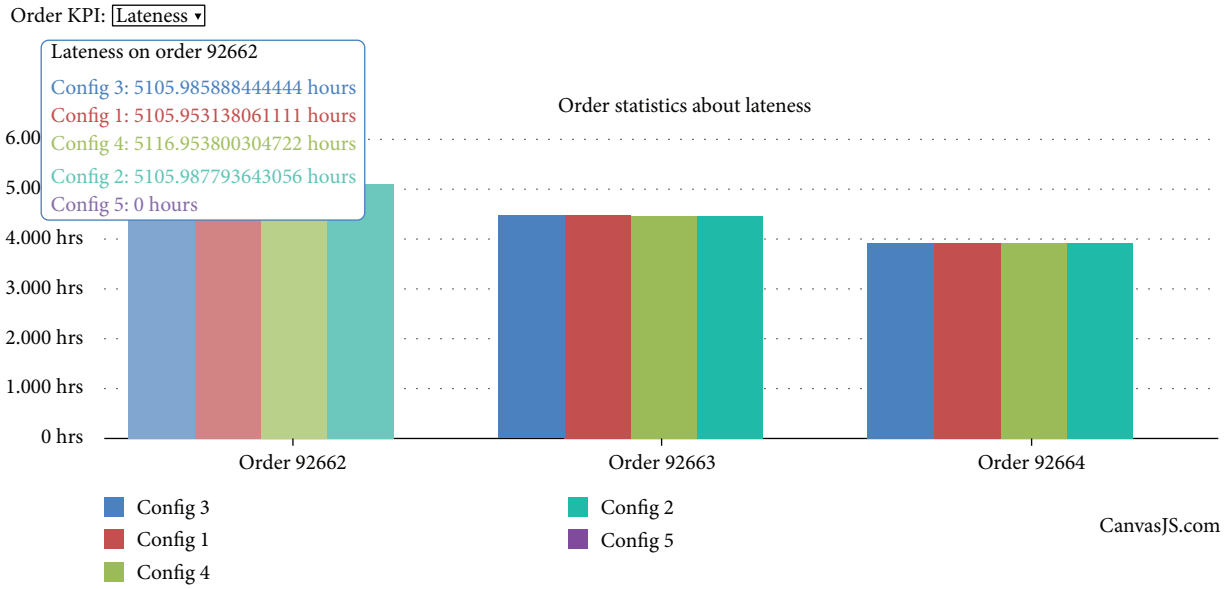

Figure 11: Statistics of the orders pulled through the system.

container instances for a particular microservice. The cloud-level autoscaling deals with allocating the optimal amount of cloud resources for the entire microservice-based infrastructure.

MiCADO is developed by integrating various tools into a common framework. For executing microservice infrastructure, a dynamically extendable and resizable Swarm [45] cluster is used. Monitoring is performed by Prometheus [40] with agents on the nodes of the cluster. The communication with the cloud API and the orchestration of the Swarm cluster is performed by Occopus [35] mentioned in previous sections. Each of the components is integrated taking into account the replaceability in the future in case a better tool appears in its area. The scaling and optimization logic is built by the COLA project as well as the submission interface. For describing the microservice infrastructure, the project has chosen the TOSCA [31] specification language where the components, requirements, relations, and so on can be easily defined in a portable way. The way of describing scaling/optimization policies is developed by the COLA project as an extension of the TOSCA specification.

The conceptual overview of the two control loops implemented by the aforementioned components and tools is shown in Figure 12. In both control loops, Policy Keeper performs controlling and decision-making on scaling while Prometheus acts as a sensor to monitor the measured targets. In the microservice control loop, the targets are the microservice containers realizing that the infrastructure can be controlled. Containers are modified (number, location, etc.) by Swarm playing as an actuator in the loop. A similar control loop is realized for the cloud resources represented by virtual machines in our case. Here, Occopus acts as an actuator to scale up/down the virtual machines (targets). The microservice control loop controls the consumers while the cloud-level control loop controls the resources. As a consequence, the microservice loop affects the cloud loop since more consumers require more resources.

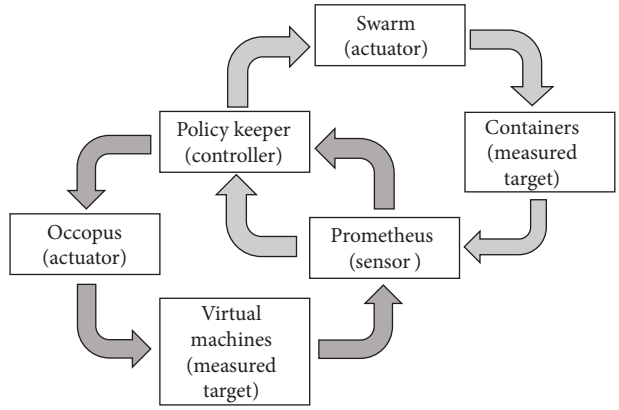

Figure 12: Control loops applied for multilevel autoscaling of virtual machines and containers in MiCADO.

The goal of MiCADO control loops is to provide an automatic scaling functionality for an infrastructure built by microservices. For automatic scaling, there are several different scenarios in which scaling can focus on optimizing the running infrastructure for various goals. The execution of the microservice infrastructure has different requirements and different measurable characteristics. For example, processing, memory, network bandwidth, and disk i/o are all resources MiCADO may reserve for the infrastructure while CPU load, memory usage, response time, or disk usage are measurable characteristics. Beyond optimizing for some of the characteristics, MiCADO is also being developed towards optimizing for costs generated by the usage of (commercial) cloud resources.

Beyond optimizing for easily measurable external characteristics, MiCADO is prepared to monitor some internal parameters of the microservice infrastructure. For example, monitoring the length of a queue enables MiCADO to perform optimization in different scenarios like keeping the

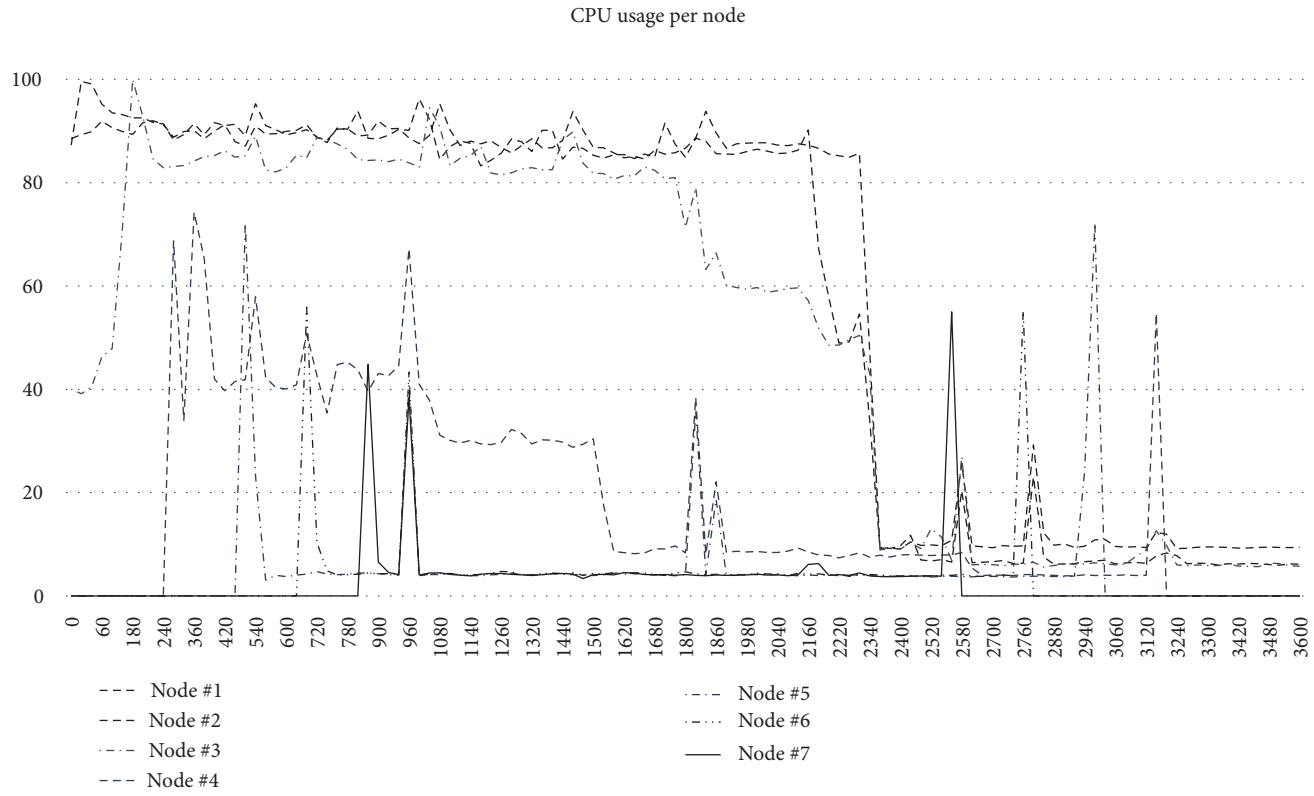

(a) CPU usage per node

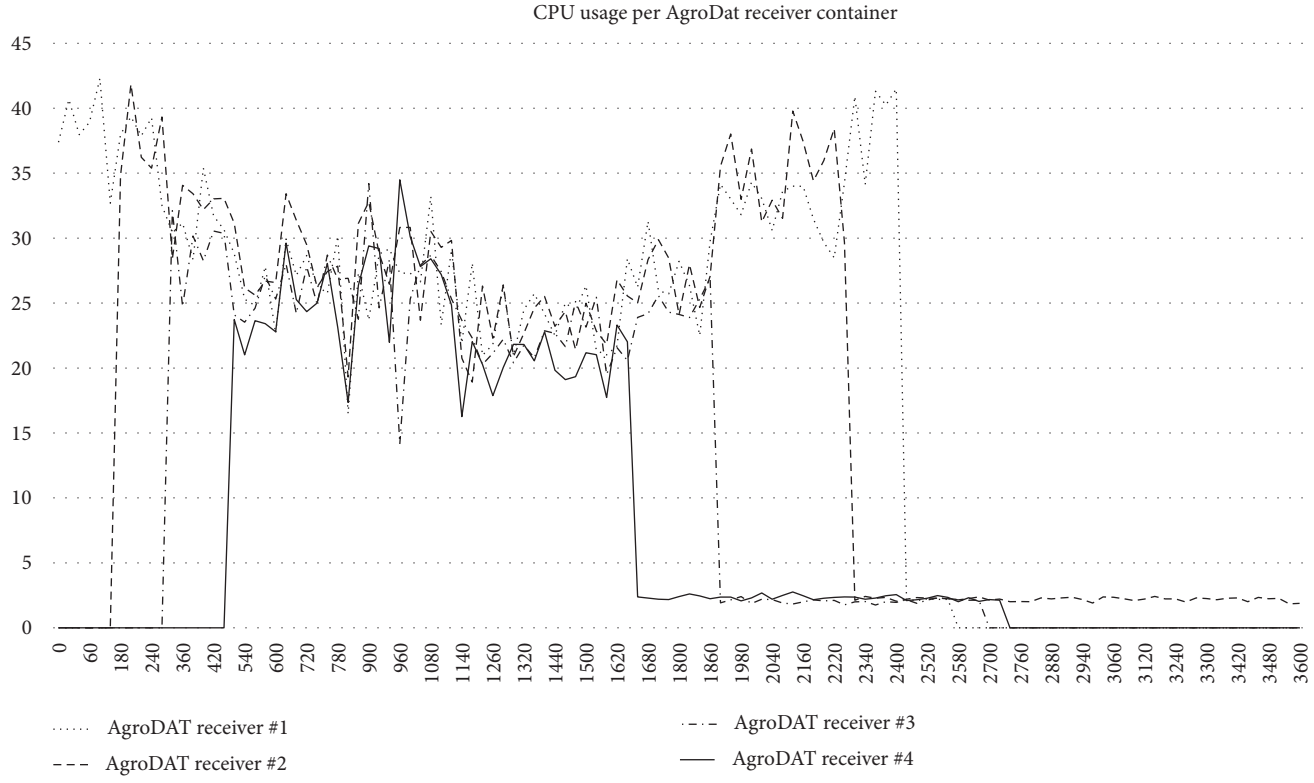

(b) CPU usage per data receiver container

Figure 13: Continued.

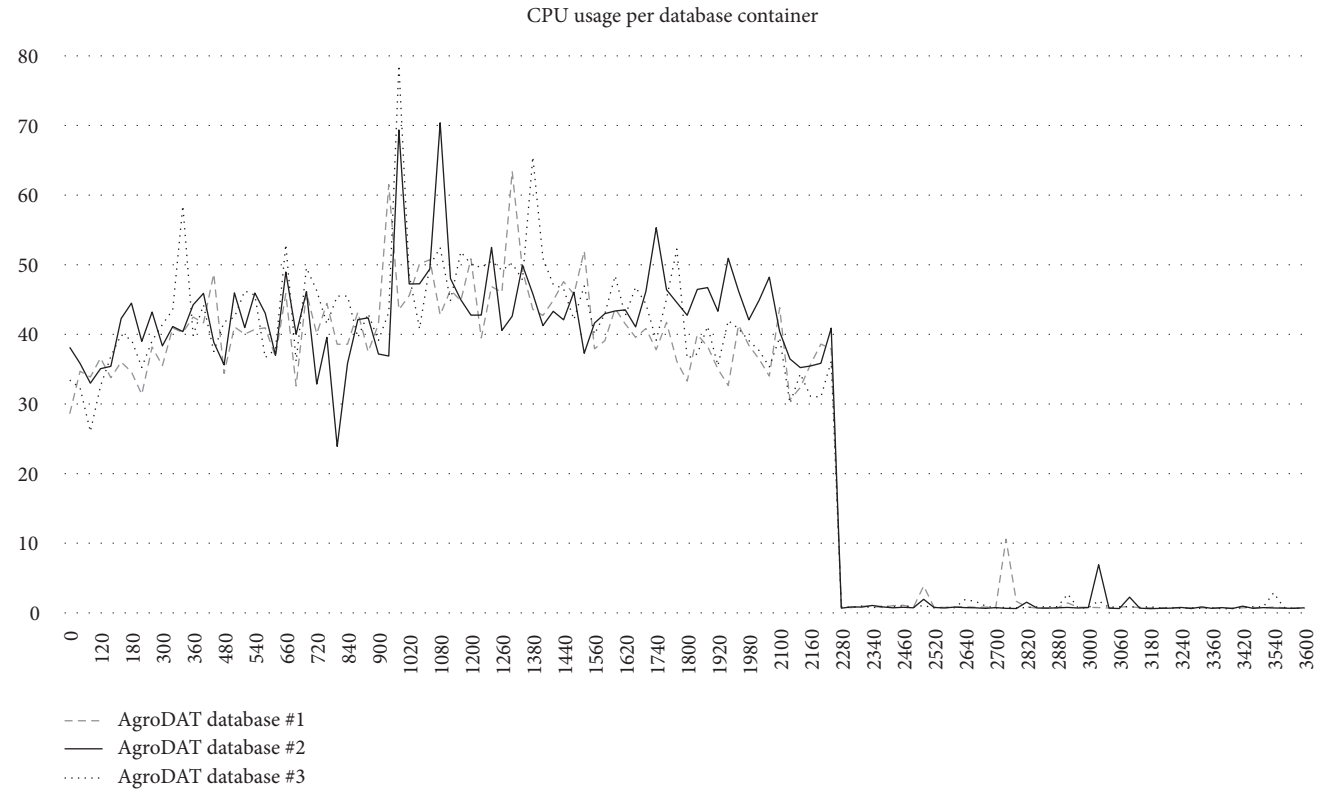

(c) CPU usage per database container

Figure 13: CPU usage per container.

number of items on a certain level, keeping a predefined processing rate of items, or making the items consumed by a predefined deadline. The different scenarios and optimization strategies are continuously developed and added to the latest version of MiCADO. The current version of MiCADO (v3) supports the performance-based policy for containers and virtual machines.

4.2.2. Results. The multilevel scaling of the back-end is handled by MiCADO. With MiCADO's dual control loops, we can scale the container-based data collectors and the host virtual machines as well. The whole data collector infrastructure is deployed in MiCADO.

All measurements were performed on an OpenNebula-based cloud within MTA SZTAKI. All nodes ran as virtual machines on AMD Opteron 6376 CPUs with all virtual CPUs (VCPUs) mapped to actual physical cores and connected via a 10 Gbit/s network. The virtual machines had 1 VCPU and 2 GB RAM allocated. The measured data are exported from MiCADO's Prometheus monitoring component. MiCADO was configured to scale up or down the containers in every minute and the workers nodes in every third minute. We only scaled the collector components automatically within the architecture. The collector components are scaled up when the average CPU usage of the collectors reaches 30 percent. This allows the saturation of the worker nodes and distribution of the incoming data between additional collector containers. The collectors are scaled down at 10-percent average CPU usage. The MiCADO worker nodes are scaled up at 60-percent CPU usage and down at 20-percent CPU usage. Measurements were performed with test sensor data, and we generated and sent 800 data packages per second to the framework. We deployed the collector infrastructure initially with one collector and three database containers. As shown in Figure 13(c), as the collectors' average CPU usage reaches the threshold, MiCADO scaled up the collector containers, and the incoming data was distributed between the increased numbers of collector containers. The number of the collector components can be seen in Figure 14(a). The balanced CPU usage of the collectors' database components can be seen in Figure 13(c). As seen in Figure 13(a) and in Figure 14(b), when the MiCADO worker nodes' average CPU usage reached the threshold, MiCADO automatically scaled up the worker nodes. Only node #4 had a high CPU load, because the number of the collector containers was enough to process the incoming data. The remaining running nodes can be considered spares in the system, or alternatively we can manually reschedule the running collector components to balance the worker nodes' CPU usage within the cluster. As shown in Figure 13(c) and in Figure 14(a), when the stream of the incoming data finished, the worker components' CPU usage lowered and MiCADO scaled down the collector's container service to the minimum number of containers. This scaling down can be observed in Figures 13(a) and 14(b), with the MiCADO worker nodes as well.

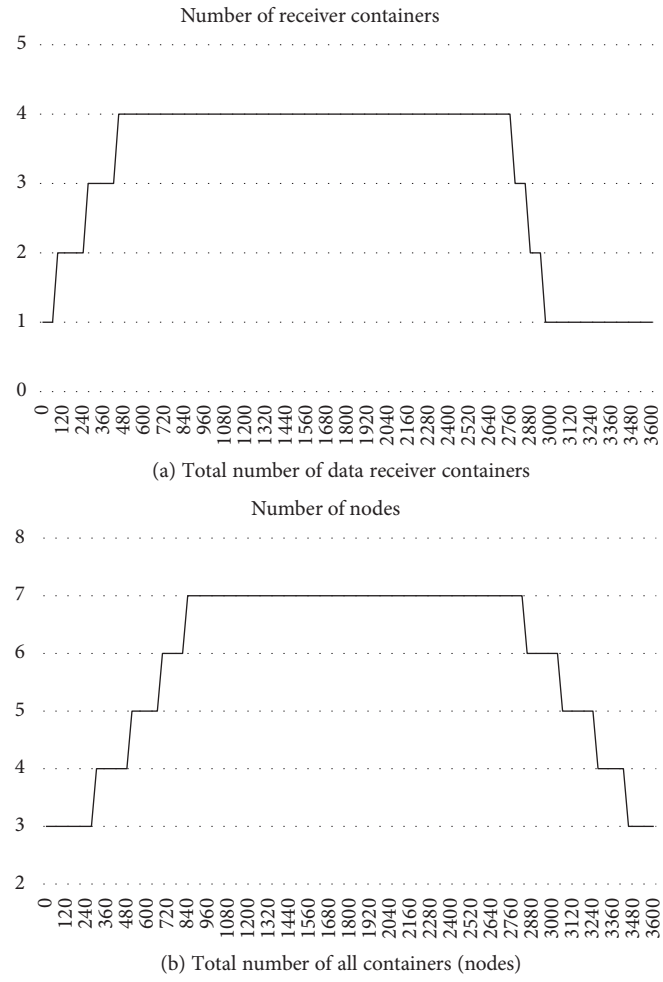

(a) Total number of data receiver containers

(b) Total number of all containers (nodes)

Figure 14: Number of containers.

5. Future Works and Conclusions

This section summarizes further the targeted use cases: (i) connected cars (see Section 5.1) and (ii) precision agriculture (see Section 5.2), and contains conclusions for the paper. In both (connected cars and precision agriculture) CPS areas, a subset of the presented back-end framework has been already applied and integrated successfully with other system components particularly for research and evaluation purposes and also for forming the baseline of new production-level services.

As additional future work, we have started to study and elaborate the adaptation of different job-based policies, including deadline and throughput, in MiCADO over the CQueue microservice infrastructure. The integration will lead to an autoscalable CQueue job execution framework with different strategies on scaling. Furthermore, the adaptation of this sensor data ingestion architecture is already in progress in two further sectors, namely, connected cars and precision farming, with some positive preliminary results based on the outlined sectoral demands.

5.1. Connected Cars. Connected car technologies have been rapidly advancing with several new digital solutions and autonomous driving features. Connected cars collect and make interpretable massive amounts of data—mostly from digital sensors of IoT systems by exchanging useful data (e.g., alerts) between other vehicles, stoplights, and back-end services [33, 46]. Even though automobiles today are equipped with significant amount of processing and storage capacities, the rapidly growing amount of raw data and the higher-level functionalities require robust and scalable back-end technologies that can handle the underlaying sophisticated processing and analytical functions. Relying on the basic principles and some components of the presented sensor data back-end architecture, our current research focuses on CAN data collection, remote device flashing, Eco-driving, and weather report and forecast with some promising initial achievements (see details in [47]).

5.2. Precision Agriculture. The ultimate aim of the Agro-Dat.hu project [48] is to create a knowledge center for precision agriculture based on the local sensor data (and also integrating semi- or unstructured data from international repositories). Concerning the sensors, more than 1000 complex sensor pillars have been deployed at various selected locations covering more than 8000 hectares of 58 farmers. The sensor pillars have modular structure [49] with facilities

to measure environmental factors (weather, soil moisture, etc.), phenotypes (sensor image data), and other parameters continuously for at least 3 years. The communication network is based on a 4G GSM network and M2M communication-enabled SIM cards. For processing and storing data and also for providing services for researchers, farmers, decision-makers, and so on, a new big data center is in operation based on the OpenStack [50] cloud. It is responsible for providing an elastic and flexible framework for the higher-level software services: (among others) back-end for data collection, processing, and decision support systems.

The back-end architecture of AgroDat.hu contains the two main functionalities: (i) data collectors for processing incoming sensor and sensor image data and (ii) a Backoffice system for additional functionalities and administrative functions. The obtained raw data is then made available for processing and analytics in the big data center.

(1) First, the data collectors are responsible for gathering and storing sensor messages in the cloud for further processing. They preprocess the data and store it in a structured format for the other cloud-based functions. Additionally, it is also stored directly in the input format to have backup for security reasons and to be available for future implemented functions and statistics. (2) The collected data can be visualized within a *Backoffice* application and is also available for further processing by analytical tools. The detailed description of these results can be found in [51].

5.3. Conclusions. In this paper, we presented different variants (based on orchestrated VMs and containers) and also the major implementation steps of a scalable sensor data back-end and predictive simulation architecture that can be adapted with low-entry barriers to other use case scenarios as well.

According to the evaluation of the orchestrated back-end framework, the solution is highly scalable and the back-end facilitates the transfer of the results achieved in the field of digital factory (DF), namely, the DES solution presented in the paper, by allowing much faster, parallelized behavior forecasting of manufacturing systems. We strongly believe that the orchestrated cloud and container-based back-end platform support industrial applications by providing the required up-to-date and cutting-edge ICT technologies.

The novelties of our cloud orchestration solution are mostly described in [35]. However, the combination of the key features such as (i) multilevel autoscaling including VMs and containers, (ii) cloud agnostic approach, and (iii) generic open-source solutions for such wide scope including various CPS problems makes our solution innovative.

We are just in the initiating phase of creating and operating the Centre of Excellence in Production Informatics and Control (EPIC CoE), and the integrated solution presented in the paper already allows us to offer complex, powerful, and affordable Industry 4.0 solutions to all stakeholders, especially to SMEs. Moreover, we recently started the innovation and knowledge transfer activities in the "Cloudification of Production Engineering for Predictive Digital Manufacturing" (CloudiFacturing) consortium [52] in order to adapt the presented sensor data back-end and predictive simulation architecture by the help of digital innovation hubs across Europe.

Conflicts of Interest

The authors declare that they have no conflicts of interest.

Acknowledgments

This work was partially funded by the European "COLA (Cloud Orchestration at the Level of Application)" project (Grant Agreement no. 731574 (H2020ICT-2016-1)), by the National Research, Development and Innovation Fund of Hungary (Grant no. VKSZ 12-1-2013-0024) (Agrodat.hu), and by the International Science and Technology Cooperation Program of China (Grant no. 2015DFE12860). On behalf of the project Occopus, the authors thank for the usage of the MTA Cloud [53] that significantly helped us achieve the results published in this paper. The research conducted with the scope of the discrete-event simulation was supported by the European Commission through the H2020 project EPIC (http://www.centre-epic.eu) (Grant no. 739592).

References

[1] L. Monostori, B. Kádár, T. Bauernhansl et al., "Cyber-physical systems in manufacturing," *CIRP Annals*, vol. 65, no. 2, pp. 621–641, 2016.

[2] C. Kardos, G. Popovics, B. Kádár, and L. Monostori, "Methodology and data-structure for a Uniform System's Specification in Simulation Projects," *Procedia CIRP*, vol. 7, pp. 455–460, 2013.

[3] A. Gupta, M. Kumar, S. Hansel, and A. K. Saini, "Future of all technologies-the cloud and cyber physical systems," *International Journal Of Enhanced Research In Science Technology & Engineering*, vol. 2, p. 2, 2013.

[4] I. Mezgár and U. Rauschecker, "The challenge of networked enterprises for cloud computing interoperability," *Computers in Industry*, vol. 65, no. 4, pp. 657–674, 2014.

[5] R. Gao, L. Wang, R. Teti et al., "Cloud-enabled prognosis for manufacturing," *CIRP Annals*, vol. 64, no. 2, pp. 749–772, 2015.

[6] J. Gubbi, R. Buyya, S. Marusic, and M. Palaniswami, "Internet of things (IoT): a vision, architectural elements, and future directions," *Future Generation Computer Systems*, vol. 29, no. 7, pp. 1645–1660, 2013.

[7] "AWS Internet of Things," October 2017, http://aws.amazon.com/iot.

[8] "Azure IoT Suite - IoT Cloud Solution," October 2017, http://www.microsoft.com/en-us/internet-of-things/azure-iot-suite.

[9] "Google IoT Core," October 2017, http://cloud.google.com/iot-core.

[10] "FIWARE architecture description: big data," October 2017, https://forge.fiware.org/plugins/mediawiki/wiki/fiware.

[11] N. Marz and J. Warren, *Big Data: Principles and Best Practices of Scalable Real-time Data Systems*, Manning Publications Co., 2015.

[12] "Highly scalable blog. In-stream big data processing," October 2017, https://highlyscalable.wordpress.com/2013/08/20/in-stream-big-data-processing/.

[13] "FIWARE architecture description: big data," October 2017, https://forge.fiware.org/plugins/mediawiki/wiki/fiware/index.php/FIWARE.ArchitectureDescription.Data.BigData.

[14] "FIWARE glossary," October 2017, https://forge.fiware.org/plugins/mediawiki/wiki/fiware/index.php/FIWARE.Glossary.Global.

[15] "Hadoop: WebHDFS REST API," October 2017, http://hadoop.apache.org/docs/current/hadoop-project-dist/hadoop-hdfs/WebHDFS.html.

[16] M. Kornacker, A. Behm, V. Bittorf et al., "Impala: a modern, open-source SQL engine for Hadoop," in *7th Biennial Conference on Innovative Data Systems Research (CIDR'15)*, Asilomar, CA, USA, January 2015.

[17] K. Shvachko, H. Kuang, S. Radia, and R. Chansler, "The Hadoop distributed file system," in *2010 IEEE 26th Symposium on Mass Storage Systems and Technologies (MSST)*, pp. 1–10, Incline Village, NV, USA, May 2010.

[18] "The Apache Cassandra project," October 2017, http://cassandra.apache.org.

[19] "Cascading: application platform for enterprise big data," October 2017, http://www.cascading.org.

[20] G. Casale, D. Ardagna, M. Artac et al., "DICE: quality-driven development of data-intensive cloud applications," in *2015 IEEE/ACM 7th International Workshop on Modeling in Software Engineering*, pp. 78–83, Florence, Italy, May 2015.

[21] "The Apache Spark project," October 2017, http://spark.apache.org.

[22] "The Apache Storm project," October 2017, http://storm.apache.org.

[23] V. Abramova and J. Bernardino, "NoSQL databases: MongoDB vs Cassandra," in *C3S2E '13 Proceedings of the International C∗ Conference on Computer Science and Software Engineering*, pp. 14–22, Porto, Portugal, July 2013.

[24] "Docker-build, ship, and run any app, anywhere," October 2017, https://www.docker.com/.

[25] B. Burns, B. Grant, D. Oppenheimer, E. Brewer, and J. Wilkes, "Borg, Omega, and Kubernetes," *Communications of the ACM*, vol. 59, no. 5, pp. 50–57, 2016.

[26] "OpenLambda," October 2017, https://open-lambda.org/.

[27] "OpenFaaS: Functions as a Service," October 2017, https://blog.alexellis.io/introducing-functions-as-a-service/.

[28] "A Kubernetes native serverless framework," October 2017, http://kubeless.io/.

[29] "Terraform by HashiCorp," October 2017, https://www.terraform.io/.

[30] T. Binz, U. Breitenbücher, O. Kopp, and F. Leymann, "TOSCA: portable automated deployment and management of cloud applications," *Advanced Web Services*, pp. 527–549, 2013.

[31] "OASIS Topology and Orchestration Specification for Cloud Applications (TOSCA)," October 2017, https://www.oasis-open.org/committees/tosca.

[32] "OASIS - advancing open standards for the information society," October 2017, https://www.oasis-open.org/.

[33] T. Haberle, L. Charissis, C. Fehling, J. Nahm, and F. Leymann, "The connected car in the cloud: a platform for prototyping telematics services," *IEEE Software*, vol. 32, no. 6, pp. 11–17, 2015.

[34] "GE. Predix platform: the foundation for digital industrial applications," March 2018, https://www.ge.com/digital/predix-platform-foundation-digital-industrial-applications.

[35] J. Kovács and P. Kacsuk, "Occopus: a multi-cloud orchestrator to deploy and manage complex scientific infrastructures," *Journal of Grid Computing*, vol. 16, no. 1, pp. 19–37, 2017.

[36] "HAProxy: the reliable, high-performance TCP/HTTP load balancer," October 2017, http://www.haproxy.org/.

[37] "The uWSGI project. uWSGI 2.0 documentation," October 2017, https://uwsgi-docs.readthedocs.io.

[38] J. Gardner, "The Web Server Gateway Interface (WSGI)," *The Definitive Guide to Pylons*, pp. 369–388, 2009.

[39] W. Reese, "Nginx: the high-performance web server and reverse proxy," *Linux Journal*, vol. 2008, no. 173, p. 2, 2008.

[40] "The Prometheus monitoring tool," November 2017, https://prometheus.io/.

[41] International Society of Automation, "ISA95, enterprise-control system integration," November 2017, https://www.isa.org/isa95/.

[42] R. Bloomfield, E. Mazhari, J. Hawkins, and Y.-J. Son, "Interoperability of manufacturing applications using the Core Manufacturing Simulation Data (CMSD) standard information model," *Computers & Industrial Engineering*, vol. 62, no. 4, pp. 1065–1079, 2012.

[43] T. Kiss, P. Kacsuk, J. Kovacs et al., "MiCADO—Microservice-based Cloud Application-level Dynamic Orchestrator," *Future Generation Computer Systems*, 2017, http://www.sciencedirect.com/science/article/pii/S0167739X17310506.

[44] "COLA: Cloud Orchestration at the Level of Application," November 2017, http://www.project-cola.eu.

[45] "Swarm mode of Docker," November 2017, https://docs.docker.com/engine/swarm/.

[46] W. He, G. Yan, and L. Da Xu, "Developing vehicular data cloud services in the IoT environment," *IEEE Transactions on Industrial Informatics*, vol. 10, no. 2, pp. 1587–1595, 2014.

[47] C. Marosi, R. L. Attila, A. Kisari, and S. Erno, "A novel IoT platform for the era of connected cars," in *2018 IEEE International Conference on Future IoT Technologies (Future IoT)*, pp. 1–11, Eger, Hungary, January 2018.

[48] "Agrodat.hu project website," October 2017, http://www.agrodat.hu.

[49] P. Gábor, S. Péter, and É. Gábor, "Power consumption considerations of GSM-connected sensors in the AgroDat.hu sensor network," *Sensors & Transducers*, vol. 189, no. 6, pp. 52–60, 2015.

[50] X. Wen, G. Gu, Q. Li, Y. Gao, and X. Zhang, "Comparison of open-source cloud management platforms: OpenStack and OpenNebula," in *2012 9th International Conference on Fuzzy Systems and Knowledge Discovery*, pp. 2457–2461, Sichuan, China, May 2012.

[51] C. Marosi, A. F. Attila, and R. Lovas, "An adaptive cloud-based IoT back-end architecture and its applications," in *Proceedings of The 26th Euromicro International Conference on Parallel, Distributed and Network-Based Processing (PDP 2018)*, Cambridge, UK, March 2018.

[52] "CloudiFacturing project website," May 2018, http://cloudifacturing.eu.

[53] "MTA Cloud," October 2017, https://cloud.mta.hu.

Hindawi
Complexity
Volume 2018, Article ID 4670159, 11 pages
https://doi.org/10.1155/2018/4670159

Research Article

Receding Horizon Control of Type 1 Diabetes Mellitus by Using Nonlinear Programming

Hamza Khan,[1,2] **József K. Tar**,[3] **Imre Rudas**,[3] **Levente Kovács**,[4] **and György Eigner**[4]

[1]*Doctoral School of Applied Informatics and Applied Mathematics, Óbuda University, Bécsi Street 96/B, Budapest 1034, Hungary*
[2]*Mathematical Sciences Research Center, Karachi, Pakistan*
[3]*Antal Bejczy Center for Intelligent Robotics (ABC iRob), Óbuda University, Bécsi Street 96/B, Budapest 1034, Hungary*
[4]*Physiological Controls Research Center, Óbuda University, Bécsi Street 96/B, Budapest 1034, Hungary*

Correspondence should be addressed to György Eigner; eigner.gyorgy@nik.uni-obuda.hu

Received 23 November 2017; Accepted 26 February 2018; Published 23 April 2018

Academic Editor: Thierry Floquet

Receding Horizon Controllers are one of the mostly used advanced control solutions in the industry. By utilizing their possibilities we are able to predict the possible future behavior of our system; moreover, we are able to intervene in its operation as well. In this paper we have investigated the possibilities of the design of a Receding Horizon Controller by using Nonlinear Programming. We have applied the developed solution in order to control Type 1 Diabetes Mellitus. The nonlinear optimization task was solved by the Generalized Reduced Gradient method. In order to investigate the performance of our solution two scenarios were examined. In the first scenario, we applied "soft" disturbance—namely, smaller amount of external carbohydrate—in order to be sure that the proposed method operates well and the solution that appeared through optimization is acceptable. In the second scenario, we have used "unfavorable" disturbance signal—a highly oscillating external excitation with cyclic peaks. We have found that the performance of the realized controller was satisfactory and it was able to keep the blood glucose level in the desired healthy range—by considering the restrictions for the usable control action.

1. Introduction

The advanced control solutions have inevitable role in today's medical practice regarding the control of physiological processes [1]. Many control solutions are under development that can be used for various kinds of control problems. Advanced control methods have been successfully applied for physiological regulation problems, for example, control of anesthesia [2, 3], angiogenic inhibition of cancer [4, 5], immune response in presence of human immunodeficiency virus [6], and regulation of blood glucose (BG) level [7–10] as well.

Diabetes Mellitus (DM) is the collective name of several chronic diseases connected to the metabolic system of the human body. In most of the cases, the DM condition appears due to the issues related to the insulin hormone [11]. The insulin is the key hormone which makes the glucose molecules possible to enter from the blood into the glucose consuming cells through the insulin-dependent gates on the cell-wall [12].

There are many types of DM. The most dangerous is the Type 1 DM (T1DM) where the metabolic system is not able to function normally due to the lack of insulin. Type 2 DM (T2DM) is the most widespread kind of DM and it occurs mostly because of the lifestyle. In this case usually the blood glucose and insulin levels continuously increase over a long period of time. Due to the extreme glucose and insulin load the cells become resistant to the insulin over time. In order to compensate this condition the body produces more and more insulin that leads to the "burnout" of the pancreatic β-cells that produce the hormone. At this point the T2DM turns into T1DM. Other frequently occurring type is the Gestational DM (GDM) from which women may suffer during pregnancy. Usually, this condition is

temporary; however, sometimes it turns into T2DM and becomes permanent [13–15].

In case of DM the application of these kinds of advanced control techniques has high importance. Due to the nature of the phenomenon to be controlled the researchers on the field have to face many challenges such as high nonlinearities, model and parameter uncertainties, and even time-delay effects, as well. However, regardless the type of DM a few common control goals can be defined: keeping the glycemia (the BG level) in a the healthy range; totally avoiding the hypoglycemic periods; and avoiding the high BG variability as much as possible [16–18].

In this research we have investigated the T1DM. As we mentioned, T1DM is the most dangerous condition because the patients need external insulin intake in order to keep their metabolic status on appropriate level. In this case the patient's pancreatic β-cells are terminated by the immune system of the patient during an autoimmune reaction. As a consequence, these patients are not able to produce insulin—which leads to short term starving, coma, or even death [11]. Furthermore, the appropriate treatment—how the insulin is administered—is also important to avoid long term side effects, for example, the chronic failure of peripheric vasculature [13].

By using advanced control techniques not just acceptable control action but higher treatment quality can be obtained. The selected control methods have to handle the already mentioned unfavorable effects—such as the nonlinearities and so on—as well. In case of T1DM many solutions are available; however, all of them have their own limitations, simplifications, and restrictions—thus, none of them are general [10]. In these days from control point of view the most beneficial approach is the Artificial Pancreas (AP) concept. This idea aims to imitate the regular operation of the pancreas from the insulin production point of view, namely, administering insulin demands on the needs determined by the BG level [19]. Thus, we have to face contradictory requirements: the generalization and personalization as well.

One of the mostly used algorithms is the modified proportional-integral-derivative (PID) solutions due to their simplicity and flexibility. Moreover, several clinical trials have been done by using this methodology and investigate its effectivity [20–22]. Linear Parameter Varying (LPV) model-based solutions have high importance, since the uncertainties can be handled with high efficiency by them [7, 9, 23]. The Tensor Product (TP) model-based techniques also represent interesting directions, since they can be combined by Linear Matrix Inequality (LMI) based control and LPV methodology as well [24, 25].

The most frequently used method is the Model Predictive Control (MPC) regarding the control of DM [19, 26–28]. MPC is a widely used approach in various research fields as well [29–32]. In general the goals of the MPC applications are tracking and stabilization [33]. In case of an MPC the actual value of the control signal $u(k)$ is obtained by solving an open-loop control problem over a finite horizon. Of course, some feedback is present because the starting point of the next horizon is the last realized point of the previous one. The type of the optimal control problem depends on the type of the control task. The classical MPC is realized in a framework of cost-function-based optimal control where the dynamics of the system to be controlled can be considered as a set of constraints. Furthermore, the cost function regularly contains terms which depend on the tracking error and the control signal itself. Optionally, a cost contribution that depends on the tracking error at the end of the horizon can be added as well.

In case of the Receding Horizon Control (RHC) via Nonlinear Programming (NP) based approximation the state variables and the control inputs of the system are considered over a discrete time grid. At each point of the grid the Lagrangian multipliers determine the reduced gradient which is driven into zero numerically to find the optimal solution. This solution consists of the estimated values of the state variables and control signals over the finite horizon. In that case if the dynamic model of the system is not precise, the optimal design can be used only for consecutive finite horizons since the actual state of the controlled system propagates according to its exact dynamics. In order to minimize the effects coming from the inaccuracies the actual measured state variable from the end of the previous horizon is applied as starting point for the next one in the next horizon-length design [34]. The RHC framework can be hardly combined with the Lyapunov function based control. However, certain approaches can be found in the literature where the Lyapunov stability [35] and RHC were successfully combined for specific cases [36–39].

Alternative solutions also exist which can be used instead of Lyapunov's stability theorem. The Robust Fixed Point Transformation (RFPT) based control [40, 41] uses Banach's fixed point theorem [42] to transform the control problem into a fixed point problem which can be solved iteratively. This method allows designing a robust iterative adaptive controller which can avoid the main limitations of RHC if these are combined.

In this study we present the first part of our research, namely, the design of an appropriate RHC controller on NP basis which can be completed by RFPT in our further work.

The paper is structured as follows. First, the applied diabetes model is introduced. After that, the RHC design based on the NP approach is presented. Then, the results are introduced with their discussion. Finally, we conclude our work and provide an outline regarding our further research.

2. Type 1 Diabetes Mellitus Model

During our research we have applied a modified Minimal Model [43] which originates from the model of Bergman [46]. This model has several beneficial properties, such as simplicity, good transformability, and flexibility and it is based on simpler biological considerations. The main goal of the model is to describe the glucose-insulin dynamics, namely, to define the connection between the blood glucose and insulin levels. However, in order to characterize the daily life of a T1DM patient this model has to be extended with additional submodels. These submodels are the absorption of the external glucose and insulin intakes. During the daily routine these substances are not directly injected to the blood

stream—however, this can occur in case of persistent hospitalization. Instead, the carbohydrate is consumed via food intake and the insulin is entered through the extracellular tissue matrix under the skin [13]. Thus, their appearance does not contain sharp peaks: it happens through longer dynamics.

The glucose and insulin absorption are described by (1)–(4), respectively. These submodels originate from the Cambridge model [44], but we applied them in appropriate dimensions to insert them into the core model. The core model is described by (5)–(7).

$$\dot{D}_1(t) = -\frac{1}{\tau_D} D_1(t) + \frac{1000 A_g}{M_{wG} V_G} C \cdot d(t), \tag{1}$$

$$\dot{D}_2(t) = -\frac{1}{\tau_D} D_2(t) + \frac{1}{\tau_D} D_1(t), \tag{2}$$

$$\dot{S}_1(t) = -\frac{1}{\tau_S} S_1(t) + \frac{1}{V_I} u(t), \tag{3}$$

$$\dot{S}_2(t) = -\frac{1}{\tau_S} S_2(t) + \frac{1}{\tau_S} S_1(t), \tag{4}$$

$$\dot{G}(t) = -\left(p_1 + X(t)\right) G(t) + p_1 G_B + \frac{1}{\tau_D} D_2(t), \tag{5}$$

$$\dot{X}(t) = -p_2 X(t) + p_3 \left(I(t) - I_B\right), \tag{6}$$

$$\dot{I}(t) = -n\left(I(t) - I_B\right) + \frac{1}{\tau_S} S_2(t). \tag{7}$$

The state variables in (1)–(7) have the meaning and purpose as follows. $D_1(t)$ mg/dL and $D_2(t)$ mg/dL are the primary and secondary compartments belonging to glucose, where the time constant τ_D determines how long it takes for the meal to be absorbed after consumption in time. $S_1(t)$ mU/L and $S_2(t)$ mU/L are the primary and secondary compartments belonging to insulin, where the time constant τ_S determines how long it takes the insulin to be absorbed after injection (to the extracellular space) in time. Variable $G(t)$ mg/dL is the blood glucose (BG) concentration—the so-called glycemia—and $I(t)$ mU/L is the blood insulin concentration and $X(t)$ 1/min is the insulin-excitable tissue glucose uptake activity—which describes the connection between the blood's glucose and insulin levels, respectively.

From system engineering point of view the external glucose, namely, the food intake, can be handled as disturbance. In this case $d(t)$ g/min is the disturbance input. It can be inserted to $D_1(t)$ via $((1000A_g)/(M_{wG}V_G))C$ complex which describes the bioavailability of the glucose from complex carbohydrates. The control signal $u(t)$ mU/min—the injected insulin—is directly connected to $S_1(t)$. More detailed description of the used model parameters can be found in Table 1 and in [43–45].

3. A Nonlinear Programming Approach with regard to the Receding Horizon Controller

3.1. Nonlinear Programming in General. The numerical approximation of a given problem can be considered in the following way:

(I) Determination of a discrete time grid which is dense enough from the given application point of view as $\{t_0, t_1 = t_0 + \Delta t, \ldots, t_{n+1} = t_n + \Delta t, \ldots, t_F\}$, where $F \in \mathbb{N}$. Here t_0 belongs to the initial and t_F belongs to the final time instant of the motion to be taken into account, respectively.

(II) Assume that the nonlinear equation of the system to be controller is $\dot{\mathbf{x}}(t) = f(\mathbf{x}(t), \mathbf{u}(t))$, where $\mathbf{x}(t) \in \mathbb{R}^M$ is the state and $\mathbf{u}(t) \in \mathbb{R}^K$ is the input vector, respectively. Furthermore, the $\mathbf{x}_0 \equiv \mathbf{x}(t_0)$ initial condition of the system is given.

(III) Consider that $\mathbf{x}^N(t_i)$ is the nominal trajectory to be tracked by the states of the system over time. Here $\mathbf{x}^N(t_i) \equiv \mathbf{x}_i^N$ in the given time grid determined by (I).

(IV) The nominal prescribed trajectory cannot be exactly realized during the execution of the control task. However, several restrictions—in order to enforce the realization of this trajectory—can be prescribed by using a predefined $J(\mathbf{x}(t), \mathbf{u}(t))$ cost function in each point of the grid.

(V) $J(\mathbf{x}(t), \mathbf{u}(t)) \geq 0$ is able to express several requirements, although these are often contradictory. It can be constructed as the sum of nonnegative terms which can be the differentiable functions of the control signal and the state variables—expediently. The drastic control signals can be avoided as well by prohibiting them via the cost function.

(VI) Terminal conditions can be embedded into the prescription depending only on $\mathbf{x}_F$ in the last step t_F.

(VII) During an optimal control approach, $\sum_{i=0}^{F-1} J(\mathbf{x}_i, \mathbf{u}_i) + \Phi(\mathbf{x}_F)$ has to be minimized, where $\Phi(\mathbf{x}_F)$ is an extra weight that belongs to the last point of the trajectory.

(VIII) The cost function $\sum_{i=0}^{F-1} J(\mathbf{x}_i, \mathbf{u}_i) + \Phi(\mathbf{x}_F)$ cannot be arbitrarily minimized due to the specificities of the system to be controlled. In the minimization the state propagation equation must be considered as a constraint. In order to process this constraint the Lagrangian multipliers can be used as follows.

(IX) $\dot{\mathbf{x}}(t)$ can be expressed from the state propagation equation and as a numerical approximation $(\mathbf{x}_{i+1} - \mathbf{x}_i)/\Delta t \approx f(\mathbf{x}_i, \mathbf{u}_i)$. By using this estimation, the control task can be expressed in the following way:

$$\min_{\substack{\{\mathbf{x}_1, \ldots, \mathbf{x}_F\} \\ \{\mathbf{u}_0, \ldots, \mathbf{u}_{F-1}\}}} \sum_{i=0}^{F-1} J\left(\mathbf{x}_i, \mathbf{u}_i\right) + \Phi\left(\mathbf{x}_F\right) \quad \text{subject to} \quad \frac{\mathbf{x}_{i+1} - \mathbf{x}_i}{\Delta t} - f\left(\mathbf{x}_i, \mathbf{u}_i\right) = \mathbf{0}, \tag{8}$$

and $\{\lambda_0, \ldots, \lambda_{F-1}\}$ are the Lagrangian multipliers—which are used in accordance with the optimization task to be solved by the reduced gradients method.

3.2. The Applied Cost Function. During the development of the appropriate cost function—which fits to the given

Table 1: The applied parameters of the models in this study [43–45].

Notation	Value	Unit	Description
G_B	110	mg/dL	Basal glucose level
I_B	1.5	mU/L	Basal insulin level
p_1	0.028	1/min	Transfer rate
p_2	0.025	1/min	Transfer rate
p_3	0.00013	L/(mU min)	Transfer rate
n	0.23	1/min	Time constant for insulin disappearance
BW	75	kg	Body weight
V_I	0.12 BW	L	Distribution volume of insulin
V_G	0.16 BW	L	Distribution volume of glucose
M_{wG}	180.1558	g/mol	Molecular weight of glucose
A_g	0.8	-	Glucose utilization
C	18.018	mmol/L	Conversion rate between mmol/L and mg/dL
τ_D	40	min	Carbohydrate (CHO) to glucose absorption constant
τ_S	55	min	Insulin absorption constant

problem—the specificities of model (1)–(7) should be taken into account.

The main limitation coming from the model is the amount of injectable insulin and the fact that we have only one control signal. The control signals at the grid points of the horizon are independent variables in the optimization problem. However, the application of a specific form of limitation on them—a "bias"—is reasonable. Thus, the control signal in this construction should be limited in accordance with the phenomenon to be controlled. Instead of the control signal itself, another variable should be selected as independent variable to avoid the initial value problems causing the rough numerical approximation at the beginning of the optimization. This is caused by the high nonlinearity in the model.

Another property of the model is that only the blood glucose level $G(t)$ can be measured. Thus, only this state variable can be embedded into the cost function to be developed. We do not have internal information about other state variables of the process to be controlled.

Accordingly we have applied a more specific form of the (8) cost function:

$$\min_{\substack{\{G_1,\ldots,G_F\}\\ \{v_0,\ldots,v_{F-1}\}}} \sum_{i=0}^{F-1} J\left(G_i, u_i\right) + \Phi\left(G_F\right) \quad \text{subject to} \quad \frac{\mathbf{x}_{i+1} - \mathbf{x}_i}{\Delta t} - f\left(\mathbf{x}_i, \mathbf{u}_i\right) = \mathbf{0}, \tag{9}$$

where $u_i = u_{\text{bias}} + \tanh(v_i)$.

We have developed a strongly nonlinear cost function in which all requirements can be embedded against the control action to be reached during control.

$$J(G,u) \stackrel{\text{def}}{=} \left|\frac{G^N - G}{A_1}\right|^{\alpha_1} + B\left|\frac{u}{A_2}\right|^{\alpha_2}, \tag{10}$$

$$\Phi\left(G_F\right) \stackrel{\text{def}}{=} \left|\frac{G^N_{\text{final}} - G_{\text{final}}}{A_3}\right|^{\alpha_3}. \tag{11}$$

The tracking error in (10) and (11), namely, the deviation of the realized blood glucose level $G(t)$ from the nominal blood glucose level $G^N(t)$, can be calculated as $G_i^N - G_i$ at the grid points. The absolute value of this difference can be determined by parameters A_1 and A_3 that contribute the belonging level of "penalty" prevailing in the cost function. In that case if $\alpha_1 > 1$ and $\alpha_3 > 1$ beside $|G^N - G| < A_1$ and $|G^N_{\text{final}} - G_{\text{final}}| < A_3$, the contribution to the cost function is low. However, if $|G^N - G| > A_1$ and $|G^N_{\text{final}} - G_{\text{final}}| > A_3$ then due to the power terms the contributions to the cost of these terms are drastically increasing. The α_1 and α_3 weighting terms can be used for different purposes. $\alpha_1 = \alpha_3 = 1$ provides proportional contribution; namely, the pure deviation will be better prohibited. However, if $\alpha_1, \alpha_3 < 1$, then the smaller deviations will be prohibited relatively better than the bigger ones. The role of A_2 and α_2 parameters are similar; namely, the applied control input can be prohibited by applying them. The B parameter allows modifying the enforcement of the effect of the control signal in the cost function.

3.3. Applied Nonlinear Programming Solver. In order to implement the reduced gradients based optimization as Nonlinear Programming task various software products can be used. Due to its complex embedded nonlinear solvers and the easy-to-use property we have selected the Microsoft's EXCEL (MS EXCEL). The MS EXCEL's "Solver" module is produced by an external firm Frontline Systems, Inc. There are various solutions implemented into the Solver module, including the Generalized Reduced Gradient (GRG) method which can be used in the given case as well. The GRG is based on [47, 48] and its usability has been proved in various fields of research. For example, it was successfully applied for macroeconomic optimization problems [49], operational research problems related to economics [50], optimization problems regarding transportation [31], decision prediction models [51], optimal control problems in continuous time domain [52], and so on.

Table 2: The parameters of the applied cost function (10).

	Scenario 1	Scenario 2
A_1	5 mg/dL	1 mg/dL
α_1	4	4
A_2	2 mU/min	15 mU/min
α_2	4	6
A_3	5 mg/dL	5 mg/dL
α_3	4	4
u_{bias}	10 mU/min	50 mU/min
G^N	90 mg/dL	90 mg/dL

The optimization framework was built up by using the "Visual Basic" packages of the software "MS EXCEL 2016" under "Windows 10" operating system. The functional dependencies have been constructed in Visual Basic, and the grid points, parameters, and so forth have been defined on dedicated Worksheets—by using these data the Solver can be easily set up.

4. Results

In order to test the realized control framework we investigated two scenarios. In the first scenario 25 g CHO was considered—5 g over 5 minutes in each 240th time instant from the 60th one.

In the second scenario we considered 50 g CHO intake 10 g over 5 minutes in each 240th time instant from the 60th time instant. In both cases 200 time horizons have been considered within 10 grid points; thus the total simulated time domain was 2000 minutes. The resolution Δt was 1 minute in accordance with the properties of the model.

The applied cost-function parameters (which represent the control parameters in this regard) can be found in Table 2.

It should be noted that we have used permanent reference trajectories in both cases denoted by $G^N = 90$ mg/dL in (9)–(11).

Therefore, in accordance with the aforementioned details, the goal of the control becomes to keep $G^N = 90$ beside respecting the predefined u_{bias}. In this manner—via the cost function—the deviations from these predefined values have been "punished"; namely, the value of the cost function became higher.

During the examinations we have considered the following range of blood glucose as "healthy" in accordance with [11]: from 70 to 180 mg/dL.

4.1. Results of Scenario 1. In the following the results of Scenario 1 are presented. First, the disturbance signal is shown by Figure 1. The applied—calculated—control signal can be seen in Figure 2. It is clear that the controller is able to administer the insulin in accordance with (9)–(11) where $u_i = u_{\text{bias}} + \tanh(v_i)$ is prevailed in the control action.

Figures 3 and 4 show the absorption of glucose and its appearance in the blood with the dynamics determined by the model. Figures 5 and 6 show the absorption of insulin from the interstitium and its appearance in blood.

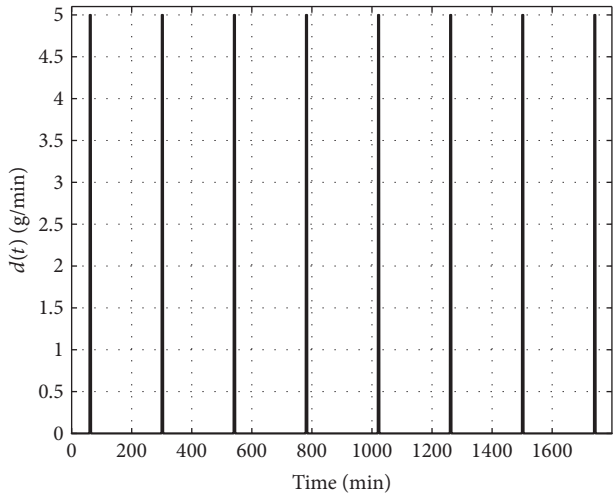

Figure 1: Applied disturbance (CHO intake)—5 g over 5 minutes at each 240th time instant.

The main point can be seen on Figure 7. The controller is able to satisfy the determined conditions and the BG level ($G(t)$) is inside the predefined range—no hypo- and hyperglycemia occurred. The BG level approaches the selected reference trajectory (G^N) as it is expected.

On Figures 8 and 9 the variation of blood insulin level and the intermediate state variable can be seen. $X(t)$ determines how the blood insulin level affects the blood glucose level, namely, the connection between them.

4.2. Results of Scenario 2. The applied disturbance input in accordance with the detailed protocol can be seen in Figure 10. In this case, we have applied higher inputs in order to be sure that the developed control framework is able to deal with unfavorable external excitation.

Figure 11 reveals the calculated and administered control signal. As it can be seen, its dynamics are significantly different from that of the previous case due to the different settings in the applied cost function.

Figures 12 and 13 represent the absorption of the glucose and its appearance in the blood with the dynamics determined by the model. Figures 14 and 15 show the absorption of insulin from the interstitium to the blood.

The main result can be seen in Figure 16. Though we have drastically increased the disturbance input signal the controller was able to deal with the situation and realized appropriate control action—without domain violation from the determined u_{bias} point of view. The blood glucose level is inside the selected healthy range without any hypo- or hyperglycemia. Moreover, the BG level oscillated around the reference trajectory—G^N—as it was expected.

Figures 17 and 18 represent the variation of the blood insulin level and the intermediate state $X(t)$. Due to the higher frequency of the control signal these are oscillating with a higher frequency as well—which is directly reflected in the blood glucose level as well, since the $X(t)$ mediates the insulin's effect on $G(t)$.

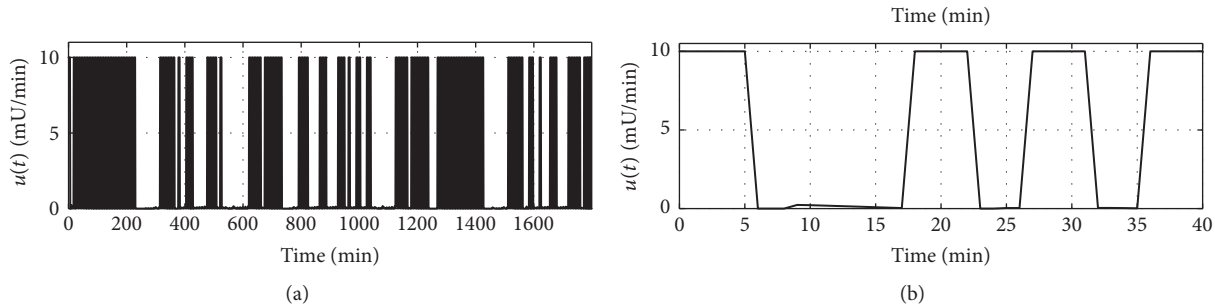

Figure 2: Calculated control signals. (a) represents the whole time horizon. (b) shows a piece of the whole time horizon between 0 and 40 minutes.

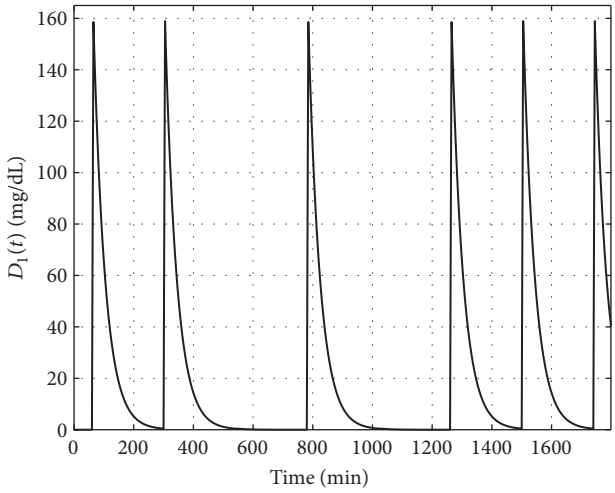

Figure 3: Variation of the first state of the glucose absorption subsystem.

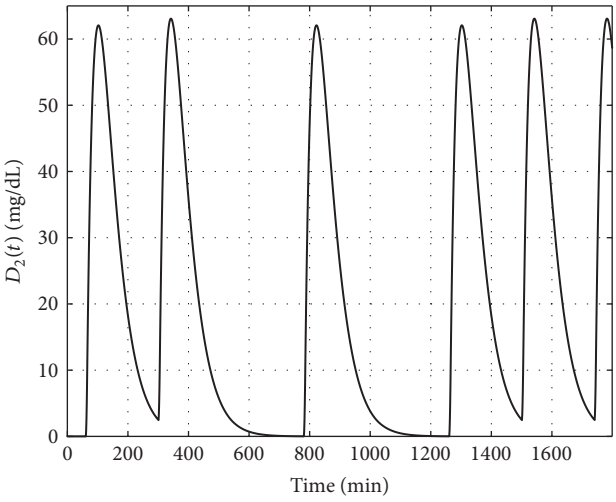

Figure 4: Variation of the second state of the glucose absorption subsystem.

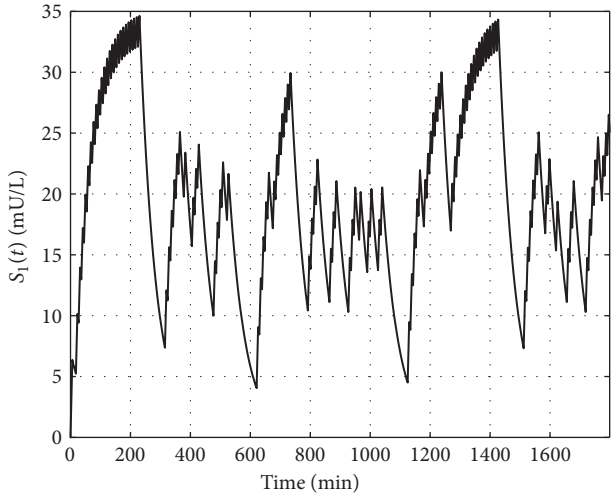

Figure 5: Variation of the first state of the insulin absorption subsystem.

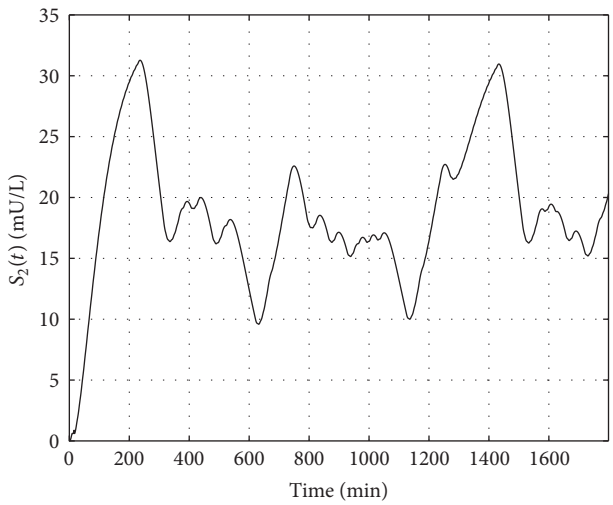

Figure 6: Variation of the second state of the insulin absorption subsystem.

5. Discussion

In this research our main goal was to design a RHC which is able to control the given patient model and, further, to do that by developing such a RHC controller which can be effectively combined with the RFPT principles in our later work by using the detailed NP environment. These goals have been reached.

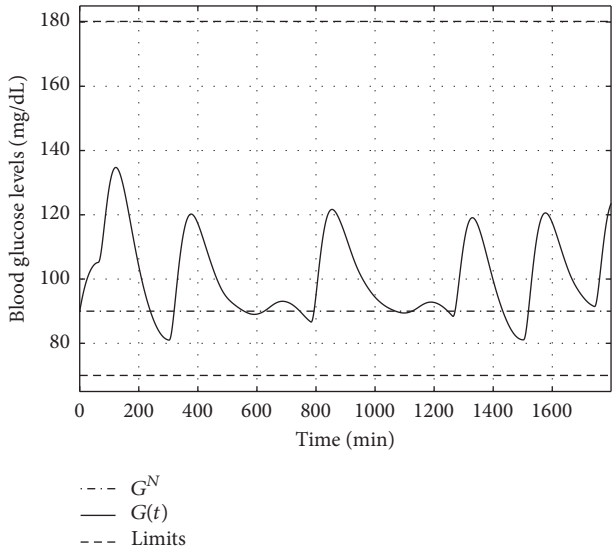

Figure 7: Variation of the blood glucose level over time.

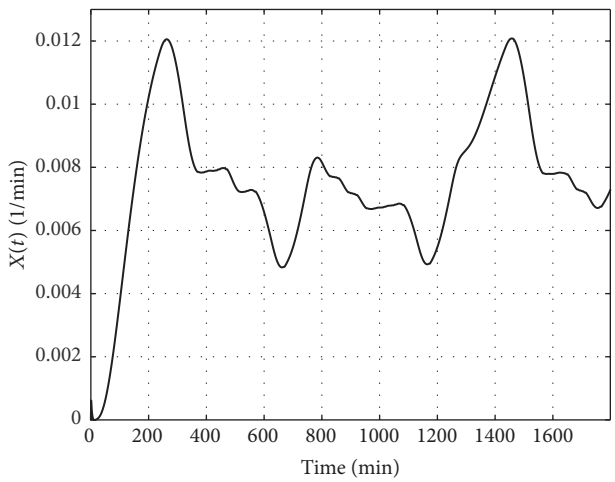

Figure 8: Variation of the insulin-excitable tissue glucose uptake activity over time.

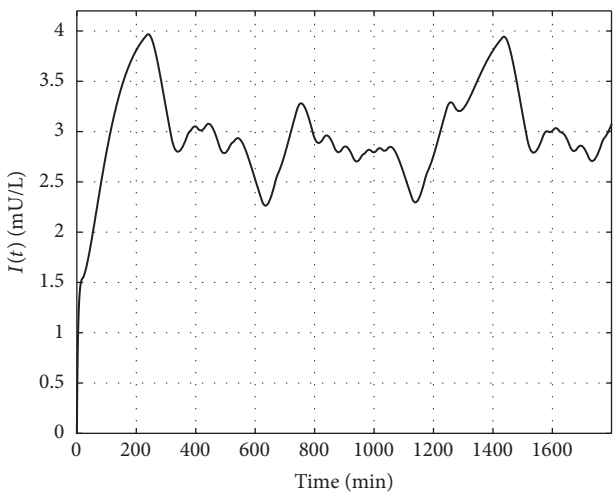

Figure 9: Variation of the blood insulin level over time.

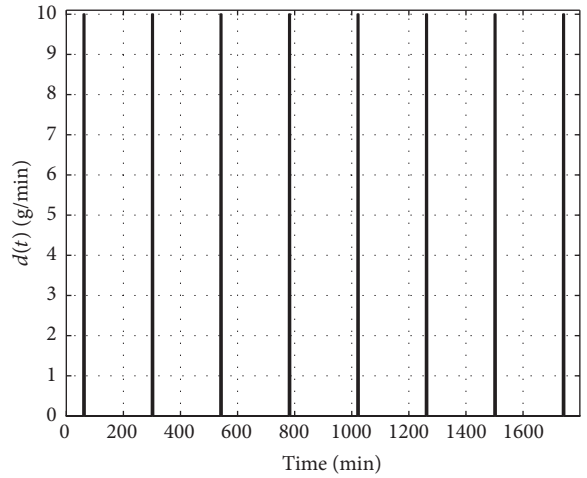

Figure 10: Applied disturbance (CHO intake)—10 g over 5 minutes at each 240th time instant.

In our first scenario we aimed to test the control environment under strict constraints—the collection of them can be found in Table 2. In detail, $A_1, A_3 = 5$ mg/dL and $\alpha_1, \alpha_3 = 4$ mean that we punished the deviation of $G(t)$ from G^N heavily above 5 mg/dL during the control action and in the terminal points of the cycles. We applied not just a restriction on the value of $u(t)$ via u_{bias}, but also we penalized the control signals above 2 mU/min as it is reflected in A_2 and α_2.

In the second scenario we investigated the "robustness" of the controller by using highly oscillating, unfavorable disturbance input in a cyclic way. As in the previous case, the controller was able to perform well—beside all of the restrictions that have been considered.

The main results can be seen in Figures 7 and 16. It is clearly visible that the main requirement has been satisfied, since the BG level was kept by the controller in the healthy range.

6. Conclusions and Future Work

In this paper we have proposed a possible design scheme for RHC controller by using a NP approach in order to control Type 1 Diabetes Mellitus. We have applied the MS EXCEL's embedded Solver solution which is based on the Generalized Reduced Gradient method in order to realize the control environment. Two different scenarios have been applied to test our approach—the results have been satisfactory.

In the first scenario we applied "soft" disturbance and smaller penalties via the developed cost function in order to make sure that the controller design is possible and appropriate control action can be achieved by using the continuous optimization. In the second test scenario we used unfavorable, cycling disturbance signal with high amplitude to test the "robustness" of the proposed controller. The developed RHC controller was able to handle the load and provided satisfactory control action. Furthermore, in both cases the BG level was kept in the predefined healthy range.

In our future work we are going to extend the developed RHC controller with an additional RFPT framework in order

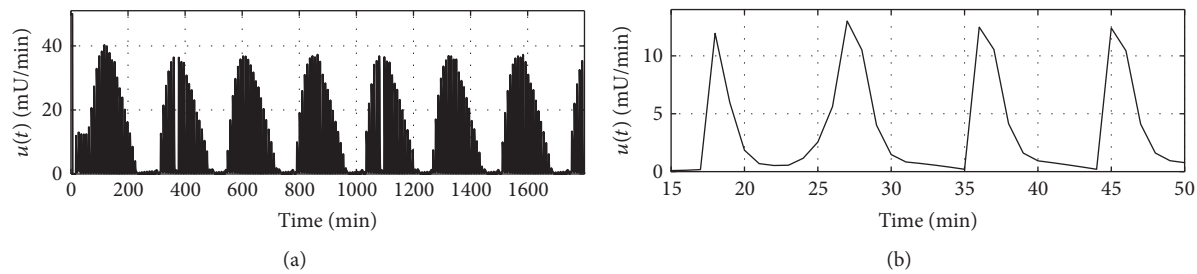

Figure 11: Calculated control signals. (a) represents the whole time horizon. (b) shows a piece of the whole time horizon between 0 and 40 minutes.

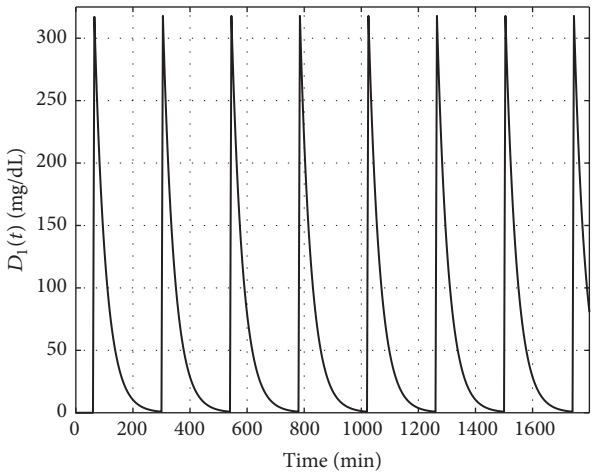

Figure 12: Variation of the first state of the glucose absorption subsystem.

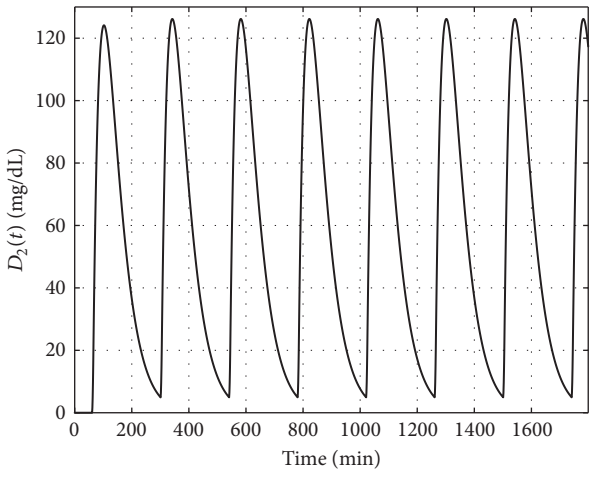

Figure 13: Variation of the second state of the glucose absorption subsystem.

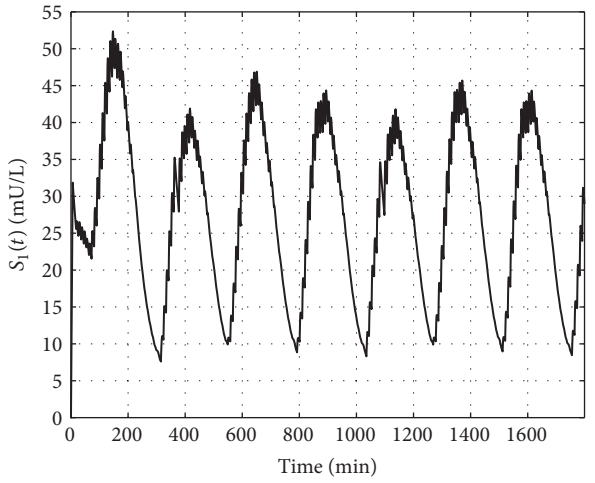

Figure 14: Variation of the first state of the insulin absorption subsystem.

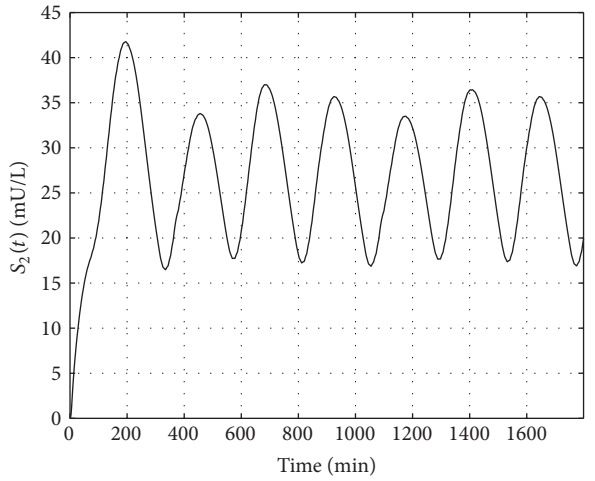

Figure 15: Variation of the second state of the insulin absorption subsystem.

to empower it with adaptive property. We will investigate the solution from robustness, adaptivity, and other aspects' points of view.

Conflicts of Interest

The authors declare that there are no conflicts of interest regarding the publication of this paper.

Acknowledgments

Gy. Eigner was supported by the ÚNKP-17-4/I New National Excellence Program of the Ministry of Human Capacities. The authors would like to acknowledge the support of the

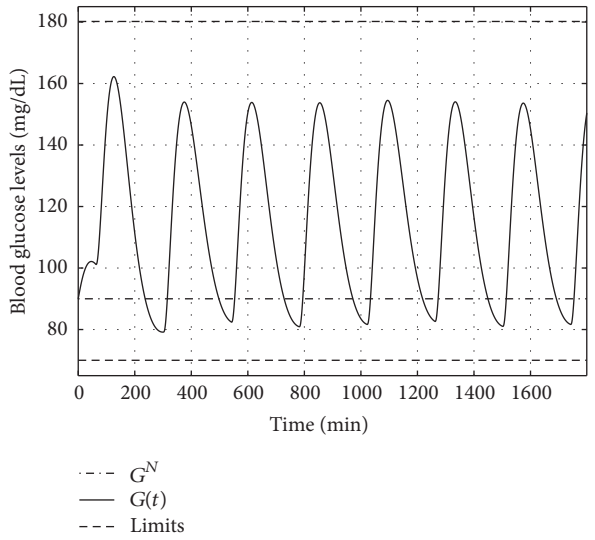

Figure 16: Variation of the blood glucose level over time.

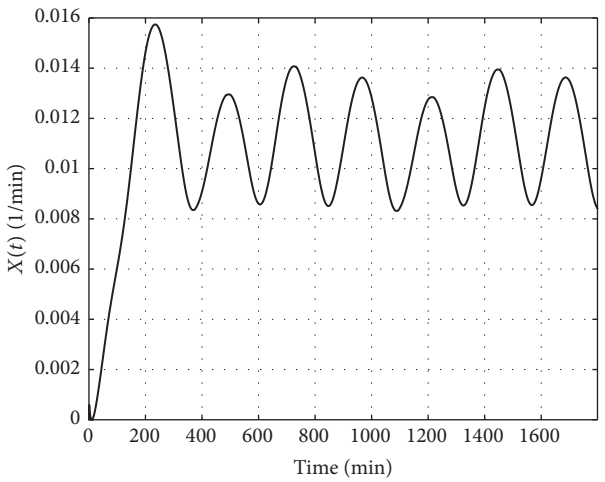

Figure 17: Variation of the insulin-excitable tissue glucose uptake activity over time.

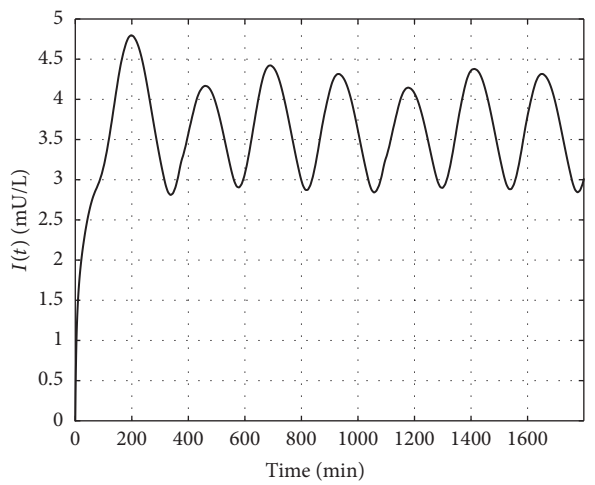

Figure 18: Variation of the blood insulin level over time.

Robotics Special College and the Research, Innovation and Service Center of Óbuda University.

References

[1] J. Bronzino and D. Peterson, *The Biomedical Engineering Handbook*, CRC Press, Boca Raton, FL, USA, 4th edition, 2015.

[2] F. Padula, C. Ionescu, N. Latronico, M. Paltenghi, A. Visioli, and G. Vivacqua, "A gain-scheduled PID controller for propofol dosing in anesthesia," *IFAC-PapersOnLine*, vol. 28, no. 20, pp. 545–550, 2015.

[3] I. Naşcu, A. Krieger, C. M. Ionescu, and E. N. Pistikopoulos, "Advanced model-based control studies for the induction and maintenance of intravenous anaesthesia," *IEEE Transactions on Biomedical Engineering*, vol. 62, no. 3, pp. 832–841, 2015.

[4] J. Sápi, D. A. Drexler, and L. Kovács, "Potential benefits of discrete-time controller-based treatments over protocol-based cancer therapies," *Acta Polytechnica Hungarica*, vol. 14, no. 1, pp. 11–23, 2017.

[5] J. Sápi, L. Kovács, D. A. Drexler, P. Kocsis, D. Gajári, and Z. Sápi, "Tumor volume estimation and quasi- continuous administration for most effective bevacizumab therapy," *PLoS ONE*, vol. 10, no. 11, Article ID e0142190, pp. 1–20, 2015.

[6] R. Zurakowski and A. R. Teel, "A model predictive control based scheduling method for HIV therapy," *Journal of Theoretical Biology*, vol. 238, no. 2, pp. 368–382, 2006.

[7] P. Colmegna, R. S. Sánchez-Peña, and R. Gondhalekar, "Linear parameter-varying model to design control laws for an artificial pancreas," *Biomedical Signal Processing and Control*, vol. 40, pp. 204–213, 2018.

[8] G. Eigner, J. K. Tar, I. Rudas, and L. Kovács, "LPV-based quality interpretations on modeling and control of diabetes," *Acta Polytechnica Hungarica*, vol. 13, no. 1, pp. 171–190, 2016.

[9] L. Kovács, "Linear parameter varying (LPV) based robust control of type-I diabetes driven for real patient data," *Knowledge-Based Systems*, vol. 122, pp. 199–213, 2017.

[10] A. Haidar, "The artificial pancreas: how closed-loop control is revolutionizing diabetes," *IEEE Control Systems Magazine*, vol. 36, no. 5, pp. 28–47, 2016.

[11] A. Fonyó and E. Ligeti, *Physiology (in Hungarian)*, Medicina, Budapest, Hungary, 3rd edition, 2008.

[12] V. Adam, *Medical Biochemistry (in Hungarian)*, Medicina Press, Budapest, Hungary, 4th edition, 2006.

[13] World Health Organization, *Global Report on Diabetes*, WHO Press, Geneva, Switzerland, 2016.

[14] American Diabetes Association, "Diagnosis and classification of diabetes mellitus," *Diabetes Care*, vol. 37, supplement 1, pp. S81–S90, 2014.

[15] World Hearth Organization, *Definition and Diagnosis of Diabetes Mellitus and Intermediate Hyperglycemia: Report of A WHO/IDF Consultation*, World Hearth Organization, 2006.

[16] T. Ferenci, A. Körner, and L. Kovács, "The interrelationship of HbA1c and real-time continuous glucose monitoring in children with type 1 diabetes," *Diabetes Research and Clinical Practice*, vol. 108, no. 1, pp. 38–44, 2015.

[17] T. Ferenci, J. Sápi, and L. Kovács, "Modelling tumor growth under angiogenesis inhibition with mixed-effects models," *Acta Polytechnica Hungarica*, vol. 14, no. 1, pp. 221–234, 2017.

[18] C. Cobelli, E. Renard, and B. Kovatchev, "Artificial pancreas: Past, present, future," *Diabetes*, vol. 60, no. 11, pp. 2672–2682, 2011.

[19] R. Nimri, N. Murray, A. Ochs, J. E. Pinsker, and E. Dassau, "Closing the Loop," *Diabetes Technology & Therapeutics*, vol. 19, no. S1, pp. S-27–S-41, 2017.

[20] J. B. Lee, E. Dassau, D. E. Seborg, and F. J. Doyle, "Model-based personalization scheme of an artificial pancreas for Type 1 diabetes applications," in *Proceedings of the 2013 American Control Conference (ACC)*, pp. 2911–2916, Washington, DC, USA, June 2013.

[21] F. Doyle, E. Dassau, D. Seborg, and J. Lee, "Model-based personalization scheme of an artificial pancreas for type I diabetes applications," 2015, uS Patent App. 14/792,524, https://www.google.com/patents/US20150306314.

[22] J. E. Pinsker, J. B. Lee, and E. Dassau, "Randomized crossover comparison of personalized mpc and pid control algorithms for the artificial pancreas," *Diabetes Care*, vol. 39, pp. 1135–1142, 2016.

[23] M. Jouini, S. Dhahri, and A. Sellami, "Design of robust super-twisting algorithm based second-order sliding mode controller for nonlinear systems with both matched and unmatched uncertainty," *Complexity*, vol. 2017, Article ID 1972921, 8 pages, 2017.

[24] J. Kuti, P. Galambos, and P. Baranyi, "Minimal volume simplex (MVS) polytopic model generation and manipulation methodology for TP model transformation," *Asian Journal of Control*, vol. 19, no. 1, pp. 289–301, 2017.

[25] L. Kovacs and G. Eigner, "Convex polytopic modeling of diabetes mellitus: A Tensor Product based approach," in *Proceedings of the 2016 IEEE International Conference on Systems, Man, and Cybernetics, SMC 2016*, pp. 3393–3398, Hungary, October 2016.

[26] L. Kovács, C. Maszlag, M. Mezei, and G. Eigner, "Robust nonlinear model predictive control of diabetes mellitus," in *Proceedings of the 15th IEEE International Symposium on Applied Machine Intelligence and Informatics, SAMI 2017*, pp. 55–60, Slovakia, January 2017.

[27] V. N. Shah, A. Shoskes, B. Tawfik, and S. K. Garg, "Closed-loop system in the management of diabetes: past, present, and future," *Diabetes Technology & Therapeutics*, vol. 16, no. 8, pp. 477–490, 2014.

[28] D. Boiroux, A. K. Duun-Henriksen, S. Schmidt et al., "Adaptive control in an artificial pancreas for people with type 1 diabetes," *Control Engineering Practice*, vol. 58, pp. 332–342, 2017.

[29] N. Moldoványi, *Model Predictive Control of Crystallisers [PhD Thesis]*, Department of Process Engineering, University of Pannonia, Veszprém, Hungary, 2012.

[30] D. Q. Mayne, J. B. Rawlings, C. V. Rao, and P. O. M. Scokaert, "Constrained model predictive control: Stability and optimality," *Automatica*, vol. 36, no. 6, pp. 789–814, 2000.

[31] N. Muthukumar, S. Srinivasan, K. Ramkumar, K. Kannan, and V. E. Balas, "Adaptive model predictive controller for web transport systems," *Acta Polytechnica Hungarica*, vol. 13, no. 3, pp. 181–194, 2016.

[32] M. Messori, G. Paolo Incremona, C. Cobelli, and L. Magni, "Individualized model predictive control for the artificial pancreas: In silico evaluation of closed-loop glucose control," *IEEE Control Systems Magazine*, vol. 38, no. 1, pp. 86–104, 2018.

[33] L. Grüne and J. Pannek, *Nonlinear Model Predictive Control*, Springer, London, UK, 2011.

[34] J. Richalet, A. Rault, J. L. Testud, and J. Papon, "Model predictive heuristic control: applications to industrial processes," *Automatica*, vol. 14, no. 5, pp. 413–428, 1978.

[35] P. Li, X. Li, and J. Cao, "Input-to-state stability of nonlinear switched systems via lyapunov method involving indefinite derivative," *Complexity*, vol. 2018, Article ID 8701219, 8 pages, 2018.

[36] A. Jadbabaie, J. Yu, and J. Hauser, "Receding horizon control of the Caltech ducted fan: A Control Lyapunov Function approach," in *Proceedings of the 1999 IEEE International Conference on Control Applications (CCA) and IEEE International Symposium on Computer Aided Control System Design (CACSD)*, pp. 51–56, August 1999.

[37] A. Jadbabaie, J. Yu, and J. Hauser, "Stabilizing receding horizon control of nonlinear systems: A control Lyapunov function approach," in *Proceedings of the 1999 American Control Conference (99ACC)*, pp. 1535–1539, June 1999.

[38] H. Khan, J. K. Tar, I. J. Rudas, and G. Eigner, "Adaptive model predictive control based on fixed point iteration," *WSEAS Transactions on Systems and Control*, vol. 12, pp. 347–354, 2017.

[39] H. Khan, A. Szeghegyi, and J. K. Tar, "Fixed point transformation-based adaptive optimal control using NLP," in *Proceedings of the 2017 IEEE 15th International Symposium on Intelligent Systems and Informatics (SISY)*, pp. 000237–000242, September 2017.

[40] J. K. Tar, J. F. Bitó, L. Nádai, and J. A. Tenreiro Machado, "Robust fixed point transformations in adaptive control using local basin of attraction," *Acta Polytechnica Hungarica*, vol. 6, no. 1, pp. 21–38, 2009.

[41] J. Tar, L. Nádai, and I. Rudas, *System and Control Theory with Especial Emphasis on Nonlinear Systems*, Budapest, Hungary, Typotex, 1st edition, 2012.

[42] S. Banach, "Sur les opérations dans les ensembles abstraits et leur application aux équations intégrales (About the Operations in the Abstract Sets and Their Application to Integral Equations)," *Fundamenta Mathematicae*, vol. 3, pp. 133–181, 1922.

[43] F. Chee and T. Fernando, *Closed-Loop Control of Blood Glucose*, Springer, 2007.

[44] R. Hovorka, V. Canonico, L. J. Chassin et al., "Nonlinear model predictive control of glucose concentration in subjects with type 1 diabetes," *Physiological Measurement*, vol. 25, no. 4, pp. 905–920, 2004.

[45] M. Naerum, "Model predictive control for insulin administration in people with type 1 diabetes," Tech. Rep., Technical University of Denmark, 2010.

[46] R. N. Bergman, Y. Z. Ider, C. R. Bowden, and C. Cobelli, "Quantitative estimation of insulin sensitivity.," *American Journal of Physiology-Endocrinology and Metabolism*, vol. 236, no. 6, p. E667, 1979.

[47] L. S. Lasdon, A. D. Waren, A. Jain, and M. Ratner, "Design and Testing of a Generalized Reduced Gradient Code for Nonlinear Programming," *ACM Transactions on Mathematical Software*, vol. 4, no. 1, pp. 34–50, 1978.

[48] D. Fylstra, L. Lasdon, J. Watson, and A. Waren, "Design and use of the Microsoft Excel Solver," *Interfaces*, vol. 28, no. 5, pp. 29–55, 1998.

[49] J. Houston, "Economic optimisation using Excels Solver: A macroeconomic application and some comments regarding its limitations," *Computers in Higher Education Economics Review*, vol. 11, no. 1, p. 2, 1997.

[50] A. Ionescu, "Microsoft Office Excel 2010 operational research in Excel 2010," *International Journal of Computer and Information Technology*, vol. 2, no. 5, pp. 1026–1064, 2013.

[51] J. Silva and A. Xabadia, "Teaching the two-period consumer choice model with EXCEL-SOLVER," *Australasian Journal of Economics Education*, vol. 10, no. 2, pp. 24–38, 2013.

[52] E. Nævdal, "Solving continuous-time optimal-control problems with a spreadsheet," *Journal of Economic Education (JEE)*, vol. 34, no. 2, pp. 99–122, 2003.

Hindawi
Complexity
Volume 2018, Article ID 4073531, 12 pages
https://doi.org/10.1155/2018/4073531

Research Article

Affine Tensor Product Model Transformation

József Kuti and Péter Galambos

Antal Bejczy Center for Intelligent Robotics, Óbuda University, Bécsi út 96/b, Budapest 1034, Hungary

Correspondence should be addressed to József Kuti; jozsef.kuti@irob.uni-obuda.hu

Received 26 October 2017; Accepted 27 December 2017; Published 20 March 2018

Academic Editor: Eulalia Martínez

This paper introduces the novel concept of Affine Tensor Product (TP) Model and the corresponding model transformation algorithm. Affine TP Model is a unique representation of Linear Parameter Varying systems with advantageous properties that makes it very effective in convex optimization-based controller synthesis. The proposed model form describes the affine geometric structure of the parameter dependencies by a nearly minimum model size and enables a systematic way of geometric complexity reduction. The proposed method is capable of exact analytical model reconstruction and also supports the sampling-based numerical approach with arbitrary discretization grid and interpolation methods. The representation conforms with the latest polytopic model generation and manipulation algorithms. Along these advances, the paper reorganizes and extends the mathematical theory of TP Model Transformation. The practical merit of the proposed concept is demonstrated through a numerical example.

1. Introduction

The importance of polytopic system descriptions is beyond doubt since the development of influential polytopic model-based analysis and synthesis methods initially introduced by Boyd et al. in [1]. These approaches offer a simple way for stability verification and robust or gain-scheduling controller design via Linear Matrix Inequality (LMI) based methods for polytopic Linear Parameter Varying (LPV) and quasi-LPV (qLPV) models.

TP Model Transformation was introduced as a numerical approach to constructing polytopic TP forms of LPV/qLPV models [2] serving as an alternative to analytical procedures such as the sector nonlinearity technique [3]. Furthermore, the separated parameter dependencies within the TP structure can be exploited during the controller design extending the polytopic model-based control analysis and synthesis methods [4, 5].

In the past decade, TP Model Transformation has been matured and became an extensive framework within polytopic model-based control [2, 3, 6]. Former related works (e.g., [7–11]) obtained the polytopic TP Model through the HOSVD-based intermediate TP form [12], although the resulting polytopic model does not really benefit from the properties of the HOSVD-based form such as complexity reduction capability and uniqueness.

A recent paper of the authors [13] established the affine geometric background of polytopic TP Model generation and proposed a direct way to determine the polytopic structures. First, it obtained the affine hulls of the subtensors of the discretized tensor and then the enclosing polytopes were established on the affine subspaces.

The paper proposes the Affine TP Model that substantially improves the polytopic TP Model generation and manipulation methodology by combining the affine geometric interpretations [13] with the benefits of higher-order SVD (HOSVD) based TP Model [2, 12, 14].

Consolidating the affine geometry-based approach, the main contribution of this paper is the introduction of a new intermediate TP Model (like the HOSVD-based form) that provides a unique description of affine geometric properties serving as direct input for polytopic model construction methods (see [13, 15–17]). Furthermore, it reserves all the benefits of the HOSVD-based form: similar uniqueness, compact representation, and capability of complexity reduction. We refer to the new intermediate form as *Affine TP Model*.

The next section discusses the abbreviations and notations used in the paper. Section 3 recalls some concepts of tensor algebra related to polytopic TP modeling; then Section 4 discusses the polytopic form of univariate functions showing its relevance to affine geometrics and introduces the affine SVD. In Section 5, affine SVD is applied to obtain the Affine TP Model. Section 6 describes the application to generate and manipulate polytopic TP Models; then Section 7 shows a simple numerical example. Finally, Section 8 concludes the paper.

2. Notations

The following abbreviations and notations are used within this paper:

(q)LPV: (quasi)Linear Parameter Varying

LMI: Linear Matrix Inequality

SVD: Singular Value Decomposition

HOSVD: higher-order singular value decomposition

TP Model: Tensor Product Model

$a, A, b, B, \ldots$: scalar values

$\mathbf{a}, \mathbf{b}, \ldots$: vectors

$\mathbf{A}, \mathbf{B}, \ldots$: matrices

H: a Hilbert space, in general

$\mathfrak{a}, \mathfrak{b}, \ldots$: elements of H, in general

$\mathbf{0}^{a\times b}$, $\mathbf{1}^{a\times b}$: $a \times b$ size matrix of zeros/ones

$\mathbf{E}^{a\times b}$: $a \times b$ size identity matrix

δ_{ij}: dirac-delta ($\delta_{ii} = 1$, $\delta_{ij} = 0$ if $i \neq j$)

$\mathfrak{A}, \mathfrak{B}, \ldots$: sets on $\mathbb{R}^a, H, \ldots$

$\mathscr{A}, \mathscr{B}, \ldots$: tensors

$\mathbf{A}_{(n)}$: n-mode unfold matrix of tensor $\mathscr{A}$

$\mathbf{A}^{(n)}$, $\mathscr{B}^{(n)}$: indexing of different matrices, tensors

$\mathscr{A} \times_n \mathbf{U}$: n-mode tensor product

$\mathscr{A} \boxtimes_{n=1}^{N} \mathbf{U}^{(n)}$: multiple tensor product as $\mathscr{A} \times_1 \mathbf{U}^{(1)} \cdots \times_N \mathbf{U}^{(N)}$

$\underline{x}$, $\overline{x}$: lower and upper bounds for the x scalar

$\mathrm{Co}(\cdots)$: convex hull (set of all convex comb.).

3. Basic Concepts

The section briefly discusses the related concepts of tensor algebra, polytopic LPV/qLPV modeling, and the goals of TP Model Transformation introducing the notations that are used in the followings.

3.1. Tensor Algebra. First, the key definitions and properties of tensor algebra of De Lathauwer et al. [18] are recalled and extended to Hilbert spaces by considering multidimensional arrays on a Hilbert space denoted by H in general.

They can be multiplied with real matrices along the nth index that is called n-mode tensor product.

Definition 1 (n-mode tensor product). The n-mode product of a tensor $\mathscr{A} \in H^{I_1\times\cdots\times I_N}$ and the matrix $\mathbf{U} \in \mathbb{R}^{L\times I_n}$, denoted by $\mathscr{A} \times_n \mathbf{U}$, is a tensor with size $I_1 \times \cdots \times I_{n-1} \times L \times I_{n+1} \times \cdots \times I_N$ that is given by

$$\left(\mathscr{A} \times_n \mathbf{U}\right)_{i_1,\ldots,i_{n-1},l,i_{n+1},\ldots,i_N} = \sum_{i_n} \mathfrak{a}_{i_1,\ldots,i_N} u_{l,i_n}. \tag{1}$$

The definition implies the following properties.

Lemma 2 (commutativity of $n \neq l$-mode tensor products). *Given the tensor $\mathscr{A} \in H^{I_1\times\cdots\times I_N}$ and the matrices $\mathbf{U} \in \mathbb{R}^{J\times I_n}$, $\mathbf{V} \in \mathbb{R}^{K\times I_l}$ ($n \neq l$), one has*

$$\left(\mathscr{A} \times_n \mathbf{U}\right) \times_l \mathbf{V} = \left(\mathscr{A} \times_l \mathbf{V}\right) \times_n \mathbf{U}. \tag{2}$$

Lemma 3 (multiple n-mode tensor products). *Given the tensor $\mathscr{A} \in H^{I_1\times\cdots\times I_N}$ and the matrices $\mathbf{U} \in \mathbb{R}^{J\times I_n}$, $\mathbf{V} \in \mathbb{R}^{M\times J}$, one has*

$$\left(\mathscr{A} \times_n \mathbf{U}\right) \times_n \mathbf{V} = \mathscr{A} \times_n (\mathbf{V}\mathbf{U}). \tag{3}$$

The inner product and norm are defined.

Definition 4 (inner product and norm of tensors). The inner product $\langle \mathscr{A}, \mathscr{B} \rangle$ of tensors $\mathscr{A}, \mathscr{B} \in H^{I_1\times\cdots\times I_N}$ is defined as

$$\langle \mathscr{A}, \mathscr{B} \rangle = \sum_{i_1} \cdots \sum_{i_N} \left\langle \mathfrak{a}_{i_1,\ldots,i_N}, \mathfrak{b}_{i_1,\ldots,i_N} \right\rangle. \tag{4}$$

Then the Frobenius norm of a tensor $\mathscr{A}$ is defined as $\|\mathscr{A}\| = \sqrt{\langle \mathscr{A}, \mathscr{A} \rangle}$.

To perform other matrix operations (e.g., SVD) along the nth index, the tensor can be unfolded to a matrix and restored back to tensor.

Definition 5 (n-mode unfold tensor). Assume an Nth-order tensor $\mathscr{A} \in H^{I_1\times\cdots\times I_N}$, where the elements can be described on an orthonormal basis with finite R elements; then its n-mode matrix unfolding is denoted by $\mathbf{A}_{(n)}$ with a size of $I_n \times (I_{n+1} \cdots I_N R\ I_1 \cdots I_{n-1})$ and it contains the rth coordinate of $\mathfrak{a}_{i_1,\ldots,i_N}$ element at the position (i_n, j_n), where

$$j_n = r + \sum_{l=1, l\neq n}^{N} (i_l - 1)\, R \prod_{m=1, m\neq n}^{l-1} I_m. \tag{5}$$

3.2. Hilbert-Space Valued Multivariate Functions. Consider the $\mathfrak{c}: X \to H$ function, where X is a hyperrectangle on the real numbers $X = [\underline{x}_1, \overline{x}_1] \times \cdots \times [\underline{x}_L, \overline{x}_L] \subset \mathbb{R}^L$ and H is a Hilbert space in general. The measure of $A \subseteq X$ set will be denoted as $V(A) = \int_A dx_1 \cdots dx_L$.

Definition 6 (inner product and norm). The inner product of $\mathfrak{b}, \mathfrak{c}: X \to H$ functions: we will use the following quantity:

$$\langle \mathfrak{b}, \mathfrak{c} \rangle = \frac{1}{V(X)} \int_{\mathbf{x} \in X} \langle \mathfrak{b}(\mathbf{x}), \mathfrak{c}(\mathbf{x}) \rangle V(d\mathbf{x}); \tag{6}$$

then their norms are as follows: $\|\mathfrak{c}\| = \sqrt{\langle \mathfrak{c}, \mathfrak{c} \rangle}$.

Along the paper, we will assume that for the considered functions this norm exists and it is finite without mentioning it.

The decomposition

$$\mathfrak{c}(\mathbf{x}) = \sum_{i=1}^{I} \mathfrak{c}_i f_i(\mathbf{x}); \tag{7}$$

will be called

(i) orthonormal, if the weighting functions are orthonormal as $\langle f_i, f_j \rangle = \delta_{ij}$ $\forall i, j = 1 \cdots I$,

(ii) homogeneous, if $f_I(\mathbf{x}) = 1$ $\forall \mathbf{x} \in \mathbf{X}$,

(iii) polytopic, if the f_i functions denote convex combinations as

$$\sum_{i=1}^{I} f_i(\mathbf{x}) = 1, \quad f_i(\mathbf{x}) \geq 0 \ \forall i \ \forall \mathbf{x} \in X. \tag{8}$$

Then, in geometric sense, the $\{\mathfrak{c}_1, \ldots, \mathfrak{c}_I\}$ vertices construct an enclosing polytope for the image of $\mathfrak{c}(\mathbf{x})$. Its elements are inside the polytope because they can be described as a convex combination of the vertices. In these cases, letter w will denote the weighting functions through the paper.

3.3. Polytopic LPV/qLPV Modeling. Consider the following form of LPV/qLPV models:

$$\begin{bmatrix} \dot{\mathbf{x}}(t) \\ \mathbf{y}(t) \\ \mathbf{z}(t) \end{bmatrix} = \begin{bmatrix} \mathbf{A}(\mathbf{p}(t)) & \mathbf{B}_u(\mathbf{p}(t)) & \mathbf{B}_w(\mathbf{p}(t)) \\ \mathbf{C}_y(\mathbf{p}(t)) & \mathbf{D}_{yu}(\mathbf{p}(t)) & \mathbf{D}_{yw}(\mathbf{p}(t)) \\ \mathbf{C}_z(\mathbf{p}(t)) & \mathbf{D}_{zu}(\mathbf{p}(t)) & \mathbf{D}_{zw}(\mathbf{p}(t)) \end{bmatrix} \begin{bmatrix} \mathbf{x}(t) \\ \mathbf{u}(t) \\ \mathbf{w}(t) \end{bmatrix}, \tag{9}$$

where

(i) $\mathbf{x}(t)$ denotes the state variables, $\mathbf{u}(t)$ the control inputs, $\mathbf{w}(t)$ the disturbances, $\mathbf{y}(t)$ the measured outputs, and $\mathbf{z}(t)$ the performance outputs,

(ii) it is defined on a hyperrectangular parameter domain:

$$\mathbf{p} \in \Omega = \left[\underline{p}_1, \overline{p}_1\right] \times \cdots \times \left[\underline{p}_N, \overline{p}_N\right] \subset \mathbb{R}^N, \tag{10}$$

(iii) for the sake of brevity, the parameter-dependent system matrices will be denoted as

$$\mathbf{S}(\mathbf{p}) = \begin{bmatrix} \mathbf{A}(\mathbf{p}) & \mathbf{B}_u(\mathbf{p}) & \mathbf{B}_w(\mathbf{p}) \\ \mathbf{C}_y(\mathbf{p}) & \mathbf{D}_{yu}(\mathbf{p}) & \mathbf{D}_{yw}(\mathbf{p}) \\ \mathbf{C}_z(\mathbf{p}) & \mathbf{D}_{zu}(\mathbf{p}) & \mathbf{D}_{zw}(\mathbf{p}) \end{bmatrix} \tag{11}$$

so we have the $\Omega \to \mathbb{S}$ function, where $\mathbb{S}$ denotes the space of real matrices with appropriate size.

That is often extended with delayed inputs, delayed states, and so on according to the dynamics of the investigated system; see [19].

Polytopic models are polytopic decomposition of the $\mathbf{S}(\mathbf{p})$ system matrix. They are described as convex combinations of so-called vertex system matrices, as

$$\mathbf{S}(\mathbf{p}) = \sum_{r=1}^{R} \mathbf{S}_r h_r(\mathbf{p}), \quad \forall \mathbf{p} \in \Omega, \tag{12}$$

and this form allows for using LMI-based control analysis and synthesis methods.

3.4. TP Model Transformation. TP Model Transformation is aimed at transforming the parameter-dependent system matrix $\mathbf{S}(\mathbf{p})$ into polytopic form with decoupled parameter dependencies, resulting in a nested parameter-wise polytopic representation that is expressed as multiple tensor products.

Definition 7 (polytopic TP Model). Polytopic TP Models are (q)LPV models with system matrices:

$$\mathbf{S}(\mathbf{p}) = \mathcal{S} \bigotimes_{n=1}^{N} \mathbf{w}^{(n)}(p_n), \tag{13}$$

in which

(i) the $\mathcal{S} \in \mathbb{S}^{J_1 \times \cdots \times J_N}$ core tensor contains the $\mathbf{S}_{j_1, \ldots, j_N}$ vertex system matrices of the polytopic model,

(ii) the $w_1^{(n)}(p_n), \ldots, w_{J_n}^{(n)}(p_n)$ n-mode weighting functions denote convex combinations $\forall p_n \in [\underline{p}_n, \overline{p}_n]$.

Let us recall its expanded form and highlight that it is polytopic for all parameter dependencies because the short TP notation can be extended as

$$\begin{aligned} \mathbf{S}(\mathbf{p}) &= \sum_{j_1=1}^{J_1} w_{j_1}^{(1)}(p_1) \sum_{j_2=1}^{J_2} \cdots \sum_{j_N=1}^{J_N} w_{j_N}^{(N)}(p_N) \mathbf{S}_{j_1, \ldots, j_N} \\ &= \sum_{j=1}^{J_n} \left(\mathcal{S}_{j_n = j} \bigotimes_{l=1, l \neq n}^{N} \mathbf{w}^{(l)}(p_l) \right) w_j^{(n)}(p_n) \end{aligned} \tag{14}$$

for all $n = 1 \cdots N$.

It is easy to see that this form is a special polytopic model. This way, the polytopic model-based control analysis and synthesis methodology can apply to them. Furthermore, the parameter separated structure can be exploited during control analysis and synthesis; for more details, see [5].

4. Affine Decomposition of Univariate Functions

The section shows the role of affine geometry in the derivation of polytopic decomposition of univariate functions, and it introduces the Affine Singular Value Decomposition to represent the geometric structure in a unique way that will be applied in the Affine TP Model.

4.1. Enclosing Polytope on the Affine Hull. Consider the univariate $\mathfrak{c} : [\underline{x}, \overline{x}] (\subset \mathbb{R}) \to H$ function, where H is a Hilbert space. Denote its image to be enclosed by the polytopic form as

$$\mathfrak{C} = \{\mathfrak{c}(x) \mid x \in [\underline{x}, \overline{x}]\} \subset H. \tag{15}$$

Although the considered Hilbert space can be higher dimensional, there may exist polytopic descriptions with a finite number of vertices. It depends on the dimension of the so-called affine hull that is the minimum dimensional affine subspace which contains every object. It can be expressed as the set of affine combinations of the values of the function

$$\mathfrak{A} = \left\{ \int_{x=\underline{x}}^{\overline{x}} \alpha(x)\, \mathfrak{c}(x)\, dx \mid \int_{x=\underline{x}}^{\overline{x}} \alpha(x)\, dx = 1 \right\} \supset \mathfrak{C}. \tag{16}$$

The dimension of the affine hull is called affine dimension and denoted by D. Then the elements of the $\mathfrak{C}$ image can be given as the sum of a value on the $(\mathfrak{a}_1, \ldots, \mathfrak{a}_D)$ basis and an $(\mathfrak{a}_{D+1})$ offset, by applying homogeneous coordinates $\mathbf{v}(x)$ as

$$\mathfrak{c}(x) = \sum_{d=1}^{D} u_d(x)\, \mathfrak{a}_d + \mathfrak{a}_{D+1} = \mathbf{v}(x) \begin{bmatrix} \mathfrak{a}_1 \\ \vdots \\ \mathfrak{a}_{D+1} \end{bmatrix}, \tag{17}$$

where $\mathbf{v}(x) = [\mathbf{u}(x)\ 1] = [u_1(x) \cdots u_D(x)\ 1]$. With this description, the objects are characterized by coordinates $\mathbf{u}(x) = [u_1(x), \ldots, u_D(x)]$ on the affine hull.

Obtaining an enclosing polytope for the $\mathbf{u}(x)$ coordinates in the D-dimensional Euclidean space with vertices $\{\mathbf{r}_1, \ldots, \mathbf{r}_J\}$ as

$$\{\mathbf{u}(x) \mid x \in [\underline{x}, \overline{x}]\} \subseteq \mathrm{Co}(\mathbf{r}_1, \ldots, \mathbf{r}_J) \subset \mathbb{R}^D, \tag{18}$$

the $\mathbf{v}(x)$ homogeneous coordinates can be expressed as convex combinations of the vertices with weights $(w_1(x), \ldots, w_J(x))$ as

$$\mathbf{v}(x) = \mathbf{w}(x)\, \mathbf{R}, \quad \text{where } \mathbf{R} = \begin{bmatrix} \mathbf{r}_1 & 1 \\ \vdots & \vdots \\ \mathbf{r}_J & 1 \end{bmatrix}, \tag{19}$$

and it provides an enclosing polytope for the $\mathfrak{C}$ image set with the following vertices:

$$\mathfrak{s}_j = \begin{bmatrix} \mathbf{r}_j & 1 \end{bmatrix} \begin{bmatrix} \mathfrak{a}_1 \\ \vdots \\ \mathfrak{a}_{D+1} \end{bmatrix} \quad (\forall j = 1 \cdots J), \tag{20}$$

because it can be described as their convex combinations:

$$\begin{aligned} \mathfrak{c}(x) &= \mathbf{v}(x) \begin{bmatrix} \mathfrak{a}_1 \\ \vdots \\ \mathfrak{a}_{D+1} \end{bmatrix} = \mathbf{w}(x)\, \mathbf{R} \begin{bmatrix} \mathfrak{a}_1 \\ \vdots \\ \mathfrak{a}_{D+1} \end{bmatrix} \\ &= \mathbf{w}(x) \begin{bmatrix} \mathfrak{s}_1 \\ \vdots \\ \mathfrak{s}_J \end{bmatrix}. \end{aligned} \tag{21}$$

This way, the polytopic description can be constructed for the original image in the H space by considering the D-dimensional geometric problem.

4.2. Affine Singular Value Decomposition of Univariate Functions. Consider the description on the affine hull in (17) and restrict it to orthogonal $(\mathfrak{a}_1, \ldots, \mathfrak{a}_D)$ bases and homogeneous, orthonormal $(v_1(x), \ldots, v_{D+1}(x))$ coordinate functions. Then we can define the following unique form that is called Affine Singular Value Decomposition.

Definition 8 (affine SVD (ASVD)). The form represented by (17) is called affine SVD of $\mathfrak{c}$ function if it is a homogeneous, orthonormal decomposition and the $\mathfrak{a}_i \in H$ $(i = 1 \cdots D)$ elements of the basis are orthogonal and ordered by their norms as

$$\begin{aligned} \left\langle \mathfrak{a}_i, \mathfrak{a}_j \right\rangle &= \delta_{ij} \sigma_i^2 \quad \forall i,\ j = 1 \cdots D, \\ \sigma_1 &\geq \cdots \geq \sigma_D > 0, \end{aligned} \tag{22}$$

which are called singular values.

The decomposition's uniqueness property is inherited from the uniqueness of SVD.

Lemma 9 (uniqueness of ASVD). *The $\sigma_1, \ldots, \sigma_D$ singular values and the $\mathfrak{a}_{D+1}$ offset are unique.*

Now consider the ordered singular values and let $(m_1, m_2, \ldots)$ denote their multiplicities such that

$$\begin{aligned} &\underbrace{\sigma_1 = \cdots = \sigma_{m_1}}_{m_1} > \underbrace{\sigma_{m_1+1} = \cdots = \sigma_{m_1+m_2}}_{m_2} > \cdots > \sigma_D \\ &> 0. \end{aligned} \tag{23}$$

Then the forms and only these forms are valid decomposition

$$\mathfrak{c}(x) = \sum_{d=1}^{D+1} v'_d(x)\, \mathfrak{a}'_d, \tag{24}$$

where

$$\begin{aligned} \left[v'_1(x) \cdots v'_D(x)\right] &= \left[v_1(x) \cdots v_D(x)\right] \mathbf{T}, \\ \left[\mathfrak{a}'_1 \cdots \mathfrak{a}'_D\right]^T &= \mathbf{T}^T \left[\mathfrak{a}_1 \cdots \mathfrak{a}_D\right]^T, \end{aligned}$$

$$v'_{D+1}(x) = v_{D+1}(x),$$
$$\mathfrak{a}'_{D+1} = \mathfrak{a}_{D+1},$$
$$\mathbf{T} = \mathit{blockdiag}(\mathbf{Q}_1, \mathbf{Q}_2, \dots), \tag{25}$$

and $\mathbf{Q}_i$ *are arbitrary real orthogonal matrices with size* $m_i \times m_i$*, respectively.*

Proof. These kinds of decomposition are ASVD because

(i) by multiplying the orthonormal $v_d(x) d = 1 \cdots D$ functions with a $\mathbf{T}$ orthogonal matrix, they remain orthonormal,

(ii) by multiplying the orthogonal $\mathfrak{a}_d$ values of the same norm with a $\mathbf{Q}_i$ orthogonal matrix, they maintain their orthogonality and norm as well. This way, the singular values and their order do not change.

Only this kind of decomposition is ASVD, because

(i) to ensure the $v'_{D+1}(x) = 1$ and the orthonormality of $v_d(x)$ functions, the offset part cannot change:

$$\int_{x=\underline{x}}^{\overline{x}} \mathfrak{c}(x) \frac{dx}{\overline{x} - \underline{x}} = \sum_{d=1}^{D+1} \langle v_d(x), 1 \rangle a_d = a_{D+1}, \tag{26}$$

(ii) the remaining part must be the SVD of function $(\mathfrak{c}(x) - \mathfrak{a}_{D+1})$ inheriting its uniqueness properties, which results in the structure of $\mathbf{T}$.

□

Obviously, if every singular value is different, only the signs of $\mathfrak{a}_d$ objects and $v_d(x)$ functions $(d = 1, \dots, D)$ can be varied, because the lemma allows for only $\mathbf{Q}_i = \pm 1$ values in these cases.

Lemma 10 (complexity trade-off). *Consider the affine SVD in (17) with D singular values, where D is the dimension of the affine hull.*

The best $d < D$*-dimensional approximation (in terms of the defined norm) can be obtained as*

$$\mathfrak{c}(x) = \sum_{l=1}^{d} v_l(x) \mathfrak{a}_l + \mathfrak{a}_{D+1}. \tag{27}$$

Proof. It was shown in (26) that the average value of $\mathfrak{c}$ function is $\mathfrak{a}_{D+1}$ so it is the best $d = 0$-dimensional approximation.

And if the best d-dimensional approximation is known, the best $d + 1$-dimensional can be obtained by adding the a product with maximal possible norm (as in the Eckhart-Young theorem [20]), which is here $\mathfrak{a}_{d+1} v_{d+1}(x)$. □

Because the complexity of enclosing polytope generation depends on the dimension of the affine hull, this property allows for its reduction with minimal error in the defined norm.

The following lemma describes the numerical reconstruction assuming a vector function given as a homogeneous, orthonormal decomposition.

Lemma 11 (ASVD from a homogen. orthonorm. decomp.). *Consider the* $\mathbf{s} : [\underline{x}, \overline{x}] \to \mathbb{R}^R$ *function, which is given as a homogeneous, orthonormal decomposition*

$$\mathbf{s}(x) = \sum_{m=1}^{M} f_m(x) \mathbf{k}_m, \tag{28}$$

in matrix form as $\mathbf{s}(x) = \mathbf{f}(x)\mathbf{K}$.

Then $\mathbf{s}(x) = \mathbf{v}(x)\mathbf{K}'$ *ASVD can be obtained as*

$$\mathbf{v}(x) = \mathbf{f}(x) \begin{bmatrix} \mathbf{U} & \mathbf{0} \\ \mathbf{0} & 1 \end{bmatrix},$$
$$\mathbf{K}' = \begin{bmatrix} \mathbf{S}\mathbf{V}^T \\ \mathbf{k}_M \end{bmatrix}, \tag{29}$$

where the matrices $\mathbf{U}$*,* $\mathbf{S}$*, and* $\mathbf{V}$ *come from the SVD computation:*

$$\mathbf{U}\mathbf{S}\mathbf{V}^T = svd\left(\begin{bmatrix} \mathbf{k}_1 \\ \vdots \\ \mathbf{k}_{M-1} \end{bmatrix} \right) \tag{30}$$

omitting the zero singular values and the corresponding columns of singular matrices.

Proof. $\mathbf{v}(x)$ is orthonormal, because $\mathbf{f}(x)$ is orthonormal and blockdiag $(\mathbf{U}, 1)$ is orthogonal. It is homogeneous because $v_{D+1}(x) = f_M(x) = 1$. The $\mathbf{k}'_d$ values $(d = 1 \cdots D)$ are orthogonal and ordered by norm from properties of SVD. □

5. Definition of Affine Tensor Product Form

This section presents the derivation of polytopic TP forms for multivariate functions

$$\mathfrak{c} : \Omega \longrightarrow H \tag{31}$$

based on the Affine TP form, which represents the affine geometric structure for all parameter dependency, respectively.

Definition 12 (Affine TP form). The following form of function (31)

$$\mathfrak{c}(\mathbf{p}) = \mathscr{C}^{\text{aff}} \bigboxtimes_{n=1}^{N} \mathbf{v}^{(n)}(p_n) \tag{32}$$

is called Affine TP form, in which the $\mathscr{C}^{\text{aff}}$ core tensor is on H as $\mathscr{C}^{\text{aff}} \in H^{(D_1+1) \times \cdots \times (D_N+1)}$, the D_n $(n = 1 \cdots N)$ values are called n-mode dimensions, and the n-mode expansion of (32)

$$\mathfrak{c}(\mathbf{p}) = \sum_{d=1}^{D_n+1} \left(\mathscr{C}^{\text{aff}}_{d_n=d} \bigboxtimes_{l=1, l \neq n}^{N} \mathbf{v}^{(l)}(p_l) \right) v_d^{(n)}(p_n) \tag{33}$$

is an ASVD with $\sigma_1^{(n)}, \dots, \sigma_{D_n}^{(n)}$ singular values for all n, respectively.

Remark 13 (ASVD on functions). The definition exploits the fact that functions with norm in Definition 6 constitute Hilbert spaces. This way, the $\mathfrak{c}(\mathbf{p})$ function can be considered as a univariate function

$$\left[\underline{p}_n, \overline{p}_n\right] \longrightarrow \mathbb{H} \tag{34}$$

for all $n = 1 \cdots N$, where $\mathbb{H}$ is the Hilbert space of functions

$$\Omega_1 \times \cdots \times \Omega_{n-1} \times \Omega_{n+1} \times \cdots \times \Omega_N \longrightarrow H \qquad \left(\Omega_i = \left[\underline{p}_i, \overline{p}_i\right]\right), \tag{35}$$

and the ASVD is defined for it.

The polytopic TP form can be obtained by determining enclosing polytopes for all $\mathbf{v}^{(n)}(p_n)$ trajectories in the D_n-dimensional spaces for all $n = 1 \cdots N$ and applying the following theorem.

Theorem 14 (derivation of polytopic TP form). *If for all $n = 1 \cdots N$ the vertices $\mathbf{r}_1^{(n)}, \ldots, \mathbf{r}_{J_n}^{(n)}$ construct enclosing polytopes for trajectories $\mathbf{v}^{(n)}(p_n)$, they can be expressed as $\mathbf{v}^{(n)}(p_n) = \mathbf{w}^{(n)}(p_n)\mathbf{R}^{(n)}$ (see (19)). Then*

$$\begin{aligned}\mathfrak{c}(\mathbf{p}) &= \mathscr{C}^{aff} \bar{\boxtimes}_{n=1}^{N} \left(\mathbf{w}^{(n)}(p_n)\,\mathbf{R}^{(n)}\right) \\ &= \left(\mathscr{C}^{aff} \bar{\boxtimes}_{n=1}^{N} \mathbf{R}^{(n)}\right) \bar{\boxtimes}_{n=1}^{N} \mathbf{w}^{(n)}(p_n)\end{aligned} \tag{36}$$

which is a polytopic TP form.

Proof. From Section 4.1, the uniqueness of the Affine TP form can be characterized by the following theorem. □

Theorem 15 (uniqueness). *The $\sigma_d^{(n)}$ singular values are unique; let $(m_1^{(n)}, m_2^{(n)}, \ldots)$ denote their multiplicities as in (23).*

If (32) is an Affine TP form, the following and only the following forms are Affine TP Models:

$$\mathfrak{c}(\mathbf{p}) = \left(\mathscr{C}^{aff} \bar{\boxtimes}_{n=1}^{N} \mathbf{T}^{(n)T}\right) \bar{\boxtimes}_{n=1}^{N} \left(\mathbf{v}^{(n)}(p_n)\,\mathbf{T}^{(n)}\right), \tag{37}$$

where the matrices are defined as $\mathbf{T}^{(n)} = diag(\mathbf{T}_0^{(n)}, 1)$ and $\mathbf{T}_0^{(n)}$ is a block-diagonal matrix constructed by arbitrary orthogonal matrices with sizes $m_1^{(n)} \times m_1^{(n)}$, $m_2^{(n)} \times m_2^{(n)}$, and so on as shown in Lemma 9.

Proof. Only these forms are allowed by uniqueness properties of ASVD (see Lemma 9) and their n-mode expansions

$$\begin{aligned}\mathfrak{c}(\mathbf{p}) = \sum_{d=1}^{D_n+1} &\left(\mathscr{C}^{\text{aff}} \bar{\boxtimes}_{l=1,l\neq n}^{N} \mathbf{v}^{(l)}(p_l) \times_n \mathbf{T}^{(n)T}\right)_{d_n=d} \\ &\cdot \left(\mathbf{v}^{(n)}(p_n)\,\mathbf{T}^{(n)}\right)_d\end{aligned} \tag{38}$$

show that these forms are ASVD, so the TP form is affine. □

The form enables the n-mode dimension reductions with the following error (regarding the defined norm) based on the properties of TP forms on orthonormal weighting functions, which are discussed in the Appendix.

Theorem 16 (complexity reduction). *The reduction of one n-mode dimension from D_n to $D_n' < D_n$ with minimal error in the defined norm can be achieved by omitting the $(D_n' + 1), \ldots, D_n$th subtensors of $\mathscr{C}^{aff}$ and the corresponding elements of $\mathbf{v}^{(n)}(p_n)$. Then the error is*

$$\|\mathfrak{c} - \widehat{\mathfrak{c}}\|^2 = \sum_{d=D_n'+1}^{D_n} \sigma_d^{(n)2}. \tag{39}$$

The approximation error of dimension reduction in multiple $(n = 1 \cdots N)$ parameter dependencies is bounded as

$$\|\mathfrak{c} - \widehat{\mathfrak{c}}\|^2 \leq \sum_{n=1}^{N} \sum_{d=D_n'+1}^{D_n} \sigma_d^{(n)2}. \tag{40}$$

Proof. Construct a tensor $\widehat{\mathscr{C}}^{\text{aff}}$ with the same sizes as $\mathscr{C}^{\text{aff}}$ that contains zeros in the omitted subtensors. Then, if $\Delta\mathscr{C}^{\text{aff}} = \mathscr{C}^{\text{aff}} - \widehat{\mathscr{C}}^{\text{aff}}$, the approximation error can be written as

$$\mathfrak{c}(\mathbf{p}) - \widehat{\mathfrak{c}}(\mathbf{p}) = \Delta\mathscr{C}^{\text{aff}} \bar{\boxtimes}_{n=1}^{N} \mathbf{v}^{(n)}(p_n). \tag{41}$$

If only one n-mode dimension is decreased, the error of the approximation can be written as (based on Lemma A.2)

$$\|\mathfrak{c} - \widehat{\mathfrak{c}}\|^2 = \sum_{d=1}^{D_n+1} \left\|\Delta\mathscr{C}^{\text{aff}}_{d_n=d}\right\|^2 = \sum_{d=D_n'+1}^{D_n} \sigma_d^{(n)2} \tag{42}$$

that is minimal as Lemma 10 indicated.

Considering the case when more than one n-mode dimension is decreased, the worst case (equality) of (40) occurs if there are zero elements in the intersection of the omitted subtensors. Otherwise, the error of the approximation is smaller. □

Finally, the method is presented for its exact derivation or at least approximate reconstruction.

Method 17 (numerical reconstruction of Affine TP form). The first step is to obtain an initial TP form with the desired parameter groups

$$\begin{aligned}\widehat{\mathfrak{c}}(\mathbf{p}) &= \mathscr{D} \bar{\boxtimes}_{n=1}^{N} \boldsymbol{\alpha}^{(n)}(p_n) \\ &= \sum_{m_1=1}^{M_1} \cdots \sum_{m_N=1}^{M_N} \mathfrak{d}_{m_1,\ldots,m_N} \prod_{n=1}^{N} \alpha_{m_n}^{(n)}(p_n).\end{aligned} \tag{43}$$

Here we describe two approaches for it.

Step 1a (analytical initial form). If the function is analytically given, the $\mathfrak{c}(\mathbf{p}) = \widehat{\mathfrak{c}}(\mathbf{p})$ initial form may be constructed analytically.

Step 1b (discretization based initial form). The function can be approximated by the TP form as $\mathfrak{c}(\mathbf{p}) \approx \widehat{\mathfrak{c}}(\mathbf{p})$ via

discretization in general: For each $\mathbf{p}_n$ parameter, choose M_n discrete points denoted as $\{\dots, \mathbf{g}_{m_n}^{(n)}, \dots\}$ and appropriate $\boldsymbol{\alpha}^{(n)}(\mathbf{p}_n)$ interpolatory functions (as Lagrange polynomials, piecewise linear/constant functions, etc.).

Then the initial TP form (43) can be constructed to approximate the function by choosing elements of the core tensor $\mathfrak{D} \in H^{M_1 \times M_2 \times \cdots \times M_N}$ denoted by $\mathfrak{d}_{m_1,\dots,m_N}$ which is the value of $\mathfrak{c}(\mathbf{p})$ function at $(\mathbf{g}_{m_1}^{(1)}, \mathbf{g}_{m_2}^{(2)}, \dots)$.

Step 2 (homogeneous orthonormalization). Determine the homogeneous, orthonormal weighting functions $\boldsymbol{\gamma}^{(n)}$: $[\underline{p}_n, \overline{p}_n] \to \mathbb{R}^{L_n}$ as $\boldsymbol{\gamma}^{(n)}(p_n)\mathbf{T}^{(n)} = \boldsymbol{\alpha}^{(n)}(p_n)$ to obtain the following orthonormal TP form:

$$\widehat{\mathfrak{c}}(\mathbf{p}) = \mathscr{F} \bar{\times}_{n=1}^{N} \gamma^{(n)}(p_n), \tag{44}$$

where

$$\mathscr{F} = \mathscr{D} \bar{\times}_{n=1}^{N} \mathbf{T}^{(n)}. \tag{45}$$

Some examples are Gram-Schmidt orthogonalization [21], the Householder transformation [22–24], or the Givens rotation [25].

Step 3 (sequential ASVD). Denote the TP form as

$$\widehat{\mathfrak{c}}(\mathbf{p}) = \mathscr{K} \bar{\times}_{n=1}^{N} \mathbf{f}^{(n)}(p_n), \tag{46}$$

whose initial value is $\mathscr{K} = \mathscr{F}$ and $\mathbf{f}^{(n)}(p_n) = \boldsymbol{\gamma}^{(n)}(p_n)$ for $n = 1 \cdots N$.

Then for index $n = 1$, compute the ASVD of $\mathbf{f}^{(n)}(p_n)\mathbf{K}_{(n)}$ form as

$$\mathbf{f}^{(n)}(p_n)\,\mathbf{K}_{(n)} = \mathbf{v}^{(n)}(p_n)\,\mathbf{K}' \tag{47}$$

(see Lemma 11) and continue with $\mathscr{K} := \text{inv\_unfold}(\mathbf{K}')$, $\mathbf{f}^{(n)}(p_n) := \mathbf{v}^{(n)}(p_n)$, and $n = n + 1$ until $n \le N$.

Then the resulting TP form is affine.

Proof. For TP forms on orthonormal weighting functions, if $\mathscr{K} \times_n \mathbf{v}^{(n)}(p_n)$ is ASVD, then

$$\left(\mathscr{K} \bar{\times}_{l=1, l\neq n}^{N} \mathbf{f}^{(l)}(p_l)\right) \times_n \mathbf{v}^{(n)}(p_n) \tag{48}$$

is ASVD as well; see Lemma A.3 of the Appendix. □

The method proves the existence of Affine TP forms for cases where the separation of parameter dependencies is possible, and it extends the previous approach by allowing exact analytical separation or the application of discretization with varying density along the parameter domain Ω with different interpolation strategies.

Remark 18. The sequential truncation approach (see [26]) can also be applied by using the complexity reductions in iterations of Step 3 in order to decrease the computational cost.

Remark 19. By applying SVD instead of ASVD in Step 3 (and optionally simple orthonormalization in Step 2), the method can be used to determine the so-called HOSVD-based TP form as well.

6. Application for LPV/qLPV Models

The results of the previous section are appropriate for system matrices $\mathbf{S}(\mathbf{p})$ of (q)LPV models (9). By defining the inner product and norm for $\mathbf{F}, \mathbf{G} \in \mathbb{S}$ system matrices as

$$\langle \mathbf{F}, \mathbf{G} \rangle = \text{trace}\left(\mathbf{F} \cdot \mathbf{G}^T\right), \quad \|\mathbf{F}\| = \sqrt{\langle \mathbf{F}, \mathbf{F} \rangle}, \tag{49}$$

the space $\mathbb{S}$ constitutes a Hilbert space and the following TP Model can be defined.

Definition 20 (Affine TP Model). The system matrix of the (q)LPV model (9) is given in Affine TP form as

$$\mathbf{S}(\mathbf{p}) = \mathcal{S}^{\text{aff}} \bar{\times}_{n=1}^{N} \mathbf{v}^{(n)}(p_n); \tag{50}$$

see Definition 12.

The elements of core tensor $\mathcal{S}^{\text{aff}}$ are system matrices and the functions $\mathbf{v}^{(n)}(p_n)$ are D_n-dimensional trajectories given by homogeneous coordinates.

The uniqueness of the description is inherited from Theorem 15. Complexity (dimension of the affine hull) reduction can be done based on Theorem 16 but it must be mentioned that it does not give guarantee about its distribution along the parameter domain in terms of dynamical effects, and thus, it is not closely related to its dynamical properties in ill-conditioned cases. It means that if the omitted details are not only numerical error (representing essential information about the system dynamics), it is recommended to apply robust design methods taking into account the neglected part as in [27].

Furthermore, it has direct link with polytopic model generation based on Theorem 14.

Corollary 21 (polytopic model generation). *The determination of vertices* $\mathbf{r}_1^{(n)}, \mathbf{r}_2^{(n)}, \dots, \mathbf{r}_{J_n}^{(n)} \in \mathbb{R}^{D_n}$ $(J_n \ge D_n + 1)$ *for all* $n = 1 \cdots N$ *constructs an enclosing polytope for the* $[v_1^{(n)}(p_n) \cdots v_{D_n}^{(n)}(p_n)]$ *trajectory and the weighting functions* $\mathbf{w}^{(n)}(p_n)$ *(interpreting convex combination for all* p_n*) in such a way that*

$$\mathbf{w}^{(n)}(p_n)\,\mathbf{R}^{(n)} = \mathbf{v}^{(n)}(p_n) \tag{51}$$

(as in (19)).

Then the polytopic TP Model (13) can be formalized with $\mathbf{w}^{(n)}(p_n)$ *weighting functions and core tensor*

$$\mathcal{S} = \mathcal{S}^{aff} \bar{\times}_{n=1}^{N} \mathbf{R}^{(n)}. \tag{52}$$

There exist numerical methods for enclosing simplex polytope generation (where $J_n = D_n + 1$) such as the Minimal

Volume Simplex Approach [13] and other simplex methods: CNO, IRNO, and SNNN [15, 17]. The classical convex hull methods [28, 29] can also be applied, but they usually result in enclosing polytopes with too many vertices (up to infinity).

Fine-tuning manipulation/optimization is an important technique in polytopic model-based design. Similarly to the polytope generation methods, manipulation techniques are also immediately connectible to the Affine TP Model.

Corollary 22 (polytopic model manipulation). *As manipulation of $\mathfrak{N} \subset \{1, \ldots, N\}$ mode enclosing polytopes, determinate the vertices $\mathbf{r}'^{(n)}_1, \mathbf{r}'^{(n)}_2, \ldots, \mathbf{r}'^{(n)}_{J'_n} \in \mathbb{R}^{D_n}$ ($J'_n \geq D_n + 1$) and weighting functions $\mathbf{w}'^{(n)}(p_n)$ for all $n \in \mathfrak{N}$ that constructs an enclosing polytope for the trajectory $[v^{(n)}_1(p_n) \cdots v^{(n)}_{D_n}(p_n)]$ in such a way that $\mathbf{w}'^{(n)}(p_n)\mathbf{R}'^{(n)} = \mathbf{v}^{(n)}(p_n)$ as in (19), taking into account the control design experience with previous enclosing polytopes.*

Then the manipulated polytopic TP Model can be formalized as

$$\mathbf{S}(\mathbf{p}) = \mathcal{S}^{man} \underset{n=1, n\notin\mathfrak{N}}{\overset{N}{\boxtimes}} \mathbf{w}^{(n)}(p_n) \underset{n\in\mathfrak{N}}{\boxtimes} \mathbf{w}'^{(n)}(p_n), \tag{53}$$

where

$$\mathcal{S}^{man} = \mathcal{S}^{aff} \underset{n=1, n\notin\mathfrak{N}}{\overset{N}{\boxtimes}} \mathbf{R}^{(n)} \underset{n\in\mathfrak{N}}{\boxtimes} \mathbf{R}'^{(n)}. \tag{54}$$

Relevant examples are the manipulation of the constraints in MVS method based on the achievable performance with the previous polytopes (see [13, 30]) or the nonsimplex method where problematic regions are cut off from the polytope [16].

7. Numerical Example

This section discusses a control-related example that gives hands-on insight into a realistic design scenario.

Consider the translational oscillator with an eccentric rotational mass actuator (TORA) system shown in Figure 1. The goal of the control effort is to stabilize its translational motion using a rotational actuator [31–35].

The equation of motion is usually reformulated in the following dimensionless form:

$$\begin{aligned} \chi'' &= -\chi + \epsilon \sin\theta, \\ \theta'' &= \frac{\epsilon\chi\cos\theta + u}{1 - \epsilon^2\cos^2\theta} - \epsilon^2 \frac{\left(\theta'^2 + 1\right)\cos\theta}{1 - \epsilon^2\cos^2\theta}\sin\theta, \end{aligned} \tag{55}$$

where

$$\begin{aligned} \chi &= \xi + \epsilon\sin\theta, \\ \xi &= \sqrt{\frac{M+m}{I+me^2}}\, q, \\ u &= \frac{M+m}{k\left(I+me^2\right)} N, \end{aligned}$$

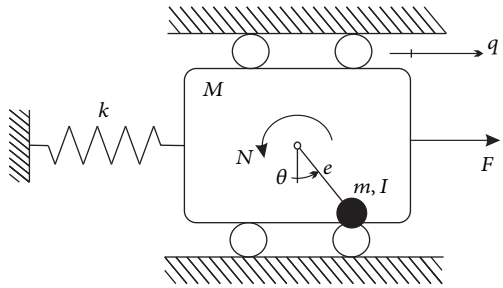

Figure 1: The mechanical model of the TORA system.

$$\begin{aligned} \tau &= \sqrt{\frac{k}{m+M}}\, t, \\ \epsilon &= \frac{me}{\sqrt{\left(I+me^2\right)(M+m)}}, \end{aligned} \tag{56}$$

where ξ denotes the dimensionless translational position, u the dimensionless input, τ dimensionless time, and ϵ the coupling parameter.

The nonlinear ODE is used for the purpose of constructing the qLPV model; the state variables are chosen as

$$\mathbf{x} = \begin{bmatrix} \chi & \chi' & \theta & \theta' \end{bmatrix}^T, \tag{57}$$

and the parameters as

$$\begin{aligned} p_1 &= |\theta|, \\ p_2 &= \frac{\left(\theta'^2 + 1\right)\cos\theta}{1 - \epsilon^2\cos^2\theta}. \end{aligned} \tag{58}$$

Then the constructed qLPV realization reads

$$\mathbf{x}' = \begin{bmatrix} \mathbf{A}(\mathbf{p}) & \mathbf{B}(\mathbf{p}) \end{bmatrix} \begin{bmatrix} \mathbf{x} \\ u \end{bmatrix} = \mathbf{S}(\mathbf{p}) \begin{bmatrix} \mathbf{x} \\ u \end{bmatrix}, \tag{59}$$

where

$$\begin{aligned} \mathbf{A}(\mathbf{p}) &= \begin{bmatrix} 0 & 1 & 0 & 0 \\ -1 & 0 & \epsilon\dfrac{\sin p_1}{p_1} & 0 \\ 0 & 0 & 0 & 1 \\ \dfrac{\epsilon\cos p_1}{G(p_1)} & 0 & -\epsilon^2 p_2 \dfrac{\sin p_1}{p_1} & 0 \end{bmatrix}, \\ \mathbf{B}(\mathbf{p}) &= \begin{bmatrix} 0 \\ 0 \\ 0 \\ \dfrac{1}{G(p_1)} \end{bmatrix}, \end{aligned} \tag{60}$$

$$G(p_1) = 1 - \epsilon^2\cos^2 p_1,$$

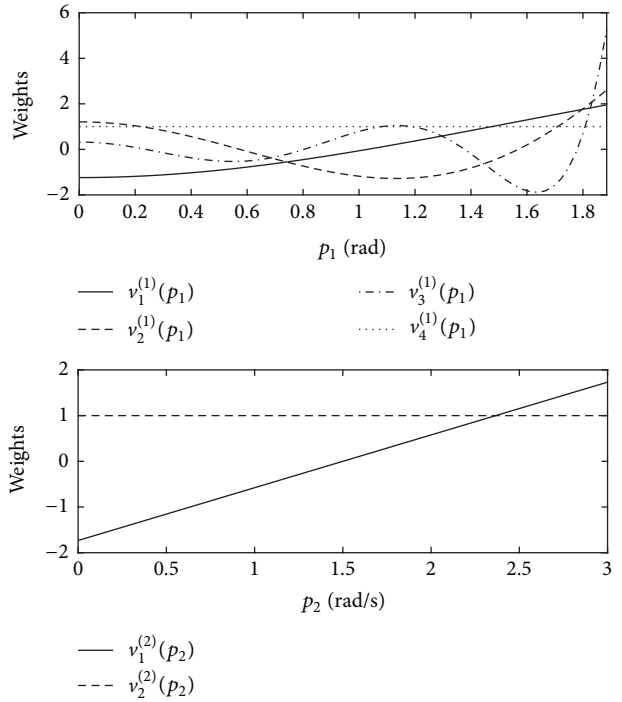

FIGURE 2: The $\mathbf{v}^{(1)}(p_1)$ and $\mathbf{v}^{(2)}(p_2)$ weighting functions in the Affine TP Model.

and here the $|\theta| < 0.6\pi$ $|\dot{\theta}| < 3$ (rad/s) domain is considered with $\epsilon = 0.2$ value.

In order to obtain the Affine TP form of function (59), the parameter dependencies are separated leading to an initial TP form with the following weighting functions:

$$\boldsymbol{\alpha}^{(1)}(p_1) = \left[\frac{\sin p_1}{p_1} \quad \frac{\cos p_1}{G(p_1)} \quad \frac{1}{G(p_1)} \quad 1\right],$$
$$\boldsymbol{\alpha}^{(2)}(p_2) = [p_2 \quad 1] \tag{61}$$

performing Step 1a of Method 17. After orthogonalization and sequential ASVD, we get the affine form

$$\mathbf{S}(\mathbf{p}) = \mathcal{S}^{\text{aff}} \times_1 \mathbf{v}^{(1)}(p_1) \times_2 \mathbf{v}^{(2)}(p_2)$$
$$= \mathcal{S}^{\text{aff}} \boxtimes_{n=1}^{2} \mathbf{v}^{(n)}(p_n), \tag{62}$$

where the n-mode dimensions are $D_1 = 3$ and $D_2 = 1$ and the corresponding weighting functions are depicted in Figure 2. The singular values: $\sigma_1^{(1)} = 9.15 \cdot 10^{-2}$, $\sigma_2^{(1)} = 5.75 \cdot 10^{-3}$, $\sigma_3^{(1)} = 1.91 \cdot 10^{-5}$, and $\sigma_1^{(2)} = 2.90 \cdot 10^{-2}$. (By applying discretization and interpolator functions, numerically reconstructed approximations of this TP form can be obtained.)

The enclosing polytope generation for p_2 dependency is trivial, because it is a one-dimensional problem. The vertices: $\mathbf{r}_1^{(2)} = [-1.731 \quad 1]$ and $\mathbf{r}_2^{(2)} = [1.731 \quad 1]$.

The three-dimensional problem of p_1 dependency is more challenging. The methods for generation of the enclosing polytope can be applied as MVS (or SNNN, CNO); see Section 6. Figure 3 shows the resulting tetrahedron enclosing polytope and Figure 4 the weighting functions (denoting convex combinations) and the vertices are

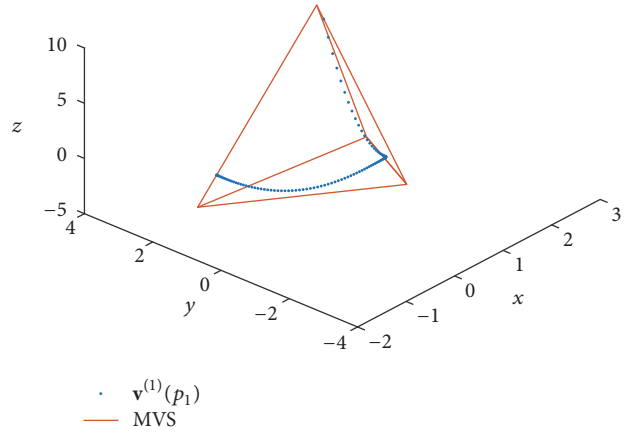

FIGURE 3: The MVS enclosing polytope for $\mathbf{v}^{(1)}(p_1)$ on the affine hull.

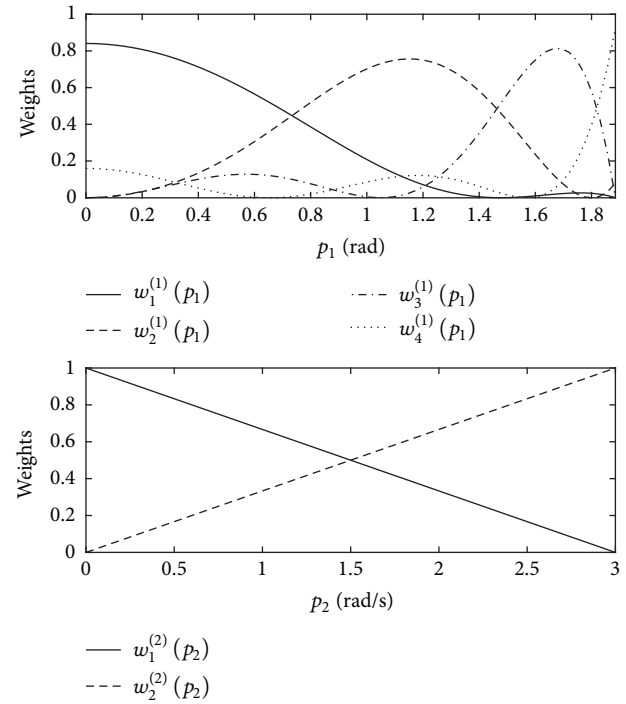

FIGURE 4: The $\mathbf{w}^{(1)}(p_1)$ and $\mathbf{w}^{(2)}(p_2)$ weighting functions in the polytopic TP Model.

$$\mathbf{r}_1^{(1)} = [-1.873 \quad 0.864 \quad -0.691 \quad 1],$$
$$\mathbf{r}_2^{(1)} = [0.201 \quad -2.311 \quad 0.661 \quad 1],$$
$$\mathbf{r}_3^{(1)} = [1.676 \quad 0.964 \quad -2.647 \quad 1],$$
$$\mathbf{r}_4^{(1)} = [2.102 \quad 3.027 \quad 5.659 \quad 1]. \tag{63}$$

The resulting polytopic TP Model has two parameter dependencies, and it has the following general form:

$$\mathbf{x}' = \mathbf{S}(\mathbf{p}) \begin{bmatrix} \mathbf{x} \\ u \end{bmatrix}, \tag{64}$$

where

$$\begin{aligned} \mathbf{S}(\mathbf{p}) &= \mathcal{S} \boxtimes_{n=1}^{2} \mathbf{w}^{(n)}(p_n) \\ &= \sum_{j_1=1}^{2} \sum_{j_2=1}^{4} w_{j_1}^{(1)}(p_1)\, w_{j_2}^{(2)}(p_2) \left[\mathbf{A}_{j_1,j_2} \quad \mathbf{B}_{j_1,j_2}\right]. \end{aligned} \tag{65}$$

For the sake of brevity, only the quadratic stabilization via state feedback problem is recalled and applied. To exploit the separated parameter dependencies, the controller-candidate depends only on the first parameter as

$$u = \mathbf{F}(p_1)\,\mathbf{x}, \quad \mathbf{F}(p_1) = \sum_{j=1}^{4} w_j^{(1)}(p_1)\,\mathbf{F}_j. \tag{66}$$

Then the closed-loop system is stable if there exist $\mathbf{X} \in \mathbb{R}^{4\times4}$ symmetric matrix and $\mathbf{M}_j \in \mathbb{R}^{1\times4}$ $j = 1\cdots4$ matrices such that

$$\begin{aligned} &\mathbf{X} > 0, \\ &\Gamma_{j_1,j_1,j_2} < 0 \quad \forall j_1 = 1\cdots4,\ j_2 = 1,2, \\ &\Gamma_{j_1,i_1,j_2} < 0 \quad \forall j_1 = 1\cdots4,\ 1 \geq i_1 < j_1,\ j_2 = 1,2, \\ &\text{where } \Gamma_{j_1,i_1,j_2} = \mathrm{He}\left(\mathbf{A}_{j_1,j_2}\mathbf{X} + \mathbf{B}_{j_1,j_2}\mathbf{M}_{i_1}\right) \end{aligned} \tag{67}$$

and the gains of the state feedback are $\mathbf{F}_j = \mathbf{M}_j\mathbf{X}^{-1}$.

Here the problem is feasible with gains:

$$\begin{aligned} \mathbf{F}_1 &= \begin{bmatrix} 0.2419 & -0.5642 & -1.8000 & -0.6950 \end{bmatrix}, \\ \mathbf{F}_2 &= \begin{bmatrix} 0.4320 & -0.6009 & -1.9145 & -0.7264 \end{bmatrix}, \\ \mathbf{F}_3 &= \begin{bmatrix} 0.5588 & -0.6120 & -1.9458 & -0.7305 \end{bmatrix}, \\ \mathbf{F}_4 &= \begin{bmatrix} 0.5935 & -0.6124 & -1.9449 & -0.7285 \end{bmatrix}. \end{aligned} \tag{68}$$

For more complex examples that apply other polytopic model generation, manipulation methods, and controller design techniques, see papers [9, 11, 13, 16, 30].

8. Conclusion

The proposed Affine TP Model Transformation is a significant development in polytopic model-based control providing a general yet practically advantageous methodology for polytopic model generation. The unique Affine TP Model as a central concept serves as starting point for complexity reduction, polytopic model creation, and various polytope manipulation/optimization approaches helping to fully exploit the directly applicable powerful LMI-based synthesis methods. The most important benefits of the proposed intermediate TP form are the geometrically appropriate representation of the LPV structure in each dimension and the capability of dimension reduction with minimal error and low computational cost. In addition to the theoretical discussion, for the sake of technical completeness, an illustrative numerical example was provided to clearly show the practical merit of the Affine TP form.

In some sense, the paper sums up and consolidates the theoretical basis of TP Model Transformation that has been evolved in the past decade through the contribution of a broader research community.

Appendix

Mathematical Background of Affine TP Form

First, the following lemma highlights important properties of orthonormal decomposition.

Lemma A.1 (inner product and norm of orthonormal decomp.). *If $\mathfrak{b}, \mathfrak{c} : X \to H$ functions are given with the same $\{\ldots, f_i(\mathbf{x}), \ldots\}$ orthonormal weighting functions, their inner product and norm can be computed as*

$$\langle \mathfrak{b}, \mathfrak{c} \rangle = \sum_{i=1}^{I} \langle \mathfrak{b}_i, \mathfrak{c}_i \rangle, \quad \|\mathfrak{c}\| = \sqrt{\sum_{i=1}^{I} \|\mathfrak{c}_d\|^2}. \tag{A.1}$$

This property appears in orthonormal TP forms in the following way.

Lemma A.2 (inner product and norm of orthonormal TP forms). *If there are two TP functions given on the same orthonormal weighting function system as*

$$\begin{aligned} \mathfrak{c}(\mathbf{p}) &= \mathscr{C} \boxtimes_{n=1}^{N} \mathbf{f}^{(n)}(p_n), \\ \mathfrak{d}(\mathbf{p}) &= \mathscr{D} \boxtimes_{n=1}^{N} \mathbf{f}^{(n)}(p_n), \end{aligned} \tag{A.2}$$

their inner product can be obtained as

$$\langle \mathfrak{c}, \mathfrak{d} \rangle = \langle \mathscr{C}, \mathscr{D} \rangle. \tag{A.3}$$

Furthermore, their norm can be derived as

$$\|\mathfrak{c}\| = \|\mathscr{C}\|. \tag{A.4}$$

This way, the functions' orthogonality depends only on the orthogonality of the core tensors. Based on this property, the following lemma formalizes an important property of the Affine TP form.

Lemma A.3 (*n*-mode ASVD of orthonormal TP forms). *If the weighting functions of TP form*

$$\mathfrak{k}(\mathbf{p}) = \mathscr{K} \boxtimes_{n=1}^{N} \mathbf{f}^{(n)}(p_n) \tag{A.5}$$

are orthonormal, the following statements are equivalent for all $n = 1 \cdots N$*:*

(i) *The following form is an ASVD along* p_n *parameter*

$$\left(\mathcal{K} \underset{l=1,l\neq n}{\overset{N}{\boxtimes}} \mathbf{f}^{(l)}\left(p_l\right) \right) \times_n \mathbf{f}^{(n)}\left(p_n\right). \tag{A.6}$$

(ii) *The form is an ASVD along* p_n *parameter*

$$\mathcal{K} \times_n \mathbf{f}^{(n)}\left(p_n\right). \tag{A.7}$$

Furthermore, their singular values are equal.

Proof. The requirements for the $\mathbf{f}^{(n)}(p_n)$ weighting functions are the same and the inner products of the bases are also equal because from Lemma A.2

$$\begin{aligned} &\left\langle \mathcal{K}_{d_n=i} \underset{l=1,l\neq n}{\overset{N}{\boxtimes}} \mathbf{f}^{(l)}\left(p_l\right), \mathcal{K}_{d_n=j} \underset{l=1,l\neq n}{\overset{N}{\boxtimes}} \mathbf{f}^{(l)}\left(p_l\right) \right\rangle \\ &\quad = \left\langle \mathcal{K}_{d_n=i}, \mathcal{K}_{d_n=j} \right\rangle; \end{aligned} \tag{A.8}$$

this way, their orthogonality, order, and norms are the same. □

Conclusively, the n-mode singular values can be obtained as norm of the n-mode subtensors of the core tensor and the ASVD on p_n parameter dependency is invariant for inner transformations among orthonormal decomposition on other p_n parameter dependencies.

Conflicts of Interest

The authors declare that they have no conflicts of interest.

Acknowledgments

The authors thankfully acknowledge the financial support of this work by the ÚNKP-16-3 and ÚNKP-16-4 New National Excellence Program of the Ministry of Human Capacities and the support of the Doctoral School of Applied Informatics and Applied Mathematics of Óbuda University and Research and Innovation Center of Óbuda University.

References

[1] S. Boyd, L. El Ghaoui, E . Feron, and V. Balakrishnan, *Linear Matrix Inequalities in System and Control Theory*, SIAM, Philadelphia, Pa, USA, 1994.

[2] P. Baranyi, "TP model transformation as a way to LMI-based controller design," *IEEE Transactions on Industrial Electronics*, vol. 51, no. 2, pp. 387–400, 2004.

[3] K. Tanaka and H. O. Wang, "Fuzzy control systems design and analysis a linear matrix inequality approach," in *1em plus 0.5em minus 0.4em*, Wiley, New York, 2001.

[4] C. Ariño and A. Sala, "Relaxed LMI conditions for closed-loop fuzzy systems with tensor-product structure," *Engineering Applications of Artificial Intelligence*, vol. 20, no. 8, pp. 1036–1046, 2007.

[5] J. Kuti, P. Galambos, and P. Baranyi, "Polytopic TP Model based control analysis and synthesis concept," *IFAC*, p. accepted, 2017.

[6] G. G. Angelis, *System analysis, modelling and control with polytopic linear models [Ph.D. thesis]*, Technische Universiteit Eindhoven, 2001, Ph.D. dissertation.

[7] J. Kuti, P. Galambos, and A. Miklós, "Output feedback control of a dual-excenter vibration actuator via qLPV model and TP model transformation," *Asian Journal of Control*, vol. 17, no. 2, pp. 432–442, 2015.

[8] P. Baranyi, "Output feedback control of two-dimensional aeroelastic system," *Journal of Guidance, Control, and Dynamics*, vol. 29, no. 3, pp. 762–767, 2006.

[9] T. T. Wang, W. F. Xie, G. D. Liu, and Y. M. Zhao, "Quasi-min-max model predictive control for image-based visual servoing with tensor product model transformation," *Asian Journal of Control*, vol. 17, no. 2, pp. 402–416, 2015.

[10] V. C. S. Campos, F. O. Souza, L. A. B. Torres, and R. M. Palhares, "New stability conditions based on piecewise fuzzy lyapunov functions and tensor product transformations," *IEEE Transactions on Fuzzy Systems*, vol. 21, no. 4, pp. 748–760, 2013.

[11] S. Chumalee and J. F. Whidborne, "Gain-scheduled H_∞ control for tensor product type polytopic plants," *Asian Journal of Control*, vol. 17, no. 2, pp. 417–431, 2015.

[12] P. Baranyi, L. Szeidl, and P. Várlaki, "Numerical reconstruction of the HOSVD based canonical form of polytopic dynamic models," in *Proceedings of the INES 2006: 10th International Conference on Intelligent Engineering Systems 2006*, pp. 196–201, gbr, June 2006.

[13] J. Kuti, P. Galambos, and P. Baranyi, "Minimal volume simplex (MVS) polytopic model generation and manipulation methodology for TP model transformation," *Asian Journal of Control*, vol. 19, no. 1, pp. 289–301, 2017.

[14] P. Baranyi, Y. Yam, and P. Várlaki, "Tensor Product Model Transformation in Polytopic Model-Based Control," in *1em plus 0.5em minus 0.4em Taylor*, Francis Group, 4em Taylor, 2013.

[15] P. Várkonyi, D. Tikk, P. Korondi, and P. Baranyi, "A new algorithm for RNO-INO type Tensor Product model representation," in *Proceedings of the INES'05: IEEE 9th International Conference on Intelligent Engineering Systems*, pp. 263–266, September 2005.

[16] J. Kuti, P. Galambos, and P. Baranyi, "Non-simplex enclosing polytope generation concept for Tensor Product model transformation based controller design," in *Proceedings of the 2016 IEEE International Conference on Systems, Man, and Cybernetics, SMC 2016*, pp. 3368–3373, Hungary, October 2016.

[17] P. Baranyi, "Convex hull generation methods for polytopic representations of LPV models," in *Proceedings of the 7th International Symposium on Applied Machine Intelligence and Informatics, SAMI 2009*, pp. 69–74, Slovakia, January 2009.

[18] L. De Lathauwer, B. De Moor, and J. Vandewalle, "A multilinear singular value decomposition," *SIAM Journal on Matrix Analysis and Applications*, vol. 21, no. 4, pp. 1253–1278, 2000.

[19] C. Briat, *Linear parameter-varying and time-delay systems*, vol. 3 of *Advances in Delays and Dynamics*, Springer, Heidelberg, 2015.

[20] C. Eckart and G. Young, "The approximation of one matrix by another of lower rank," *Psychometrika*, vol. 1, no. 3, pp. 211–218, 1936.

[21] Å. Björck, "Numerics of Gram-Schmidt orthogonalization," *Linear Algebra and its Applications*, vol. 197, pp. 297–316, 1994.

[22] A. S. Householder, "Unitary triangularization of a nonsymmetric matrix," *Journal of the ACM*, vol. 5, pp. 339–342, 1958.

[23] R. Cabrera, T. Strohecker, and H. Rabitz, "The canonical coset decomposition of unitary matrices through Householder transformations," *Journal of Mathematical Physics*, vol. 51, no. 8, Article ID 082101, 2010.

[24] L. N. Trefethen, "Householder triangularization of a quasimatrix," *IMA Journal of Numerical Analysis (IMAJNA)*, vol. 30, no. 4, pp. 887–897, 2010.

[25] D. Bindel, J. Demmel, W. Kahan, and O. Marques, "On computing Givens rotations reliably and efficiently," *ACM Transactions on Mathematical Software*, vol. 28, no. 2, pp. 206–238, 2002.

[26] J. Pan and L. Lu, "TP model transformation via sequentially truncated higher-order singular value decomposition," *Asian Journal of Control*, vol. 17, no. 2, pp. 467–475, 2015.

[27] V. c. Campos, L. A. Tôrres, and R. M. Palhares, "Revisiting the TP model transformation: interpolation and rule reduction," *Asian Journal of Control*, vol. 17, no. 2, pp. 392–401, 2015.

[28] C. B. Barber, D. P. Dobkin, and H. Huhdanpaa, "The quickhull algorithm for convex hulls," *ACM Transactions on Mathematical Software*, vol. 22, no. 4, pp. 469–483, 1996.

[29] D. Avis and D. Bremner, "How good are convex hull algorithms?" in *Proceedings of the the eleventh annual symposium*, pp. 20–28, Vancouver, British Columbia, Canada, June 1995.

[30] J. Kuti, P. Galambos, P. Baranyi, and P. Varlaki, "A Hands-On Demonstration of Control Performance Optimization Using Tensor Product Model Transformation and Convex Hull Manipulation," in *Proceedings of the IEEE International Conference on Systems, Man, and Cybernetics, SMC 2015*, pp. 2609–2614, Hong Kong, October 2015.

[31] D. K. Lindner, T. P. Celano, and E. N. Ide, "Vibration Suppression Using a Proofmass Actuator Operating in Stroke/Force Saturation," *Journal of Vibration and Acoustics*, vol. 113, no. 4, p. 423, 1991.

[32] M. E. Polites, "New method for scanning spacecraft and balloon-borne/space-based experiments," *Journal of Guidance, Control, and Dynamics*, vol. 14, no. 3, pp. 548–553, 1991.

[33] R. H. Rand, R. J. Kinsey., and D. L. Mingori, "Dynamics of spinup through resonance," *International Journal of Non-Linear Mechanics*, vol. 27, no. 3, pp. 489–502, 1992.

[34] C.-J. Wan, D. S. Bernstein, and V. T. Coppola, "Global stabilization of the oscillating eccentric rotor," in *Proceedings of the 1994 33rd IEEE Conference on Decision and Control*, pp. 4024–4029, Lake Buena Vista, FL, USA.

[35] R. T. Bupp, D. S. Bernstein, and V. . Coppola, "A benchmark problem for nonlinear control design," *International Journal of Robust and Nonlinear Control*, vol. 8, no. 4-5, pp. 307–310, 1998.

Hindawi
Complexity
Volume 2018, Article ID 1069839, 9 pages
https://doi.org/10.1155/2018/1069839

Research Article

Intermittent Control for Cluster-Delay Synchronization in Directed Networks

Jianbao Zhang,[1,2,3] **Yi Wang**,[4] **Zhongjun Ma**,[5] **Jianlong Qiu**,[3,6] **and Fawaz Alsaadi**[6]

[1]*School of Information Science and Technology, Linyi University, Linyi 276005, China*
[2]*School of Automation, Southeast University, Nanjing 210096, China*
[3]*Key Laboratory of Complex Systems and Intelligent Computing in Universities of Shandong (Linyi University), Linyi 276005, China*
[4]*School of Data Sciences, Zhejiang University of Finance and Economics, Hangzhou 310018, China*
[5]*School of Mathematics and Computing Science, Guilin University of Electronic Technology, Guilin 541004, China*
[6]*Department of Information Technology, King Abdulaziz University, Jeddah 21589, Saudi Arabia*

Correspondence should be addressed to Zhongjun Ma; mzj1234402@163.com

Received 30 September 2017; Revised 8 January 2018; Accepted 24 January 2018; Published 18 February 2018

Academic Editor: Imre J. Rudas

We investigate cluster-delay synchronization of a directed network possessing cluster structures by designing an intermittent control protocol. Based on Lyapunov stability theory, we proved that synchronization can be realized for oscillators in the same cluster and cluster-delay synchronization can be realized for the whole network. By simplifying the obtained sufficient conditions, we carry out a succinct and utilitarian corollary. In addition, comparative researches are carried out to show the differences and the usefulness of the obtained results with respect to other similar controllers from the recent literature. Finally we provide two numerical examples to show the effectiveness of the control schemes.

1. Introduction

Chaos theory is an interdisciplinary theory studying the unstable aperiodic behavior of dynamical systems. The most distinguishing characteristic of chaotic systems is the highly sensitive dependence on initial conditions [1], which implies that even if the present determines the future, the approximate present does not approximately determine the future. Therefore, it is difficult to control an unpredictable chaotic system in the long term. However, due to the wide applications of chaos theory, more and more researchers are devoting themselves to studying chaos control theory in many fields of science and engineering.

In 1990, it was discovered surprisingly that two chaotic systems started from different initial conditions could synchronize with each other [2], and the great discovery immediately attracted lots of attention and became an important issues of chaos control. Since then, several effective methods have been applied to study synchronization of chaos oscillators. In 1998, the famous master stability function method was proposed to study the local stability of the synchronous state [3], which is based on the calculation of the maximum Lyapunov exponent for the least stable transversal mode of the synchronous manifold and the eigenvalues of the connection matrix. Later, Lyapunov function method was employed to investigate global stability of the synchronous state [4]. Based on the two methods mentioned above, many other surveys have been carried out to explore the mysterious mechanisms of chaos synchronization and chaos control. As the study develops in depth, various kinds of synchronization protocols have been put forward and deeply studied, such as complete synchronization [5], exponential synchronization [6, 7], projective synchronization [8, 9], lag synchronization [10], and cluster synchronization [11–13]. The above-mentioned results only discussed synchronization induced by mutual coupling and the intrinsic structure of the network.

During the past decades, many external control strategies have been carried out to synchronize complex networks, such as adaptive control [14, 15], impulsive control [16], sliding

mode control [17], pinning control [18–20], sliding mode control [21], and intermittent control [22, 23]. Those control strategies have been widely investigated and used in many network control problems. The primary concern of this paper is cluster synchronization under external control, which has attracted widespread attention [24, 25]. By designing adaptive pinning-control schemes on both coupling strengths and feedback gains, it was shown that a network can realize cluster synchronization under weak coupling strengths and small feedback gains [15]. Later, another feedback controller was designed to realize cluster synchronization under the condition that the topology of each cluster has a directed spanning tree [25, 26]. All in all, great efforts have been devoted to the investigation of cluster synchronization under external control. It has been shown to be an effective method to control a complex network to a desired synchronized state.

Up to now, to the best of our knowledge, there are few results concerning cluster-delay synchronization, which is a special type of collective behavior between complete synchronization and cluster synchronization. In our opinion, cluster-delay synchronization implies that the nodes in a complex network are split into several clusters, and all the nodes in the same cluster behave in a synchronous fashion, but nodes in different clusters follow distinct time evolutions with different time delays. It is a new type of collective behavior in complex networks worthy of detailed investigation, and this paper studies cluster-delay synchronization of a complex network via pinning control with intermittent effect. To achieve cluster lag synchronization in community networks, Wu and Fu designed several linear pinning controllers in view of lower cost and more convenient implementation [23]. Recently, motivated by the interesting investigation, we provided some primary theoretical analyses and numerical experiment [27]. Different from the previous results [23, 27], this paper proposes a leader-following system and derives sufficient conditions for cluster-delay synchronization via pinning control with intermittent effect. We first prove that all the oscillators in the same cluster synchronize with each other and then prove that the oscillators in different clusters behave in a synchronous mode but with different time delays. Numerical simulations show that the modified pinning-control scheme works effectively and serves different purposes in practice.

The rest of this paper is organized as follows. Section 2 introduces some necessary preliminaries and builds a modified clustered network model with an intermittent leader-following controller. Then, both cluster synchronization and cluster-delay synchronization of the network model are investigated through Lyapunov theory in Section 3. Comparative researches with respect to previous controllers are also given there. In Section 4, two examples of numerical simulations are carried out to show the validity of the proposed control schemes. Finally, the main results of this paper are briefly summarized in Section 5.

2. Preliminaries

In this section, we make some mathematical preparations for the oscillator network model. Suppose the topology structure of the communication network is represented by a directed graph $\mathcal{G} = \{\mathcal{V}, \mathcal{E}\}$, which is composed of a set of nodes $\mathcal{V} = \{1, \ldots, N\}$ and a set of edges $\mathcal{E} = \mathcal{V} \times \mathcal{V}$. The graph exhibits a clustered structure, which implies that the N nonidentical oscillators are divided into n nonempty subsets called clusters. Let $\mathcal{V}_k = \{m_{k-1} + 1, \ldots, m_k\}$ denote the index set of all the nodes in the kth cluster, where $k = 1, 2, \ldots, n$, $m_0 = 0$, $m_n = N$. For convenience, we define a function $\varphi : \{1, \ldots, N\} \to \{1, \ldots, n\}$, where $\varphi(i) = k$ implies that the node $i \in \mathcal{V}_k$.

Let $x_i(t) = (x_{i1}(t), \ldots, x_{id}(t))^\top$ be the state variable of the ith oscillator, the state equations of the network are given by

$$\dot{x}_i(t) = f(x_i(t)) + \sum_{l=1}^{n} \sum_{j \in \mathcal{V}_l} a_{ij} x_j(t) + u_i(t), \quad i = 1, 2, \ldots, N, \tag{1}$$

where $t \in [0, +\infty)$ is a continuous time, $f(\cdot)$ is a continuous function that describes the local dynamics of each node, $A = (a_{ij})_{N \times N}$ is the coupling matrix with $a_{ij} \geq 0$ for $i \neq j$, and $\sum_{j=1}^{N} a_{ij} = 0$ for $i = 1, 2, \ldots, N$. Denoting the state variables of the oscillators in kth cluster as $X_k(t) = (x_{m_{k-1}+1}^\top(t), \ldots, x_{m_k}^\top(t))^\top$, $U_k(t) = (u_{m_{k-1}+1}^\top(t), \ldots, u_{m_k}^\top(t))^\top$, and $F(X_k(t)) = (f(x_{m_{k-1}+1}(t))^\top, \ldots, f(x_{m_k}(t))^\top)^\top$, the network (1) can be rewritten as follows:

$$\frac{dX_k(t)}{dt} = F(X_k(t)) + \sum_{l=1}^{n} (A_{kl} \otimes I_d) X_l(t) + U_k(t), \quad k = 1, 2, \ldots, n, \tag{2}$$

where $A_{kl} \in R^{(m_k - m_{k-1}) \times (m_l - m_{l-1})}$ are defined by the block matrix

$$A = \begin{bmatrix} A_{11} & A_{12} & \cdots & A_{1n} \\ A_{21} & A_{22} & \cdots & A_{2n} \\ \cdots & \cdots & \cdots & \cdots \\ A_{n1} & A_{n2} & \cdots & A_{nn} \end{bmatrix}. \tag{3}$$

For convenience, we decompose matrix A into two matrices as follows:

$$A = \overline{A} + \widetilde{A}, \tag{4}$$

where

$$\overline{A} = \left\{\overline{A}_{kl}\right\}_{n \times n} = \left\{\overline{a}_{ij}\right\}_{N \times N} = \begin{cases} 0, & \varphi(i) \neq \varphi(j); \\ a_{ij}, & \varphi(i) = \varphi(j),\ i \neq j; \\ -\sum_{j=1, j \neq i}^{N} \overline{a}_{ij}, & i = j \end{cases} \tag{5}$$

representing the intracluster couplings, and

$$\widetilde{A} = \left\{\widetilde{A}_{kl}\right\}_{n\times n} = \left\{\widetilde{a}_{ij}\right\}_{N\times N} = \begin{cases} 0, & \varphi(i) = \varphi(j),\ i \neq j; \\ a_{ij}, & \varphi(i) \neq \varphi(j); \\ -\sum_{j=1, j\neq i}^{N} \widetilde{a}_{ij}, & i = j \end{cases} \tag{6}$$

representing the intercluster couplings.

The dynamics of the virtual leaders in the oscillator network are described by

$$\dot{s}_k(t) = f\left(s_k(t)\right) - \theta_k(t)\left(s_k(t) - s_1\left(t - \tau_k\right)\right), \quad k = 1, 2, \ldots, n, \tag{7}$$

where $s_k(t)$ is the state variable of the kth virtual leader, τ_k is the time delay, and

$$\theta_k(t) = \begin{cases} \Theta_k, & t \in [mT, (m+\zeta)T); \\ 0, & t \in [(m+\zeta)T, (m+1)T), \end{cases} \tag{8}$$

where Θ_k is a positive constant representing the feedback control gain, $\zeta \in (0, 1)$ is the control width, $k = 1, 2, \ldots, n$, $m = 0, 1, 2, \ldots$. In this paper, we suppose that the time delay $\tau_1 = 0$, which implies that $\dot{s}_1(t) = f(s_1(t))$. Different from the previous result on cluster lag synchronization [23], the leader systems in this paper are not isolated nodes $\dot{s}_k(t) = f(s_k(t))$. Instead, linear control laws are designed for the leader systems to realize cluster-delay synchronization. This paper aims to make the leader of the kth cluster track the trajectory of the leader of the first cluster with a time delay τ_k, $k = 1, \ldots, n$.

Analyzing systems (2) and (7) comprehensively, we design the control inputs for system (2):

$$\begin{aligned} U_k(t) = {} & \theta_k(t)\, \iota_{m_k - m_{k-1}} \otimes \left[s_k(t) - s_1\left(t - \tau_k\right)\right] \\ & - \sum_{l=1}^{n} \left(\widetilde{A}_{kl} \otimes I_d\right) X_l(t) \\ & - \sigma_k \left[X_k(t) - \iota_{m_k - m_{k-1}} \otimes s_1\left(t - \tau_k\right)\right], \end{aligned} \tag{9}$$

where the vector $\iota_{m_k - m_{k-1}} = (1, \ldots, 1)^\top \in R^{m_k - m_{k-1}}$; the constant $\sigma_k \geq 0$ is the feedback control gain; $T > 0$ is the control period; $k = 1, 2, \ldots, n$.

3. Main Results

In this section, we will derive some sufficient conditions for both cluster synchronization and cluster-delay synchronization. Before that, it is necessary to introduce the following assumptions.

Assumption 1. There exists a positive constant δ such that the vector function f satisfies that

$$(x - y)^T \left(f(x) - f(y)\right) \leq \delta (x - y)^T (x - y) \tag{10}$$

for any $x, y \in R^d$.

It has been checked that many well-known chaotic systems, such as cellular neural networks, Lorenz system, Chen system, Rössler system, and Chua's circuit, satisfy Assumption 1 [28, 29].

3.1. Cluster Synchronization Analysis. Now, we first introduce the following definition of both cluster synchronization and cluster-delay synchronization [27].

Definition 2. Define the synchronization errors $e_i(t) = x_i(t) - s_{\varphi(i)}(t)$, $E_k(t) = X_k(t) - \iota_{m_k - m_{k-1}} \otimes s_k(t)$, $E(t) = (E_1^\top(t), \ldots, E_n^\top(t))^\top$, $e_k^\tau(t) = s_k(t) - s_1(t - \tau_k)$, $E^\tau(t) = (e_1^{\tau^\top}(t), \ldots, e_n^{\tau^\top}(t))^\top$. The oscillator network (2)–(7) is said to realize cluster synchronization, if the synchronization errors satisfy

$$\lim_{t\to\infty} \sum_{i=1}^{N} \left\|e_i(t)\right\| = \lim_{t\to\infty} \sum_{k=1}^{n} \left\|E_k(t)\right\| = \lim_{t\to\infty} \left\|E(t)\right\| = 0. \tag{11}$$

The oscillator network (2)–(7) is said to realize cluster-delay synchronization, if the synchronization errors satisfy equality (11) and

$$\lim_{t\to\infty} \sum_{k=2}^{n} \left\|e_k^\tau(t)\right\| = \lim_{t\to\infty} \left\|E^\tau(t)\right\| = 0. \tag{12}$$

The preliminaries above, together with Lyapunov function method, bring us to the following theorem for cluster synchronization, which implies that the $m_k - m_{k-1}$ oscillators in cluster $\mathcal{V}_k$ to synchronize with each other, $k = 1, 2, \ldots, d$.

Theorem 3. *Suppose that Assumption 1 holds; the oscillator network (2)–(7) with the control protocol (9) realizes cluster synchronization if the matrix* $D - (\overline{A} + \overline{A}^\top)/2$ *is negative definite, where* $D = \mathrm{diag}\{(\delta - \sigma_1) I_{m_1 - m_0}, \ldots, (\delta - \sigma_n) I_{m_n - m_{n-1}}\}$.

Proof. Noticing that $E_k(t) = X_k(t) - \iota_{m_k - m_{k-1}} \otimes s_k(t)$, we obtain the error system of the kth cluster as follows:

$$\begin{aligned} \frac{dE_k(t)}{dt} &= \frac{dX_k(t)}{dt} - \iota_{m_k - m_{k-1}} \otimes \frac{ds_k(t)}{dt} \\ &= \left[F\left(X_k(t)\right) - \iota_{m_k - m_{k-1}} \otimes f\left(s_k(t)\right)\right] \\ &\quad + \sum_{l=1}^{n} \left(\overline{A}_{kl} \otimes I_d\right) X_l(t) \\ &\quad - \sigma_k \left[X_k(t) - \iota_{m_k - m_{k-1}} \otimes s_1\left(t - \tau_k\right)\right] \\ &= \left[F\left(X_k(t)\right) - F\left(\iota_{m_k - m_{k-1}} \otimes s_k(t)\right)\right] \\ &\quad + \sum_{l=1}^{n} \left(\overline{A}_{kl} \otimes I_d\right) E_l(t) - \sigma_k E_k(t). \end{aligned} \tag{13}$$

Consider the following Lyapunov function:

$$V_1(t) = \frac{1}{2} \sum_{k=1}^{n} E_k^\top(t)\, E_k(t). \tag{14}$$

The derivative of $V_1(t)$ along the trajectories of the error systems (13) can be calculated as follows:

$$\begin{aligned}\frac{dV_1(t)}{dt} &= \sum_{k=1}^{n} E_k^{\top}(t)\frac{dE_k(t)}{dt} = \sum_{k=1}^{n} E_k^{\top}(t)\\ &\cdot\left[\left(F\left(X_k(t)\right) - F\left(\iota_{m_k-m_{k-1}}\otimes s_k(t)\right)\right)\right.\\ &\left.+\sum_{l=1}^{n}\left(\overline{A}_{kl}\otimes I_d\right)E_l(t) - \sigma_k E_k(t)\right]\\ &\le \sum_{k=1}^{n}\left(\delta-\sigma_k\right)E_k^{\top}(t)E_k(t) + \sum_{l=1}^{n} E_k^{\top}(t)\left(\overline{A}_{kl}\otimes I_d\right)\\ &\cdot E_l(t) = E^{\top}(t)\left[\left(D - \frac{\left(\overline{A}+\overline{A}^{\top}\right)}{2}\right)\otimes I_d\right]E(t).\end{aligned} \tag{15}$$

According to the conditions of Theorem 3 and Lyapunov stability theory, the solutions of the oscillator network satisfy that $\lim_{t\to\infty}\|E_k(t)\| = 0$ for all $k = 1, 2, \ldots, n$. Hence, the oscillator network (2)–(7) with the control protocol (9) realizes cluster synchronization. The proof is completed. □

Noticing that matrix $\overline{A}$ represents the intracluster couplings and matrix $\widetilde{A}$ represents the intercluster couplings, one gets that the results of Theorem 3 is irrelevant to the intercluster couplings. In other words, cluster synchronization can be guaranteed by the intracluster couplings of each cluster, and the intercluster couplings can be chosen arbitrarily.

3.2. Cluster-Delay Synchronization Analysis. Now, we are in a position to carry out the following theorem on cluster-delay synchronization, which implies that the oscillators in the same cluster behave in a synchronous fashion, but oscillators in different clusters follow distinct time evolutions with different time delays.

Theorem 4. *Suppose that Assumption 1 holds, the oscillator network (2)–(7) with the control protocol (9) realizes cluster-delay synchronization if*

(i) *the matrix* $D - (\overline{A} + \overline{A}^{\top})/2$ *is negative definite;*

(ii) *there exists a positive constant* α *such that the matrix* $(\delta + \alpha)I_n - \Theta$ *is negative semidefinite, where* $\Theta = \mathrm{diag}\{\Theta_1, \Theta_2, \ldots, \Theta_n\}$;

(iii) *the constant* $\delta - \delta\zeta - \alpha\zeta \le 0$.

Proof. According to Theorem 3 and condition (i) of Theorem 4, it is easy to prove that

$$\lim_{t\to\infty}\sum_{i=1}^{N}\|e_i(t)\| = \lim_{t\to\infty}\sum_{k=1}^{n}\|E_k(t)\| = \lim_{t\to\infty}\|E(t)\| = 0. \tag{16}$$

Now, we will prove that

$$\lim_{t\to\infty}\sum_{k=2}^{n}\left\|e_k^{\tau}(t)\right\| = \lim_{t\to\infty}\left\|E^{\tau}(t)\right\| = 0. \tag{17}$$

Consider the following Lyapunov function:

$$V_2\left(E^{\tau}(t)\right) = \frac{1}{2}\sum_{k=1}^{n} e_k^{\tau^{\top}}(t)\,e_k^{\tau}(t) = \frac{1}{2}E^{\tau^{\top}}(t)\,E^{\tau}(t). \tag{18}$$

From the oscillator network (2)–(7) with the control protocol (9), it is easy to get the following error system:

$$\begin{aligned}\frac{de_k^{\tau}(t)}{dt} &= \frac{ds_k(t)}{dt} - \frac{ds_1(t-\tau_k)}{dt}\\ &= f\left(s_k(t)\right) - f\left(s_1(t-\tau_k)\right) - \theta_k(t)\,e_k^{\tau}(t),\\ &\qquad k = 1, 2, \ldots, n.\end{aligned} \tag{19}$$

Calculating the derivative of $V_2(E^{\tau}(t))$, one obtains

$$\begin{aligned}\frac{dV_2\left(E^{\tau}(t)\right)}{dt} &= \sum_{k=1}^{n} e_k^{\tau^{\top}}(t)\frac{de_k^{\tau}(t)}{dt} = \sum_{k=1}^{n} e_k^{\tau^{\top}}(t)\\ &\cdot\left[f\left(s_k(t)\right) - f\left(s_1(t-\tau_k)\right) - \theta_k(t)\,e_k^{\tau}(t)\right]\\ &\le \sum_{k=1}^{n}\delta e_k^{\tau^{\top}}(t)\,e_k^{\tau}(t) - \sum_{k=1}^{n}\theta_k(t)\,e_k^{\tau^{\top}}(t)\,e_k^{\tau}(t).\end{aligned} \tag{20}$$

On the interval $t \in [mT, (m+\zeta)T)$, $m = 0, 1, 2, \ldots$, inequality (20) can be reduced to the following form:

$$\begin{aligned}\frac{dV_2\left(E^{\tau}(t)\right)}{dt} &\le \sum_{k=1}^{n}\delta e_k^{\tau^{\top}}(t)\,e_k^{\tau}(t) - \sum_{k=1}^{n}\Theta_k e_k^{\tau^{\top}}(t)\,e_k^{\tau}(t)\\ &= E^{\tau^{\top}}(t)\left[(\delta+\alpha)I_n - \Theta\right]\otimes I_d E^{\tau}(t)\\ &\quad - \alpha E^{\tau^{\top}}(t)\,E^{\tau}(t) \le -2\alpha V_2\left(E^{\tau}(t)\right).\end{aligned} \tag{21}$$

Integrating the above inequality over the interval $[mT, (m+\zeta)T)$, one has

$$V_2\left(E^{\tau}(t)\right) \le V_2\left(E^{\tau^{\top}}(mT)\right)e^{-2\alpha(t-mT)}. \tag{22}$$

On the interval $t \in [(m+\zeta)T, (m+1)T)$, the inequality (20) can be reduced to the following form:

$$\frac{dV_2\left(E^{\tau}(t)\right)}{dt} \le \sum_{k=1}^{n}\delta e_k^{\tau^{\top}} e_k^{\tau} \le 2\delta V_2\left(E^{\tau}(t)\right), \tag{23}$$

which is equivalent to

$$V_2\left(E^{\tau}(t)\right) \le V_2\left(E^{\tau}\left((m+\zeta)T\right)\right)e^{2\delta(t-(m+\zeta)T)}. \tag{24}$$

Now, we will prove the following inequality by mathematical induction on parameter m:

$$\begin{aligned}V_2\left(E^{\tau}(t)\right) &\le V_2\left(E^{\tau}(0)\right)e^{2m(\delta+\alpha)(1-\zeta)T-2\alpha t},\\ &\qquad mT \le t < (m+\zeta)T;\\ V_2\left(E^{\tau}(t)\right) &\le V_2\left(E^{\tau}(0)\right)e^{2\delta t-2(m+1)(\delta+\alpha)\zeta T},\\ &\qquad (m+\zeta)T \le t < (m+1)T;\\ V_2\left(E^{\tau}\left((m+1)T\right)\right) &\le V_2\left(E^{\tau}(0)\right)e^{2(m+1)(\delta-\delta\zeta-\alpha\zeta)T}.\end{aligned} \tag{25}$$

Firstly, we will show the validity of the base case. In case of parameter $m = 0$, inequalities (22) and (24) can be reduced as follows:

$$\begin{aligned} &V_2\left(E^{\tau}(t)\right) \le V_2\left(E^{\tau}(0)\right) e^{-2\alpha t}, \quad 0 \le t < \zeta T, \\ &V_2\left(E^{\tau}(t)\right) \le V_2\left(E^{\tau}(\zeta T)\right) e^{2\delta(t-\zeta T)} \\ &\qquad \le V_2\left(E^{\tau}(0)\right) e^{2\delta t - 2(\alpha+\delta)\zeta T}, \quad \zeta T \le t < T, \end{aligned} \tag{26}$$

where

$$\begin{aligned} V_2\left(E^{\tau}(\zeta T)\right) &\le V_2\left(E^{\tau}(0)\right) e^{-2\alpha\zeta T}, \\ V_2\left(E^{\tau}(T)\right) &\le V_2\left(E^{\tau}(0)\right) e^{2\delta T - 2(\alpha+\delta)\zeta T}. \end{aligned} \tag{27}$$

It can be concluded from the above two inequalities that inequality (25) holds for $m = 0$.

Secondly, assuming that inequality (25) is correct for $m = k$, we will show its correctness for $m = k + 1$. In fact, if $m = k + 1$, inequalities (22) and (24) can be reduced as follows:

$$\begin{aligned} &V_2\left(E^{\tau}(t)\right) \le V_2\left(E^{\tau^{\top}}((k+1)T)\right) e^{-2\alpha(t-(k+1)T)} \\ &\qquad \le V_2\left(E^{\tau}(0)\right) e^{2(k+1)(\delta+\alpha)(1-\zeta)T - 2\alpha t}, \\ &\qquad\qquad (k+1)T \le t < (k+1+\zeta)T, \\ &V_2\left(E^{\tau}(t)\right) \le V_2\left(E^{\tau}((k+1+\zeta)T)\right) e^{2\delta(t-(k+1+\zeta)T)} \\ &\qquad \le V_2\left(E^{\tau}(0)\right) e^{2\delta t - 2(k+2)(\delta+\alpha)\zeta T}, \\ &\qquad\qquad (k+1+\zeta)T \le t < (k+2)T, \end{aligned} \tag{28}$$

where

$$\begin{aligned} &V_2\left(E^{\tau}((k+1+\zeta)T)\right) \\ &\quad \le V_2\left(E^{\tau}(0)\right) e^{2(k+1)(\delta-\delta\zeta-\alpha\zeta)T - 2\alpha\zeta T}, \\ &V_2\left(E^{\tau}((k+2)T)\right) \le V_2\left(E^{\tau}(0)\right) e^{2(k+2)(\delta-\delta\zeta-\alpha\zeta)T}. \end{aligned} \tag{29}$$

Then, based on the principle of mathematical induction, we declare that inequality (25) holds for $m = 0, 1, 2, \ldots$.

Combining the monotonic property of the exponential function and the inequality (25), we obtain that

$$V_2\left(E^{\tau}(t)\right) \le V_2\left(E^{\tau}(0)\right) e^{2m(\delta-\delta\zeta-\alpha\zeta)T}. \tag{30}$$

Noticing condition (iii) of Theorem 4, we can derive that cluster synchronization of the controlled network (2)–(7) is achieved. Hence the proof is completed. □

To make Theorem 4 more applicable, we give the following corollary.

Corollary 5. *Suppose that Assumption 1 holds, the oscillator network (2)–(7) with the control protocol (9) realizes cluster-delay synchronization if*

(i) *the constants* $\delta - \sigma_k - \overline{\lambda}_k < 0$, *where* $\overline{\lambda}_k$ *are the eigenvalues of the symmetric matrix* $(\overline{A} + \overline{A}^{\top})/2$, $k = 1, 2, \ldots, n$;

(ii) *there exists a positive constant* α *satisfying that*

$$\left(\frac{1}{\zeta} - 1\right)\delta \le \alpha \le \Theta_k - \delta, \quad k = 1, 2, \ldots, n. \tag{31}$$

It is worth noting that condition (ii) can be simplified into an inequality $\le \Theta_k\zeta$, $k = 1, 2, \ldots, n$. The proof of this corollary is not particularly difficult and will not be given here.

3.3. Comparative Studies with Previous Results. In [23], cluster lag synchronization of the undirected networks (1) has been studied by using the intermittent pinning-control method. Enlightened by the design schemes of the controllers with intermittent effect, we proposed the leader-following system (2)–(7) and designed the intermittent pinning controller (9) to realize cluster-delay synchronization.

In order to verify the usefulness of the obtained controller with respect to the previous controllers, we carry out some comparative studies to show the differences from two aspects. The first difference is the definition of cluster lag synchronization with respect to the time delays τ_{φ_i}, which implies that there holds $\lim_{t\to+\infty}\|x_i(t) - s_{\varphi_i}(t - \tau_{\varphi_i})\| = 0$, where $\dot{s}_{\varphi_i}(t - \tau_{\varphi_i}) = f_{\varphi_i}(s_{\varphi_i}(t - \tau_{\varphi_i}))$, $i = 1, 2, \ldots, N$. In this paper, we proposed the definition of cluster-delay synchronization (Definition 2) in two steps and developed a series of sufficient conditions for both cluster synchronization and cluster-delay synchronization. The second difference is the design schemes of the controllers with intermittent effect. In [23], Wu and Fu designed N controllers for each oscillator as follows:

$$u_i(t) = \begin{cases} -\varepsilon\theta_i(t)\left(x_i(t) - s\left(t - \tau_{\varphi_i}\right)\right) - \varepsilon\sum_{j=1}^{N} c_{ij}\Gamma s\left(t - \tau_{\varphi_i}\right), & i \in \overline{\mathscr{V}}_{\varphi_i} \\ 0, & i \in \mathscr{V}_{\varphi_i} - \overline{\mathscr{V}}_{\varphi_i}, \end{cases} \tag{32}$$

where the intermittent feedback control gain $\theta_i(t)$ was defined by (8). In this paper, we designed n controllers for each cluster in (9) and simplified the complexity of the previous design schemes to some extent.

Based on the aforementioned comparison and analysis, we show the characteristics and advantages of the proposed method with respect to the previous controllers. In our view, the proposed method might serve different purposes in practice.

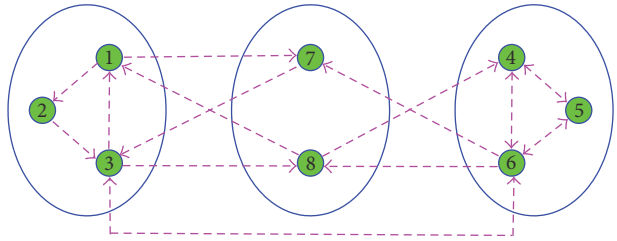

Figure 1: Topology structure of a directed network consisting of 8 nodes, which are divided into 3 clusters. If there is a directed link from node j to node i ($j \neq i$), then $a_{ij} = 1$, otherwise $a_{ij} = 0$.

4. Numerical Simulations

In this section, we carry out some numerical simulations to illustrate the effectiveness of the theoretical results obtained in this paper.

4.1. Numerical Example 1. At first, we consider a directed complex network consisting of 8 nodes separated into three different clusters, the topology of which is shown in Figure 1.

Define connectivity matrix A as an asymmetric matrix with zero row-sums, and the off-diagonal elements $a_{ij} = 1$ if the jth node can receive information from the ith node for $j \neq i$; otherwise, define $a_{ij} = 0$. Choose the node dynamics of the network as the well-known Chua oscillators; then the oscillator network (2)–(7) with the control protocol (9) can be rewritten as follows:

$$\begin{aligned}
\dot{x}_i &= -Dx_i + Tg\left(x_i\right) + \sum_{j=1}^{8} a_{ij}x_j + u_i\left(t\right), \\
u_i\left(t\right) &= \theta_{\varphi(i)}\left(t\right)\left[s_{\varphi(i)}\left(t\right) - s_1\left(t - \tau_{\varphi(i)}\right)\right] - \sum_{j=1}^{8} \widetilde{a}_{ij}x_j \\
&\quad - \sigma_{\varphi(i)}\left[x_i\left(t\right) - s_1\left(t - \tau_{\varphi(i)}\right)\right], \\
\dot{s}_{\varphi(i)}\left(t\right) &= f\left(s_{\varphi(i)}\left(t\right)\right) \\
&\quad - \theta_{\varphi(i)}\left(t\right)\left[s_{\varphi(i)}\left(t\right) - s_1\left(t - \tau_{\varphi(i)}\right)\right],
\end{aligned} \tag{33}$$

where $x_i \in R^3$, $D = I_3$, $g(x_i) = (g(x_{i1}), g(x_{i2}), g(x_{i3}))^\top$, $i = 1, 2, \ldots, 8$, $g(s) = (|s+1| - |s-1|)/2$, and

$$T = \begin{pmatrix} 1.25 & -3.2 & -3.2 \\ -3.2 & 1.1 & -4.4 \\ -3.2 & 4.4 & 1.0 \end{pmatrix}. \tag{34}$$

It is easy to derive that the nonlinear function f in system (33) satisfies Assumption 1 by choosing the matrix $\Delta = 5.5685I_3$. Then, one can choose $\delta = 5.5685$, $\sigma_1 = 10$, $\sigma_2 = 12$, $\sigma_3 = 14$ such that condition (i) of Theorem 4 holds, and choose $\alpha = 4.4$, $\Theta_1 = \Theta_2 = \Theta_3 = 10$ such that condition (ii) holds. By taking $T = 1$, it can be verified that the feedback control width $\zeta = 0.557$ satisfies condition (iii) of Theorem 4.

Choose the initial conditions randomly; Figure 2 is plotted to show the evolutions of the state variable of the 8 nodes and the cluster errors. From (a), (b), and (c), one can see that the evolutions of the nodes in the same cluster synchronize with each other. And (d) shows more clearly that the cluster errors $e_i(t) = x_i(t) - s_{\varphi(i)}(t)$ tend to zero. Therefore, Figure 2 illustrates that cluster-delay synchronization is achieved under the conditions of Theorem 4.

Next, we keep all the parameters unchanged except the feedback control gains decreasing from $\sigma_1 = 10$, $\sigma_2 = 12$, $\sigma_3 = 14$ to $\sigma_1 = \sigma_2 = \sigma_3 = 2$. Then the conditions of Theorems 3 and 4 cannot be satisfied. The time evolutions of the Chua oscillators $x_{i1}(t), x_{i2}(t), x_{i3}(t)$ $(i = 1, 2, \ldots, 8)$ in the network (33) are plotted in Figure 3. One can see clearly that the evolutions of nodes 7 and 8 do not synchronize with each other though they are in the same cluster. Therefore, neither cluster synchronization nor cluster-delay synchronization is achieved.

4.2. Numerical Example 2. In the following numerical simulations, we consider an undirected network consisting of 100 $x_{\cdot 2}$-coupled Lorenz systems separated into two clusters. The network topology is shown in Figure 4. If there is an undirected link between node j and node i ($j \neq i$), then $a_{ij} = a_{ji} = 1$; otherwise $a_{ij} = a_{ji} = 0$.

The uncoupled Lorenz system $\dot{x}_i = f(x_i, t)$ is described by

$$\begin{aligned}
\dot{x}_{i1} &= \sigma\left(x_{i2} - x_{i1}\right), \\
\dot{x}_{i2} &= rx_{i1} - x_{i2} - x_{i1}x_{i3}, \\
\dot{x}_{i3} &= -bx_{i3} + x_{i1}x_{i2},
\end{aligned} \tag{35}$$

where $\sigma = 10$, $r = 28$, $b = 8/3$. According to [30], there exists a positive constant δ such that Assumption 1 holds. Then, one can choose appropriate values for other parameters in the network (2)–(7) with the controller (9) such that the conditions of Theorem 4 are satisfied. The time evolutions of the 100 Lorenz systems are shown in Figure 5. As indicated by Figure 5, the first fifty nodes fall into the same cluster, and the rest of the nodes fall into another cluster. All the nodes in the same cluster behave in the same synchronous fashion, but nodes in different clusters follow distinct time evolutions with time delays. Therefore, cluster-delay synchronization has been realized in the network consisting of 100 $x_{\cdot 2}$-coupled Lorenz systems.

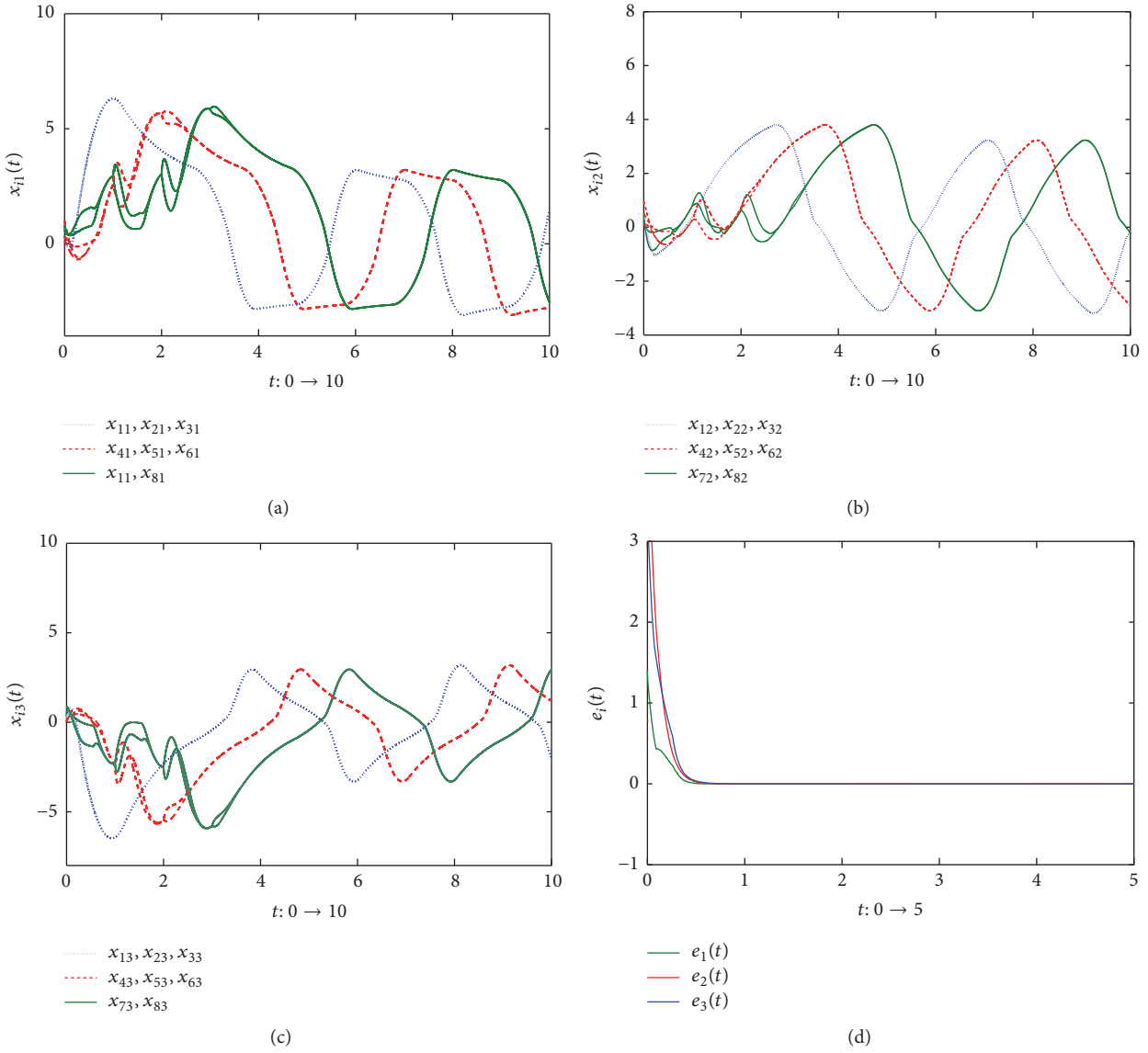

FIGURE 2: Cluster-delay synchronization of the network (33). (a), (b), and (c) show the time evolutions of the state variable of the 8 nodes splitting into three different clusters, and (d) describes the time evolutions of the cluster errors.

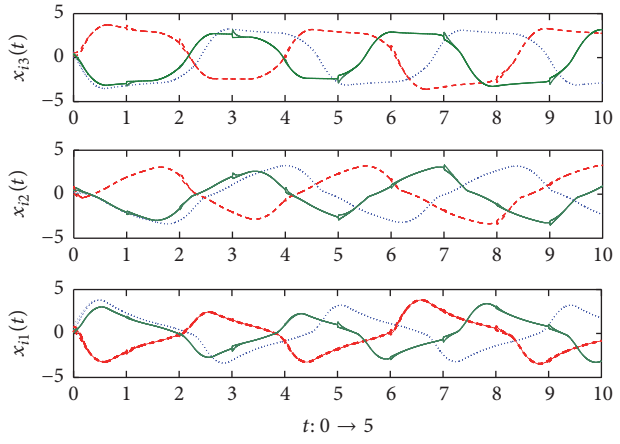

FIGURE 3: Time evolutions of the Chua oscillators $x_{i1}(t)$, $x_{i2}(t)$, $x_{i3}(t)$ $(i = 1, 2, \ldots, 8)$ in the network (33) with the feedback control gains $\sigma_1 = \sigma_2 = \sigma_3 = 2$.

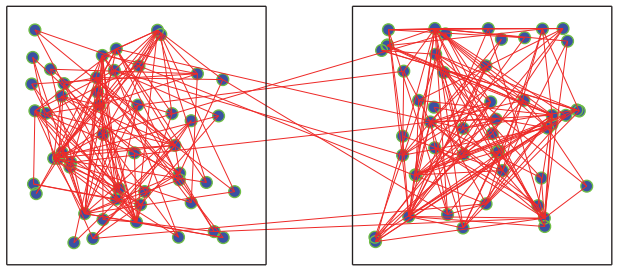

Figure 4: Topology structure of the undirected network consisting of 100 nodes, which are separated into two equal clusters. If there is an undirected link between node j and node i ($j \neq i$), then $a_{ij} = a_{ji} = 1$, otherwise $a_{ij} = a_{ji} = 0$.

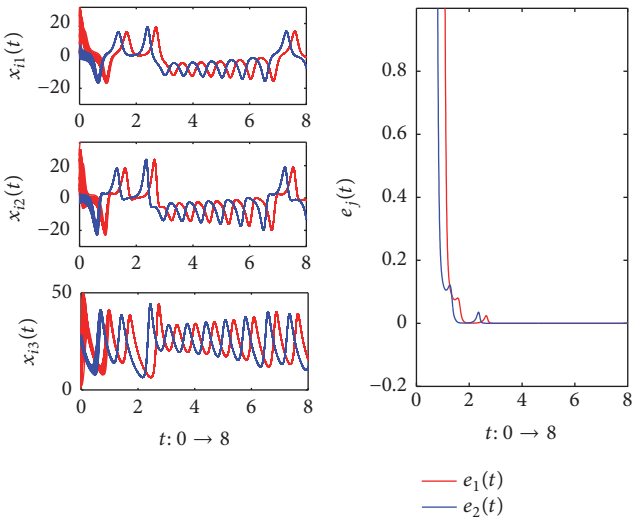

Figure 5: Time evolutions of the $x_{\cdot 2}$-coupled Lorenz systems $x_{i1}(t)$, $x_{i2}(t)$, $x_{i3}(t)$ ($i = 1, 2, \ldots, 100$) in the network (2)–(7) with the controller (9).

5. Conclusions

In this paper, the cluster-delay synchronization problem of a directed network with cluster structure has been discussed. First, a control protocol with intermittent effect has been presented to realize cluster synchronization via periodically intermittent control. The proposed control methods can be applied to discuss many real-world networks with intermittent effect. Second, we extended the criterion on cluster synchronization to the cluster-delay synchronization problem, which implies that the oscillators in the following clusters track the trajectory of those in the leader clusters with different time delays. Finally, we presented two delayed dynamical networks as illustrative examples and carry out some simulated results to show the feasibility of the proposed control methods.

Conflicts of Interest

The authors declare that they have no conflicts of interest regarding the publication of this paper.

Acknowledgments

This work was supported by NNSF of China (11447005, 11562006, 61703193, and 61663006), Jiangsu Planned Projects for Postdoctoral Research Funds (1701017A), NSF of Shandong Province (ZR2016JL021), NSF of Guangxi Province (2016GXNSFDA380031), the Key Research and Development Project of Shandong Province of China (2017GGX10143), and the Key Research and Development Project of Linyi City of China (2017GGH009).

References

[1] J. Guckenheimer, "Sensitive dependence to initial conditions for one-dimensional maps," *Communications in Mathematical Physics*, vol. 70, no. 2, pp. 133–160, 1979.

[2] L. M. Pecora and T. L. Carroll, "Synchronization in chaotic systems," *Physical Review Letters*, vol. 64, no. 8, pp. 821–824, 1990.

[3] L. M. Pecora and T. L. Carroll, "Master stability functions for synchronized coupled systems," *Physical Review Letters*, vol. 80, no. 10, pp. 2109–2112, 1998.

[4] V. N. Belykh, I. V. Belykh, and M. Hasler, "Connection graph stability method for synchronized coupled chaotic systems," *Physica D: Nonlinear Phenomena*, vol. 195, no. 1-2, pp. 159–187, 2004.

[5] W. Lu and T. Chen, "New approach to synchronization analysis of linearly coupled ordinary differential systems," *Physica D: Nonlinear Phenomena*, vol. 213, no. 2, pp. 214–230, 2006.

[6] C.-D. Yang, J.-L. Qiu, and H.-B. He, "Exponential synchronization for a class of complex spatio-temporal networks with space-varying coefficients," *Neurocomputing*, vol. 151, pp. 401–407, 2015.

[7] Y.-P. Luo, L. Shu, and B.-F. Zhou, "Global exponential synchronization of nonlinearly coupled complex dynamical networks with time-varying coupling delays," *Complexity*, vol. 2017, Article ID 7850958, 2017.

[8] Z. Wu and X. Fu, "Cluster projective synchronization between community networks with nonidentical nodes," *Physica A: Statistical Mechanics and its Applications*, vol. 391, no. 23, pp. 6190–6198, 2012.

[9] J. Guan, "Adaptive modified generalized function projection synchronization between integer-order and fractional-order chaotic systems," *Optik - International Journal for Light and Electron Optics*, vol. 127, no. 10, pp. 4211–4216, 2016.

[10] H. Liu, W. Sun, and G. Al-mahbashi, "Parameter identification based on lag synchronization via hybrid feedback control in uncertain drive-response dynamical networks," *Advances in Difference Equations*, vol. 2017, no. 1, article no. 122, 2017.

[11] J. Zhang, Z. Ma, and G. Chen, "Robustness of cluster synchronous patterns in small-world networks with inter-cluster co-competition balance," *Chaos: An Interdisciplinary Journal of Nonlinear Science*, vol. 24, no. 2, article no. 023111, 2014.

[12] A. Hu, J. Cao, M. Hu, and L. Guo, "Cluster synchronization in directed networks of non-identical systems with noises via random pinning control," *Physica A: Statistical Mechanics and its Applications*, vol. 395, pp. 537–548, 2014.

[13] C. Yang, J. Cao, T. Huang, J. Zhang, and J. Qiu, "Guaranteed cost boundary control for cluster synchronization of complex spatio-temporal dynamical networks with community structure," *Science China Information Sciences*, vol. 61, no. 5, article no. 052203, pp. 1–13, 2018.

[14] S. Cai, Q. Jia, and Z. Liu, "Cluster synchronization for directed heterogeneous dynamical networks via decentralized adaptive intermittent pinning control," *Nonlinear Dynamics*, vol. 82, no. 1-2, pp. 689–702, 2015.

[15] H. Su, Z. Rong, M. Z. Q. Chen, X. Wang, G. Chen, and H. Wang, "Decentralized adaptive pinning control for cluster synchronization of complex dynamical networks," *IEEE Transactions on Systems, Man, and Cybernetics, Part B: Cybernetics*, vol. 43, no. 1, pp. 394–399, 2013.

[16] J. Lu, J. Kurths, J. Cao, N. Mahdavi, and C. Huang, "Synchronization control for nonlinear stochastic dynamical networks: Pinning impulsive strategy," *IEEE Transactions on Neural Networks and Learning Systems*, vol. 23, no. 2, pp. 285–292, 2012.

[17] J. Guan and K. Wang, "Sliding mode control and modified generalized projective synchronization of a new fractional-order chaotic system," *Mathematical Problems in Engineering*, vol. 2015, Article ID 941654, 2015.

[18] W. Yu, G. Chen, J. Lu, and J. Kurths, "Synchronization via pinning control on general complex networks," *SIAM Journal on Control and Optimization*, vol. 51, no. 2, pp. 1395–1416, 2013.

[19] R. Rakkiyappan and N. Sakthivel, "Cluster synchronization for T-S fuzzy complex networks using pinning control with probabilistic time-varying delays," *Complexity*, vol. 21, no. 1, pp. 59–77, 2015.

[20] H.-X. Hu, Q. Xuan, W. Yu, C.-G. Zhang, and G. Xie, "Second-order consensus for heterogeneous multi-agent systems in the cooperation–competition network: a hybrid adaptive and pinning control approach," *Nonlinear Analysis: Hybrid Systems*, vol. 20, pp. 21–36, 2016.

[21] X. Chen, J. H. Park, J. Cao, and J. Qiu, "Adaptive synchronization of multiple uncertain coupled chaotic systems via sliding mode control," *Neurocomputing*, vol. 273, pp. 9–21, 2018.

[22] S. Cai, P. Zhou, and Z. Liu, "Pinning synchronization of hybrid-coupled directed delayed dynamical network via intermittent control," *Chaos: An Interdisciplinary Journal of Nonlinear Science*, vol. 24, no. 3, Article ID 033102, 2014.

[23] Z. Wu and X. Fu, "Cluster lag synchronisation in community networks via linear pinning control with local intermittent effect," *Physica A: Statistical Mechanics and its Applications*, vol. 395, pp. 487–498, 2014.

[24] J. Feng, P. Yang, and Y. Zhao, "Cluster synchronization for nonlinearly time-varying delayed coupling complex networks with stochastic perturbation via periodically intermittent pinning control," *Applied Mathematics and Computation*, vol. 291, pp. 52–68, 2016.

[25] C. Yu, J. Qin, and H. Gao, "Cluster synchronization in directed networks of partial-state coupled linear systems under pinning control," *Automatica*, vol. 50, no. 9, pp. 2341–2349, 2014.

[26] W. Sun, S. Wang, and J. Zhang, "Counting spanning trees in prism and anti-prism graphs," *Journal of Applied Analysis and Computation*, vol. 6, no. 1, pp. 65–75, 2016.

[27] Z. Ma, Y. Wang, and X. Li, "Cluster-delay consensus in first-order multi-agent systems with nonlinear dynamics," *Nonlinear Dynamics*, vol. 83, no. 3, pp. 1303–1310, 2016.

[28] T. Chen, X. Liu, and W. Lu, "Pinning complex networks by a single controller," *IEEE Transactions on Circuits and Systems I: Regular Papers*, vol. 54, no. 6, pp. 1317–1326, 2007.

[29] Q. Song and J. Cao, "On pinning synchronization of directed and undirected complex dynamical networks," *IEEE Transactions on Circuits and Systems I: Regular Papers*, vol. 57, no. 3, pp. 672–680, 2010.

[30] J.-B. Zhang, Z.-J. Ma, and G. Zhang, "Control schemes for synchronizing two subnetworks with weak couplings," *Chinese Physics B*, vol. 23, no. 1, Article ID 010507, 2013.

Hindawi
Complexity
Volume 2018, Article ID 4283634, 17 pages
https://doi.org/10.1155/2018/4283634

Research Article

Immersive Technology for Human-Centric Cyberphysical Systems in Complex Manufacturing Processes: A Comprehensive Overview of the Global Patent Profile Using Collective Intelligence

Usharani Hareesh Govindarajan[1], **Amy J. C. Trappey**[2] **and Charles V. Trappey**[3]

[1]*Department of Industrial Engineering and Engineering Management, International Intercollegiate Ph.D. Program, National Tsing Hua University, Hsinchu, Taiwan*
[2]*Department of Industrial Engineering and Engineering Management, National Tsing Hua University, Hsinchu, Taiwan*
[3]*Department of Management Science, National Chiao Tung University, Hsinchu, Taiwan*

Correspondence should be addressed to Amy J. C. Trappey; trappey@ie.nthu.edu.tw

Received 13 September 2017; Revised 19 December 2017; Accepted 9 January 2018; Published 8 February 2018

Academic Editor: Peter Galambos

Immersive technology for human-centric cyberphysical systems includes broad concepts that enable users in the physical world to connect with the cyberworld with a sense of immersion. Complex systems such as virtual reality, augmented reality, brain-computer interfaces, and brain-machine interfaces are emerging as immersive technologies that have the potential for improving manufacturing systems. Industry 4.0 includes all technologies, standards, and frameworks for the fourth industrial revolution to facilitate intelligent manufacturing. Industrial immersive technologies will be used for smart manufacturing innovation in the context of Industry 4.0's human machine interfaces. This research provides a thorough review of the literature, construction of a domain ontology, presentation of patent metatrend statistical analysis, and data mining analysis using a technology function matrix and highlights technical and functional development trends using latent Dirichlet allocation (LDA) models. A total of 179 references from the IEEE and IET databases and 2,672 patents are systematically analyzed to identify current trends. The paper establishes an essential foundation for the development of advanced human-centric cyberphysical systems in complex manufacturing processes.

1. Introduction

Industry 4.0 (I4.0) is the latest standard for data and computation oriented advanced manufacturing [1, 2]. The emphasis is placed on the deployment of technologies such as cyberphysical systems (CPS), Internet of Things (IoT), and big data analytics to achieve cost and quality benefits in the manufacturing sectors. The deployment helps overcome issues such as scalability, distribution, timeliness, reliability, security, and fault tolerance. The wide array of differential and affordable sensors at the physical level, the increased processing at the computational level, and the variety of data available for analytics at the data level form a three-pillar foundation for the transition from Industry 1.0 to Industry 4.0 [3–8]. Table 1 shows the industrial evolution transition that leads to technology shifts from Industry 1.0 to the Industry 4.0 [9]. Further advances from the basic user interface (UI) to VR-enabled CPS are explained in [10].

The current generation of products has short lifespans due to dynamically changing consumer demand. When coupled with the need for increased product quality and increasing labor costs for mass customization, smart factories become the goal of I4.0 [3]. In principle, CPS gives industrial objects microintelligence. IoT provides the ability for things to connect to the Internet and to combine big data analytic solutions to optimize production systems with continuous learning capabilities. Immersive technologies help visualize the data and actions in real-time facilitating dynamic

Table 1: Technology evolution from Industry 1.0 to Industry 4.0.

Time	Evolutional transition	Defining technology
1800s	Industry 1.0	Mechanical manufacturing
1900s	Industry 2.0	Assembly line (mass production)
1970	Industry 3.0	Robotic manufacturing (flexible manufacturing)
2010	Industry 3.5	Cyber physical systems
2012 Forward	Industry 4.0	Virtual manufacturing

responses to demand [11]. Immersive technologies create a human-centric virtual world where humans and machines interact seamlessly.

Immersive technologies provide an environment for objects that are otherwise virtual in nature through the integration of vision, sound, and tactile feedback [12]. There are three levels for immersive technologies [13]. The nonimmersive level is a desktop computer experience where the virtual environment is generated without the need for specialized hardware. The semi-immersive level uses elements of the real world to construct virtual reality applications for applications such as construction modeling, flight simulators, and robotic navigation. The user navigates a representation of themselves within the virtual environment. The fully immersive or neural-direct mode achieves the highest level of virtual reality. This level provides an immersion into the virtual world where the human brain is directly interlinked to the database system and the viewer's current orientation and position in the virtual world are experienced as it unfolds.

This research is a continuation of earlier research in the area of Industry 4.0 [14], industrial CPS, and IoT linking towards human-centric Industry 4.0 [15, 16]. The research objective is to integrate and propagate industrial immersive technologies (IIT). The study provides technical specifications and an ontology for IIT. Quantitative and qualitative analyses of technical publications and patents form the basis for the current IIT development. The datasets for analytics are extracted from global governing bodies including the Institute of Electrical and Electronic Engineers (IEEE), the International Organization for Standardization (ISO), the Institution of Engineering and Technology (IET), the International Electrotechnical Commission (IEC), the Advancement of Medical Instrumentation (AMI), the United States Patent and Trademark Office (USPTO), the World Intellectual Property Organization (WIPO), and the Guobiao Standards (Standardization Administration of China, GB). The research findings and analysis identify market potential by outlining growth benefits for embedding immersive technologies into advanced manufacturing.

2. Domain Definition and Motivation

The domain of this research includes virtual reality (VR), augmented reality (AR), and brain-machine interface (BMI) that is interchangeable referred to as brain-computer interfaces (BCI). Background studies show brain research increasing in the virtual reality area [5, 10, 11, 13, 17–20]. The motivation for this research comes from an immersive technology background review covering IEEE and IET online databases. The methodology developed in this research is generic; additional literature databases can be added to enhance the comprehensive background study. The review points towards BMI related research which will act as an enabler to translate virtual world interactions into real world actions. The background information helps form hypotheses that BMI will play a key role in the next industrial revolution. Milgram's reality-virtuality continuum is remodeled in Figure 1 [21]. This assumption is supported by Lexinnova's generic VR patent landscape analysis report [22]. The domain definitions are explained in the following paragraphs.

VR provides innovative ways for designers and engineers to interact and collaborate which accelerates creativity and productivity. VR is a host of technologies that mimic interactive 3D environments. This virtual world is designed so that users find it hard to distinguish the differences between real and virtual. The VR world can be created by wearing VR-enabled helmets or goggles [23]. Users see events from all angles in immersion and can manipulate virtual elements or constructs in the virtual world.

Augmented reality (AR) combines Mixed Reality (MR) or Substitutional Reality (SR) where the virtual world and the real world are blended in the immersive settings. AR helps designers and developers create images within applications that blend elements of the real world. Users are able to interact with real world virtual content and make distinctions [23]. The brain-machine interface is a framework that helps to create a communication channel between the human brain and the machine. There are three categories, that is, invasive, semi-invasive, and noninvasive BMIs. Invasive BMIs are microelectrode arrays surgically placed into the cortex area of the brain. Semi-invasive BMIs are electrodes placed on the exposed surface of the brain using electrocorticography (ECoG). Noninvasive BMIs use sensors and circuits placed on the scalp to measure the electrical potentials produced by the brain electroencephalography and the magnetic fields of the brain called magnetoencephalography. Noninvasive BMI using electroencephalography shows significant advancements in signals and systems [11]. Steady-state visually evoked potentials are based on the brains electrical signals generated when the retina is excited by a visual stimulus. This technique is preferred in brain interfacing research because of good signal-to-noise ratio [24]. The focus of our current research is an evaluation of noninvasive BMI, which is viewed as the technical evolution of VR and AR which enables users to translate action conceived in the virtual world into actions in the real world.

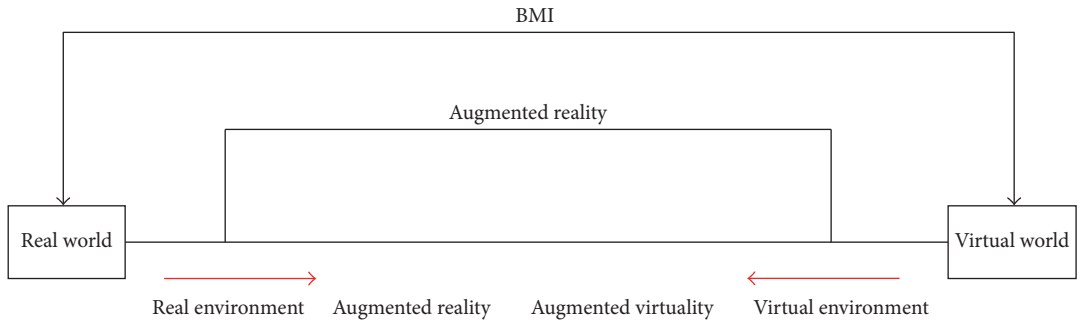

Figure 1: Milgram's reality-virtuality continuum extended.

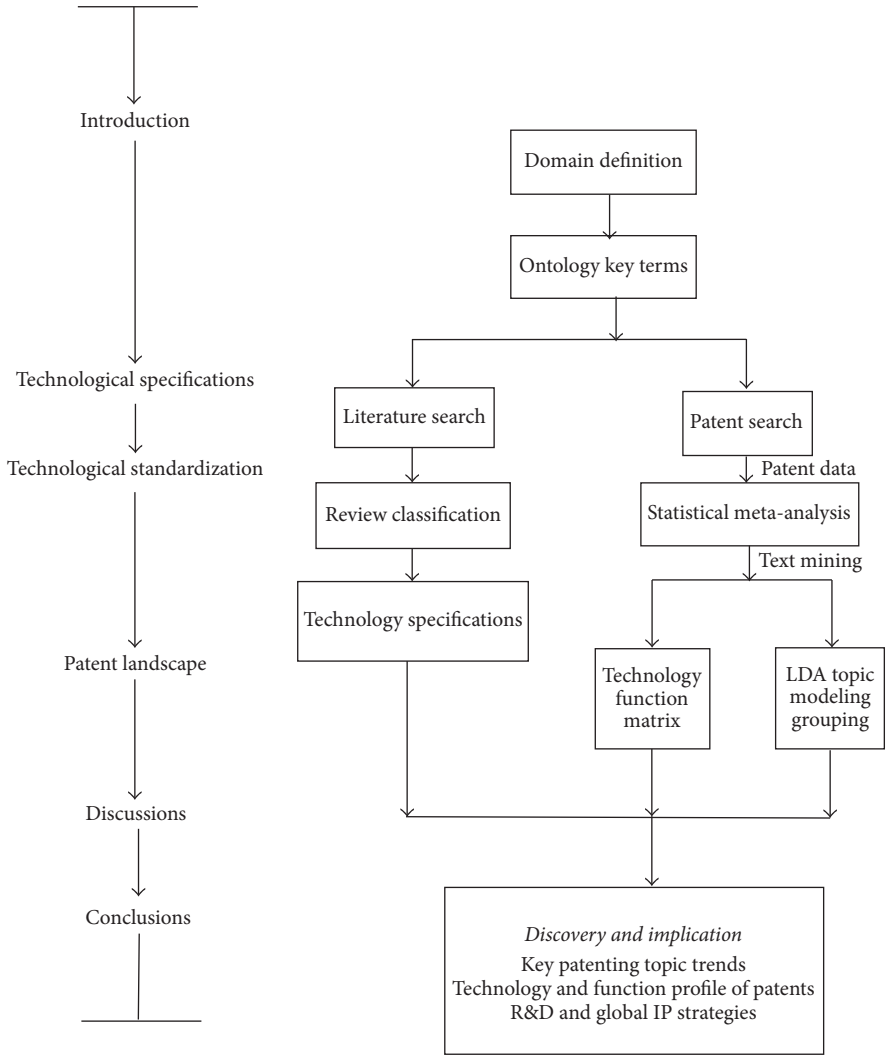

Figure 2: The research flow of a comprehensive IIT overview.

3. Research Methodology and Structure

A systematic review cross-references technical publications and essential patents. The detailed methodology is presented as a research structural flow in Figure 2. The domain definition is the primary building block for this research and reflects the current state of the science. A principal domain technology review (for domain definition) is followed by key term identification and ontology generation. The domain ontology and schema key terms serve as query input for further literature and patent searches. The result of query execution is a high volume of publication and

patent data. The publication data is manually reviewed, classified, and organized on the basis of citation count. This approach helps ensure high coverage of publications related to the current state of IIT. The patent documents are text and data mined, using computer-assisted algorithms, to depict the underlying patent landscape. The results are cross-referenced to improve review accuracy. Further, the results act as input to identifying key technical development trends.

The goal of this research is to learn the structure and opportunities for technology, standards, and intellectual property in the domain of IIT. The methodology begins with domain definition to identify related terms. The domain scope considered for this research is immersive technology in industries and manufacturing. The domain definition is followed by the literature review and the creation of the key term corpus. The IEEE and IET web explorer is used as the search platform to collect literature and key terms and the review are based on the order of citations in descending order. A top-down and bottom-up approach is used to build the key term corpus, organize technological specifications, and create a domain ontology. The ontology is enhanced iteratively every time a relevant key term is identified. The ontology generated is tested and refined using expert review. A patent search is executed using intellectual property search interfaces on the web. Conventional analysis transforms patent volume information into basic inferences such as top assignees and patent codes. The cross-referencing of these results helps validate the direction of research. Further, the analysis uses a technology function matrix (TFM) and latent Dirichlet allocation (LDA) to model IIT patent groupings.

A TFM is a patent map that helps visualize quantitative patent information with respect to the technical and functional features in the patent landscape. TFM consists of key technology terms on one axis and key function terms on another. Normalized Term Frequency (NTF) values are calculated for the key terms. The higher the NTF value, the more important the term. A one hundred key term limit is applied to each term library to ensure accuracy. The patent text mining is executed where the frequencies of terms in each patent are used to calculate the NTF value. The patent document NTF vector is compared with the term libraries NTF vector to determine if the patent belongs to a specific technology or function and assigned to the corresponding cell in the TF matrix. The final TFM is ready when all patents in the patent dataset are fully iterated.

Topic modeling is a statistical approach for finding topics that occur in an archived corpus. LDA is an unsupervised algorithmic approach for proficient information examination [25]. Topic modeling is utilized widely in numerous industries for different mining functions [26–32]. The results are used to formulate business objectives and core strategies where understanding patent dynamics are beneficial. LDA application allows identification of current industry trends and emerging applications useful for additional research and commercialization. A consistency check is performed by cross-referencing technology specifications with the patent analytics results.

4. Immersive Technology Ontology and Key Terminologies

Ontology is a collection of terms in a domain linked to visualize properties, relationships, and associations. An ontology structures domain knowledge, enables reuse of domain knowledge, and makes domain assumptions explicit [33]. The technology review combined with expert evaluation is used to generate the ontology represented in Figure 3. Since many subtopics in VR and AR are highly correlated, they are merged into one technology group. This approach increases query performance and reduces redundancy. There are some abbreviations commonly applied as the domain terminologies. The following abbreviations used to represent the ontology schema for IIT are shown in Figure 3:

(1) 3D: three-dimensional space

(2) EEG: electroencephalogram

(3) SBCI: self-paced brain-computer interface

(4) CNC: computer numerical control

(5) PLC: programmable logic controller.

The ontology represented in Figure 3 has immersive technologies as the top most layer followed by VR, AR, and BMI. Key terms that fall under each domain are arranged alphabetically under each section. Knowledge from heterogeneous sources is combined to form a single schema for a consolidated view. The key terms for VR and AR are derived from [10, 13, 34–47]. The key terms for BMI are derived from [17–20, 24, 48–52]. The key terms are preprocessed to eliminate redundant values and are reviewed by subject matter expert before ontology integration. Ontology offers a perspective towards solving interoperability problems brought about by semantic obstacles [53]. The results represent explicit knowledge contained within VR, AR, and BMI domain types software applications within the industrial and manufacturing domain. Ontology validation is explained in Sections 6, 7, 8, and 9 by cross-referencing patent and technology analysis results.

5. Technology Review and Specifications

During the 1990s, many companies failed to deliver VR products and services to the marketplace. Nintendo Virtual Boy was discontinued a year after market introduction [54]. The increase in the processing power of computers has enabled the current market success of immersive technologies. VR, AR, and BMI are being introduced across a number of market channels that include industrial and consumer applications [23]. The theoretical and methodological contributions and current knowledge from IEEE and IET publications are used to collect data for immersive technologies. IEEE and IET databases represent the research of the broad scientific community along with tools to facilitate advanced search optimization and downloads. The diverse coverage of research journals, conference, eBooks, and technical standards helps users collect data related to the current state of the art. The search reflects the tabulated publication data. The 2010–2016

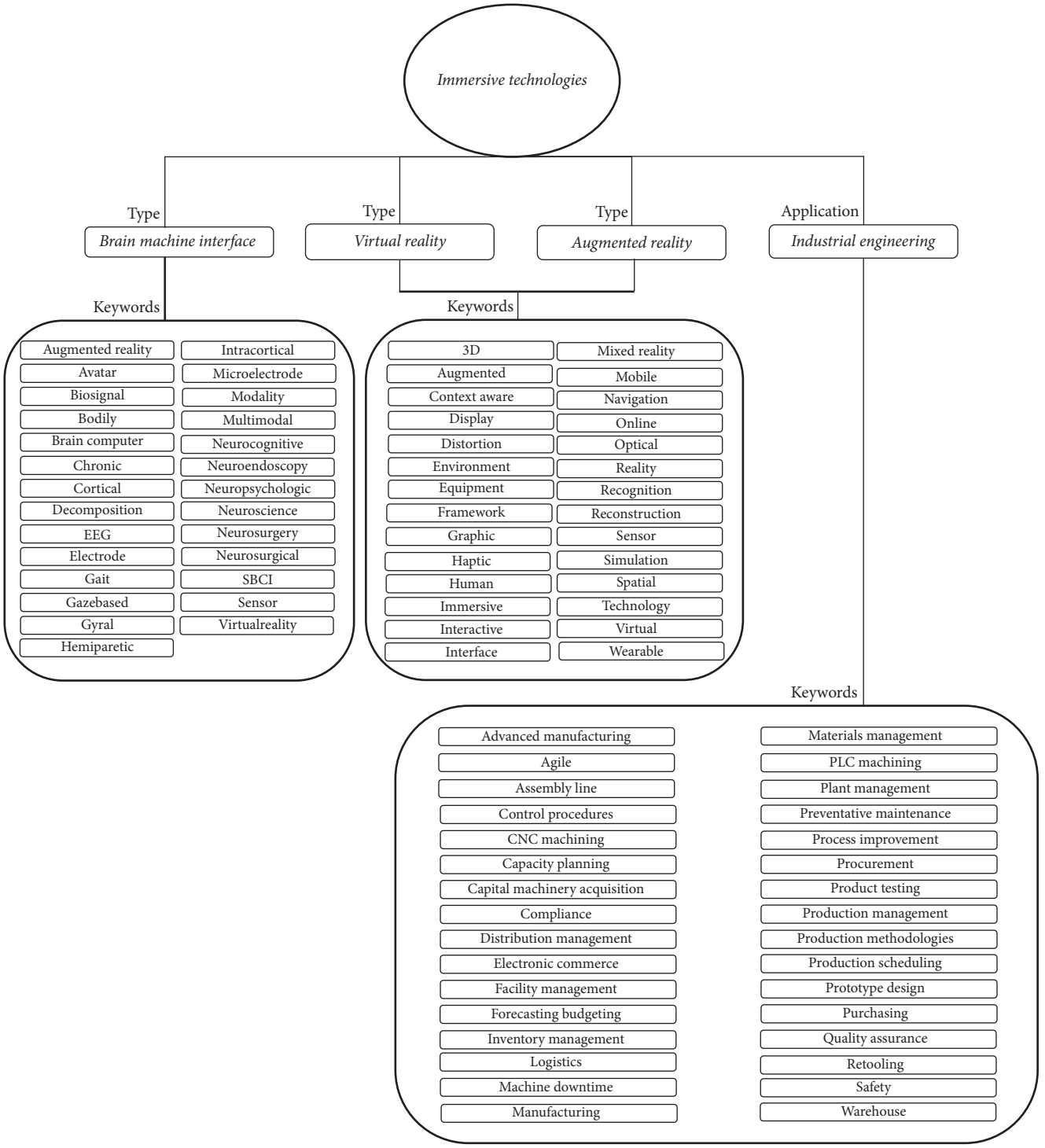

Figure 3: Ontology schema of IIT.

dataset, row 2, Table 2, is used to derive the preliminary background and inferences. The dataset from row 4, Table 2, is used for the literature review and ontology generation for IIT.

Literature classification requires a subject matter expert (SME) to cluster the publication dataset as shown in Figure 4. Publications belonging to the application group encapsulates research of IIT integration for product/concept design, robotics control, and equipment for manufacturing. Publications in the training group encapsulate research on professional training systems for manufacturing, skill transfer, and human resource development using 3D manipulators.

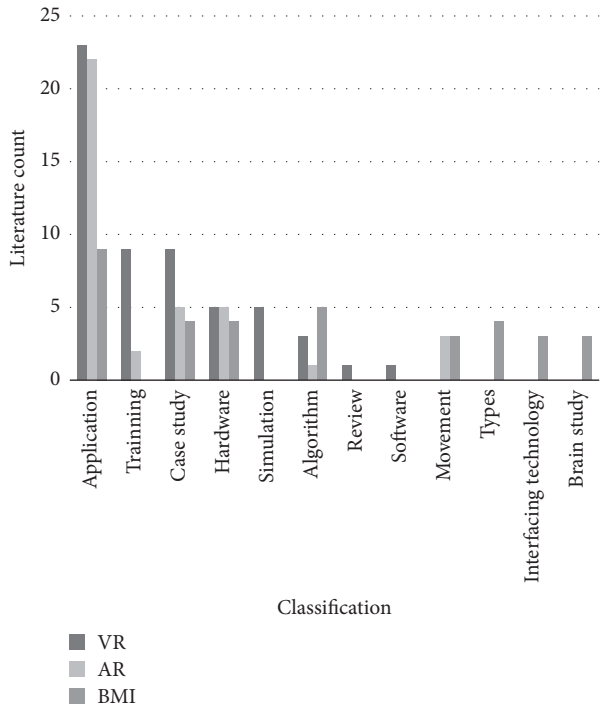

Figure 4: SME classification results.

Table 2: Publication counts by categories (indicating R&D trends and distributions).

Timeline	VR	AR	BMI
2007–2016	5,277	4,903	1,138
2010–2016	1,034	1,524	320
2016	594	716	158
2007–2016 (industrial specialization)	58	45	76

Publications in the case studies group encapsulate IIT studies conducted on industrial robotics, semiconductor chip forming and breakages, perception mechanism for assembly line environments, interaction with Computer-Aided Design (CAD), and visual communication methods. Publications in the hardware group encapsulate research on IIT customizations for motion capture devices, brain wave capture, customized displays for vehicular environments, and specialized head mounted displays. Publications in the simulation group encapsulate research on escape vehicles, precision welding, power cell production, and fixtures for grinding wheels. Publications in the algorithm group encapsulate research for feature extraction for EEG signals, correction of geometric distortions, and genetic algorithms for structure optimization. Publications in the review group consist of literature reviews related to VR production lines in China. Publications in the software group encapsulate research on motion tracking and eye positioning in VR displays. Publications in the movement group encapsulate research on navigation methods and kinesiology for human and robotics in IIT environments. Publications in the interfacing technology group encapsulate research for IIT interoperability for the brain with 3D applications for hardware devices and software platforms. Publications in the brain study group encapsulate research on a wheelchair, unmanned aircraft control, a virtual avatar for gait adaptation, temporal perception using VR neurocognitive, and brain imaging for concussion assessment.

An overlap across topics such as VR, application, research, and the interface is observed from manual review and clustering. The overlap strengthens the assumption (Figure 1) that Milgram's reality-virtuality continuum is an enabler for future industrial VR and AR products. The following sections present a consolidation of key points from literature and technological specifications. The dataset is ordered by citations and time in descending order to ensure maximum coverage of key technology specifications.

Technology analysts predict that immersive technologies such as AR and BCI/BMI will be commercial successful [23]. Immersive VR and AR are used to train pilots to overcome fear of height as well as disorientation from flight maneuvers. With the help of VR, scientists better visualize models and comprehend chemical reactions with enhanced visual details. Architects use VR to visualize and change the angle of view of structures and simulate walking through prototype buildings. VR also offers the potential for museums and art galleries to allow visitors greater access from remote distances. The VR computer is the portal for access to physical experiences and visualization. The leading immersive frameworks include Oculus Rift and Microsoft HoloLens. These cost efficient applications have gained considerable market share as Computer-Aided Design (CAD) interface solutions. Immersive technologies enable designers and engineers to collaborate on projects from multiple locations. Microsoft, Apple, Samsung, HTC, Facebook, and Sony are leading investors in these technologies [23]. Immersion, when combined with the Internet of Things (IoT), promises a new era of technologies for Industry 4.0 called the Internet of Presence (IoP) or the Internet of Experience (IoE). The SME classification results represented in Figure 4 show that the application related literature has the highest number of publications followed by training, case studies, and simulations. The technology specifications from industrial VR publications with high citation are provided in the following paragraphs.

The industrial virtual reality literature shows that industrial training has a high demand for innovation in higher education. 3D visualization and computer hardware advancements lead to a growing range of training materials. Companies, professionals, and researchers are creating interactive VR educational environments [36], such as the Mathematical Virtual Learning Environment (MAVLE) using VR [55]. The Microsoft Visual C++ programming platform has been used to identify opportunities, reduce cost, and increase competitiveness in many parts of the product development life cycle [56]. A VR based aircraft carrier management system for the French navy (GASPAR) demonstrates further industrial VR's capabilities. GASPAR simulates environment modeling, procedure organization, and validation using VR applications [57]. Virtual walk around for factories increases productivity. Motion-capturing sensors record the user's

indoor movements and the algorithm digitizes these movements for the virtual world. Virtual walk around reduces health problems, decreases labor turnover, and reduces costs [38]. VR manufacturing reduces costs and the time needed to go from product concept to production. Advancements in processing, optical visualization, power management, and data sciences are making VR a viable solution for traditional manufacturing and product realization [37, 58].

Industrial augmented reality literature has the highest number of publications followed by case studies, hardware customization for industrial machines, and movement related studies. SME classifications show that all publications with high citations are application related that support industrial processes. Industrial AR is applied in areas such as design, planning and production, abd service and maintenance. The German manufacturer Volkswagen has continuously worked on AR-based factory planning processes. Volkswagens reports that AR system application increases reliability [39]. AR applied in aeronautical maintenance allows for the efficient transfer of knowledge by offering new perspectives with dramatic improvements in maintenance tasks [41]. AR applied in acceptance testing helps real-time comparison planned for a given project. The comparisons are realistic and use an expert heuristic for automatic validations [42]. Operator safety in industrial material management and processing is critical. AR systems deployed in radioactive material processing can superimpose virtual digital models onto video streams which increase the operator's viewing scope and decrease fatigue. The concept is validated by superimposing radiation information on real data streams [46].

The IIT brain interface literature is divided into invasive, semi-invasive, and noninvasive classes. The industrial BMI area is noninvasive-centered. SME classification shows that noninvasive industrial BMI publications are concentrated in the VR area, followed by algorithms and case studies. Top citations are distributed across a spectrum of case studies, simulations, mobility research, EEG research, monitoring, software, algorithm, and hardware. Key points denoting technology specifications are presented below. BCI as a support system for video game control offers a new means of navigation and interaction in 3D environments. The interactions are supported by the noninvasive capture of cerebral activity, recorded using EEG electrodes. This helps to create a "think-and-play" user experience for games of the future and has been successfully applied to robotics control [18, 48]. Another widely used technology is called functional magnetic resonance imaging (fMRI), a neuroimaging procedure based on magnetic resonance imaging. fMRI brain activity is measured by detecting changes in blood flow. fMRI technology results in higher activation and improves task performance [51]. BCI in VR allows individuals to interact directly with an environment rather than a computer monitor ensuring higher immersion and interaction with the computer [19]. BMI applications for wheelchair control is a case analogous to driving a car. Motor execution and motor imagery simulations indicate control and accuracy [20, 49]. Technology specifications indicate the potential for industrial brain interface applications for robotic arm control. The future growth in the area requires collaboration among physical scientists, neuroscientists, engineers, and social and behavioral scientists [17]. Finally, the geographical analysis of publication metadata indicates that China has the largest number of publications in the area of industrial VR and AR, followed by Germany. The USA has the largest number of publications in the area of BMI/BCI research and publications followed by Japan and Canada.

6. Patent Search and Statistical Analysis

The ontology represented in Figure 3 is used to generate a search query for the Derwent Innovation (DI) system. The DI system automatically converts the search query to Boolean format. The DI search ensures an accurate and broader set of data for analysis and inference generation. The search scope includes patent databases from prominent global manufacturing economies. The dataset is filtered using a nine-year range from 2007 to 2016.

The ontology in Figure 3 represents the IIT hierarchy. An ontology is a higher dimension visual representation which needs dimensional reduction and simplification. The ontology in this step is converted into a search query that the DI patent search system uses as input to generate the patent dataset. This conversion is carried out using prior experience in patent search query optimization. High-frequency words identified during the literature review are subject to independent expert review. Table 3 represents the key terms represented in the DI system input format: column 2 represents a topic, keyword filtering criteria, and scope filtering while column 3 shows the generated Boolean search query.

The result of the above queries is split into 2 categories according to the derived ontology. VR and AR contain 1,995 patents in 629 Derwent world patents index (DWPI) classification families and BMI contain 677 patents under 427 DWPI families. When analyzing patent data for landscaping, data are assessed from a qualitative and a quantitative perspective. Quantitative analysis is statistical and helps determine metrics and ratios. The quantitative information in this section represents top assignees and international patent classification (IPC) analysis for VR, AR, and BMI.

Table 4 presents a statistical meta-analysis that identifies the top 10 assignees of technology in the field of IIT. Top assignees analysis shows that Seiko Epson has the most patents in the industrial VR and AR domain with 28 patents. Seiko Epson is one of the largest Japanese owned imaging related manufacturers, followed by Korea Electronics Telecomm with 11 patents. LG Display and Hyundai Motor have 10 patents each. From the technology specification in Section 5, VR technology is extensively used in the automotive industry [39]. The placement of Hyundai Motor as the third is a cross-reference between literature review and patent data analysis. Table 5 presents Samsung Electronics as the largest assignee in the BMI area with 26 patents and accounts for 15.76 percent of the market. Panasonic is the next largest assignee with 13 patents. Thalmic labs has 13 patents and is the creator of wearable technology. Microsoft has patents in VR, AR, and BMI. Microsoft holds 8 patents in

Table 3: The search query key terms.

Number	Key term	Boolean format
(1)	*Topic:* "Virtual reality" "VR" "Augmented reality" "AR" "Mixed reality" "MR" *Filtering criteria: Title/Abstract/Claims:* "Advanced manufacturing" OR "Agile" OR "Assembly line" OR "Control procedures" OR "CNC machining" OR "Capacity planning" OR "Capital machinery acquisition" OR "Compliance" OR "Distribution management" OR "Electronic commerce" OR "Facility management" OR "Forecasting budgeting" OR "Inventory management" OR "Logistics" OR "Machine downtime" OR "Manufacturing" OR "Materials management" OR "PLC machining" OR "Plant management" OR "Preventative maintenance" OR "Process improvement" OR "Procurement" OR "Product testing" OR "Production management" OR "Production methodologies" OR "Production scheduling" OR "Prototype design" OR "Purchasing" OR "Quality assurance" OR "Retooling" OR "Safety" OR "Warehouse" *Scope (Publication and application year):* (PY >= (2007) AND PY <= (2016)) OR (AY >= (2007) AND AY <= (2016)	*Query:* SSTO = ("Mixed Reality" "Augmented Reality" "Virtual Reality") AND TAB = ("Advanced manufacturing" OR "Agile" OR "Assembly line" OR "Control procedures" OR "CNC machining" OR "Capacity planning" OR "Capital machinery acquisition" OR "Compliance" OR "Distribution management" OR "Electronic commerce" OR "Facility management" OR "Forecasting budgeting" OR "Inventory management" OR "Logistics" OR "Machine downtime" OR "Manufacturing" OR "Materials management" OR "PLC machining" OR "Plant management" OR "Preventative maintenance" OR "Process improvement" OR "Procurement" OR "Product testing" OR "Production management" OR "Production methodologies" OR "Production scheduling" OR "Prototype design" OR "Purchasing" OR "Quality assurance" OR "Retooling" OR "Safety" OR "Warehouse") AND (PY >= (2007) AND PY <= (2016)) AND (AY >= (2007) AND AY <= (2016));
(2)	*Topic*: "Brain machine interface" "BMI" "Brain computer interface" "BCI" *Filtering criteria1: SSTO:* "Mixed reality" or "Augmented reality" or "Virtual reality" *Scope (Publication and application year):* (PY >= (2007) AND PY <= (2016)) OR (AY >= (2007) AND AY <= (2016)	*Query:* (SSTO = ("Brain machine interface" "BMI" "Brain computer interface" "BCI") AND (PY >= (2007) AND PY <= (2016)) AND (AY >= (2007) AND AY <= (2016))); *Sub query:* (SSTO = ("Mixed reality" "Augmented reality" "Virtual reality")

Table 4: Top assignees of VR and AR patents.

Assignee	Patent count	Percentage
Seiko Epson	28	22.58%
Korea Electronics Telecomm	11	8.87%
LG Display	10	8.06%
Hyundai Motor	10	8.06%
BOE Technology Group	9	7.26%
Microsoft	8	6.45%
Denso	8	6.45%
Flextronics	5	4.03%
Essilor	5	4.03%
Sony	5	4.03%

Table 5: Top assignees of BMI patents.

Assignee	Patent count	Percentage
Samsung Electronics	26	15.76%
Panasonic	13	7.88%
Thalmic Labs	13	7.88%
Morikawa Koji	11	6.67%
Matsushita Denki Sangyo	10	6.06%
Univ Tianjin	9	5.45%
Microsoft Technology Licensing	9	5.45%
Microsoft	8	4.85%
French Alternative Energies and Atomic Energy Commission	7	4.24%
Advanced Telecommunications Research Institute International	7	4.24%

VR and AR which represent around 6 percent of all patents. Microsoft holds 8 patents in the BMI alongside extra 9 patents in brain interfacing technologies through its auxiliary Microsoft Technology Licensing.

The top IPC classes for global VR, AR, and BMI utility patents are shown in Table 6. There is an overlap between VR, AR, and BMI in terms of IPC classes. IPC category analysis shows the top three IPC in both categories are G06F referencing electrical digital data processing. The G06F subclass contains patents dealing with processing or transporting of data and data processing equipment such as electric digital data processors. The G02B categorizes optics and the subclasses contain patents dealing with lens or prisms (an optical system designed to produce realistic images); G06T categorizes imaging and subclasses containing patents

Table 6: Top IPC classes and their patent counts.

IPC	VR/AR	BMI	Content
G06F	983	414	Electric digital data processing
G02B	606	29	Optical elements, systems, apparatus
G06T	278	37	Computing, calculating, counting
G06Q	167	11	Data processing systems
H04N	146	27	Pictorial communication
B60K	86	0	Arrangements or mounting of units
G06K	76	38	Recognition of data
B60R	73	0	Vehicles, vehicle fittings
A61B	71	206	Diagnosis, surgery
G02F	69	0	Devices, arrangements
A61F	0	32	Prostheses, orthopedic, nursing appliances, treatment or protection of eyes or ears
H04W	0	15	Wireless communication networks
G06N	0	18	Computer systems based on biological models

dealing with image acquisition, feedback, watermarking, and compression. Table 6 shows that IPC classes A61B, H04W, and G06K are specialized for brain interfacing. The A61B class is focused on invasive and semi-invasive brain interfacing. This class refers to diagnosis and surgery and its subclasses deal with prostheses, orthopedic, nursing appliances, and treatment or protection of eyes or ears. The H04W class is focused on wireless communication needed for noninvasive interfacing with focus on protocols, connectivity, and information. The G06N class deals with algorithms, platforms, and architectures required for biological computing [59].

An application on a year-by-year basis for VR and AR patent domains shows exponential growth from the year 2014 with the publication counts of 339, 394, and 579 against the application count of 118, 138, and 79 for years 2014, 2015, and 2016. BMI patent data shows low volumes until 2014 with steady growth in patenting. There are a total of 81 grants against 24 applications during the year 2016. This ratio is due to a reduction in the cost of sensors, actuators, and controller technology coupled with advanced manufacturing demand [14].

A geographical patent distribution analysis shows China companies as the leading assignees in industrial VR related patents. This growth results from mobile platform companies including Xiaomi, Huawei, Pico VR, Baofeng Mojing, and Deepoon. Followed by the USA, Korea is in the 3rd place. The US companies are the leading assignees in BMI mind-machine interface (MMI) and direct neural interface (DNI) patents. The US has a large number of industrial companies and research centers for brain research combined with governmental policies and incentives. The following sections are text mining techniques applied to construct the TFM and group patents based on LDA to map insights and the inferences from IIT data set and external cross-references.

7. Patent Technology Function Matrix Construction

A technology function matrix (TFM) is a unique approach to patent data analytics. A patent map visualizes quantitative patent information with respect to the technical and functional features in the patent landscape [15]. A TF framework consists of technology columns and function columns. The conventional method of constructing a matrix is to read the patent documents manually and fit them into a matrix. IIT TFM uses text mining for a qualitative overview of underlying IP dynamics. The TFM is constructed using the ontology represented in Figure 3. The steps to generate a TFM are presented as a flow chart in Figure 5. TFM is constructed using VR, AR, and BMI technologies and industrial engineering function key terms from the ontology.

The TFM construction uses the patent dataset and IIT ontology as the primary input. The ontology is split for technology and function term libraries. The TFM structure is created with technology keywords related to immersive building blocks assigned to the technology axis. Industrial application functionality keywords are assigned to the function axis. Normalized Term Frequency (NTF) based text mining terms are applied to extract the key terms represented in

$$\mathrm{NTF}(a,b,n) = \mathrm{tf}_{ab} \times \frac{1}{\mathrm{WN}_b} \times \frac{\sum_{d=1}^{n} \mathrm{WN}_d}{n}. \quad (1)$$

$\mathrm{NTF}(a,b,n)$ is the multiplication of tf_{ab}, the reciprocal of WN_b, and the summation of WN_d divided by n, where a is one of the terms in all document collections, b is one of the documents in all document collections, n is the total number of all the document collections, tf_{ab} is the frequency of term a appearing in the document b, WN_b is the total number of words in document b, and $\sum_{d=1}^{n} \mathrm{WN}_d$ is the

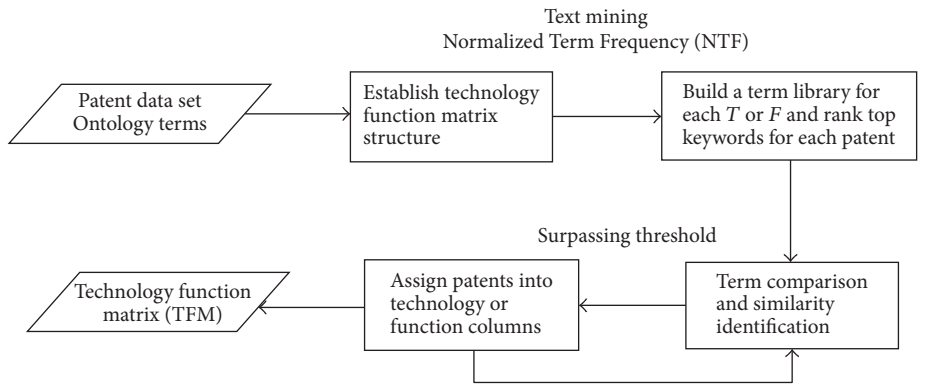

Figure 5: TFM construction process.

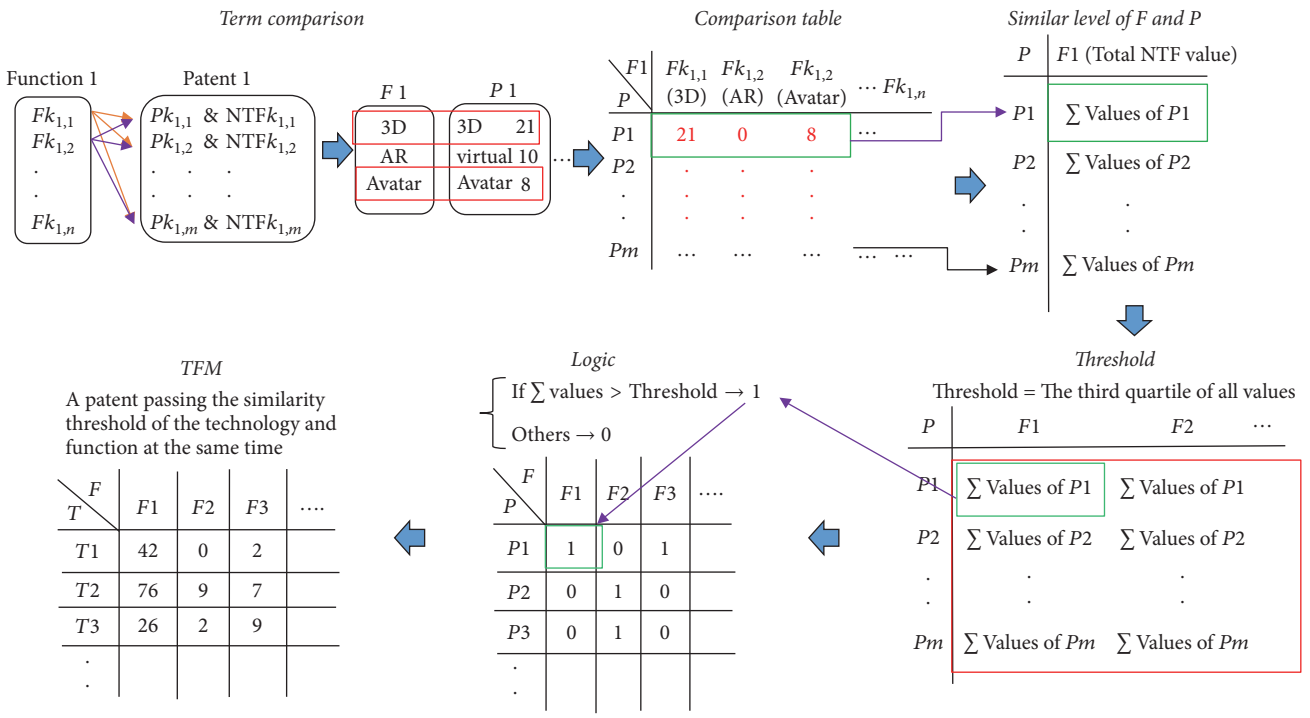

Figure 6: An example of TFM generation process.

total number of words in all document collections. Figure 6 is an example of the TFM generation process. The NTF value of each word is the weighted value and a term library comparison is made for each indicator for patents in the IIT data set. The assumption is that patents with high-term repetitions belong to a certain technology or function. The degree of association between the patent and the term library is represented by the sum of NTF value that appears in the keywords of patent and term library simultaneously. Since patent size influences term frequencies, matrix standardization needs to be carried out on the total NTF value as shown in

$$Z = \frac{X - \overline{X}}{S}. \quad (2)$$

X is the dependent variable (NTF value), $\overline{X}$ is the population mean, and S is the population standard deviation. A threshold value is applied to remove less relevant patents for a given term. The threshold used is the third quartile value which is the middle value between the median and the highest value of the given dataset. The logic for assignment into the cell for the TFM is to determine whether the words under each indicator and the words below the patent match. If equal, the assigned value for the cell is 1; otherwise, it is 0. The term comparison table for each indicator with patents is constructed with a summation value of each patent word NTF value under each indicator term library. The keywords represent each patent and each technology or function indicator. The summation value is considered to be the similarity level between each patent and each technology or function indicator. The patent

Table 7: IIT technology function matrix.

Technology function matrix		Functions															
		*F*1	*F*2	*F*3	*F*4	*F*5	*F*6	*F*7	*F*8	*F*9	*F*10	*F*11	*F*12	*F*13	*F*14	*F*15	Total
Technology	3D	42	0	2	13	43	8	26	48	3	16	2	8	55	0	5	271
	Augmented reality	76	9	7	18	124	26	99	94	6	59	11	30	134	1	8	702
	Avatar	26	2	9	12	44	10	31	35	1	21	8	19	45	0	9	272
	Brain computer	40	34	6	10	62	29	63	44	8	33	7	31	76	1	3	447
	EEG	27	11	5	11	13	2	42	39	18	31	14	16	41	0	0	270
	Electrode	1	2	0	0	1	0	2	0	0	0	0	1	0	0	0	7
	Graphic	29	6	4	4	38	4	21	22	3	12	2	9	50	0	1	205
	Immersive	33	2	9	15	44	12	39	62	13	18	13	13	49	0	7	329
	Mixed Reality	12	0	0	1	16	3	11	14	0	4	0	2	13	0	0	76
	Neurocognitive	0	1	0	2	3	2	1	1	0	3	0	0	2	0	2	17
	Neuropsychological	25	7	9	13	30	11	39	37	7	36	7	17	41	5	3	287
	Recognition	40	9	13	15	32	7	51	55	7	34	10	18	43	4	9	347
	Sensor	54	26	12	24	69	14	107	93	40	60	19	33	101	0	1	653
	Virtual reality	42	15	4	11	49	9	52	64	12	20	4	22	78	0	2	384
	Wearable	16	3	5	2	52	2	32	20	2	14	2	1	43	0	1	195
	Total	463	127	85	151	620	139	616	628	120	361	99	220	771	11	51	

*F*1: assembly line; *F*2: CNC machining; *F*3: capital machinery; *F*4: distribution management; *F*5: electronic commerce; *F*6: facility management; *F*7: logistics; *F*8: manufacturing; *F*9: preventative maintenance; *F*10: process improvement; *F*11: product testing; *F*12: production management; *F*13: prototype design; *F*14: safety; *F*15: warehouse.

is then regarded as belonging to the set of functions or the technology set. The results of the technology and the function patent counts are computed independently and the two matrices are multiplied to obtain the final TFM.

The IIT TF Matrix is presented in Table 7. TFM suggest growth in AR, and sensors are favouring patenting across industrial functional domains. Demands for a diverse array of sensors in logistics and prototype design functions are triggers for the growing volume of 653 patents in sensor technology. The role of integration and convergence of engineering tools, methods, and the need for processing in the context of interfacing, brain-computer, and virtual reality technologies occupies consecutive positions with 447 and 384 patents. Compared to the sensor technology, there are fewer patents for electrode technology which shows IIT favouring noninvasive sensing methods, against invasive or semi-invasive methods. Correlating the result of this TFM with the top IPC analysis presented in Section 6, it can be inferred that optics, sensing, and processing are the most competitive areas. Since there are fewer patents in the industrial safety area this could be a future area of patenting expansion. Optical sensing and processing are crucial elements for immersive systems because human eye limitations for the display are placed 3 to 4 cm away from the eye. Advancements in optics will make lenses in immersive technologies more human-friendly. A reduction in the number of core VR patents can be seen from the TFM numbers. This represents VR technology reaching maturity and leveraging technologies like AR and BMI. The finding further supports the Milgram's reality-virtuality continuum expansion hypotheses proposed in Section 2. AR technologies progressive patenting in prototyping, e-commerce, logistics, and manufacturing design functions in the industrial ecosystem suggest the need for future standardization research for sustainable industrial interoperability.

8. LDA Patent Topic Modeling

LDA is a generative statistical model for topic modeling. LDA is used in modeling descriptions for given documents called topics [27, 30, 31]. LDA was initially introduced for textual data modeling and uses words in a document. Topics generated are based on the probability distribution of words in a document compared to conventional stripped word frequencies. The models assumption is that words carry strong semantics information and documents with similar topics will use similar groups of words. Hence, documents are seen as a probability distribution over latent topics and topics are probability distributions over words. LDA model has been extended to various other applications such as semantic annotation in satellite imaging, social media tagging, natural language processing, object recognition, spam filtering, web-mining, and fault identification [26–32]. LDA is chosen for the probabilistic patent analysis because of prior application and validation against various bag of words model and proof of higher efficiency in unstructured literature data clustering for systematic reviews [60]. This section is an implementation of LDA model using online method to model topics for IIT patent data [61].

LDA is a generative model for sematic words of a patent based on generic continuous latent parameters for mixtures of hidden topics. Each topic is characterized by words in vocabulary V and represented with per word topic distribution. A mixture of topics is used to represent a corpus of a patent using its per topic patent distribution. Assume that there are $|V|$ words in vocabulary V and K topics in the

patent corpus D with M patents. Let $N_{d=1,\ldots,M}$ represent the number of words in the dth patent in corpus D and the prior parameter vectors for Dirichlet distribution are $\boldsymbol{\alpha}$ and $\boldsymbol{\eta}$. In per topic patent distribution, let $z_{d,n=1,\ldots,N_d} \in \{1,\ldots,K\}$ be the topic that the nth word in dth patent may belong and let $z_{d,n}$ be a multinomial distributed random variable with parameter vector $\theta_d \in (0,1)^K$ drawn from Dirichlet$(\boldsymbol{\theta}_d;\boldsymbol{\alpha})$. Since a word structure stands for a topic, per word topic distribution is needed. For per word topic distribution, let $w_{d,n=1,\ldots,N_d} \in V$ be the nth word in dth patent and the word $w_{d,n}$ may be assigned to a topic, namely, $z_{d,n}$. Since a topic is composed by words, let $w_{d,n} \mid z_{d,n}$ be a random variable with multinomial distribution $(\beta_{z_{d,n}=k})$, where $\beta_k \in (0,1)^{|V|}$ is sampled from Dirichlet$(\beta_k;\boldsymbol{\eta})$ [25]. The structure relation among the above parameters of the model is represented in the plate notation shown in Figure 7. The joint distribution of per word topic and per topic patent distributions is described in

$$P\left(\mathbf{w_d},\mathbf{z_d},\boldsymbol{\theta}_\mathbf{d},\mathbf{B};\boldsymbol{\alpha},\boldsymbol{\eta}\right)=\prod_{j=1}^{N_d}\prod_{k=1}^{K}P\left(w_{d,j}\mid\boldsymbol{\beta}_{z_{d,j}=k}\right)\text{Dirichlet}\left(\boldsymbol{\beta}_\mathbf{k};\boldsymbol{\eta}\right)P\left(z_{d,j}\mid\boldsymbol{\theta}_d\right)\text{Dirichlet}\left(\boldsymbol{\theta}_d;\boldsymbol{\alpha}\right), \tag{3}$$

where $\mathbf{B}$ is a matrix with dimension $K \times |V|$ spanned by row vectors $\boldsymbol{\beta}_{\mathbf{k=1},\ldots,\mathbf{K}}$. Further, by integrating $\boldsymbol{\theta}_1,\ldots,\boldsymbol{\theta}_M$ and $\mathbf{B}$, the joint distribution in (3) is derived as $(\mathbf{w},\mathbf{z};\boldsymbol{\alpha},\boldsymbol{\eta})$. Thereafter, the prior parameter vectors $\boldsymbol{\alpha}$ and $\boldsymbol{\eta}$ are approximated by using the online method [61, 62]; the final patent topic assignment is determined. For example, for a patent with N words, to determine whether it contains latent topic k, (4) is utilized. For any $\varepsilon \in [0,1]$,

$$I_{z=k}\left(\mathbf{w}\right)=\begin{cases}1, & \sum_{n=1}^{N}P\left(w_n,z_n=k;\boldsymbol{\alpha},\boldsymbol{\eta}\right)>\varepsilon\\ 0, & \text{Otherwise.}\end{cases} \tag{4}$$

The flowchart presented in Figure 8 gives an overview of the steps involved in the LDA application. IIT patent information from sections title, abstract, summary, and claims is extracted, filtered by cleaning, preprocessing, and normalization to form the patent data corpus. A document term matrix is then generated on which LDA object is trained for term generation. A selection criterion is used to filter terms of interest. Terms surpassing a minimum number of patents are considered as resultant patent topics. Extracted LDA topics are grouped and analyzed.

LDA application models the VR, AR, and BMI dataset of 2,672 patents across 467 topics with an average of 22 patents per topic. Patent documents contain high volumes of technological legal information that is subjective. The automatic selection of the optimal number of topics to represent the corpus in consideration is still a problem to be solved. Since an insufficient number of topics render the patent groups as too coarse, an excessive number of topics are selected. Exhaustive subject matter expertise is further used to make interpretations and validations. The subject matter expert uses prior experience in the patent pooling and licensing management area to determine the best fit. A similar validation approach was applied in validating human mobility region discovery using LDA [63]. An IPC class code cross-verification is applied manually to further verify the results obtained. The outcome demonstrates that while topics with higher patent frequencies represent a broader technological domain, topics with lower patent frequencies represent very specific technological inventions. Further, 188 topics having comparative semantics are reduced to common terms. The SME driven manual term reduction yields a specific IIT patent topic dictionary (Table 8).

The reduced terms obtained from the analysis form six groups. The optics group has an average of 36 patents and contains patents related to inventions related to the behavior of light and displays and its association with three-dimensional planes in IIT context. The ownership summary below provides a snapshot of termwise institutional holdings. The summary encompasses sample technology based on the analysis of details corresponding to the reduced terms. Seiko Epson leads with patents for manufacturing light guide devices, virtual image display apparatus, optical elements, image display devices, and polarized light separation devices. Denso and companies like LG, Samsung, Motorola, and Qualcomm have patents in display apparatus and heads-up display manufacturing. The hardware group is a collection of physical components that constitute IIT including sensors, actuators, circuits, and computation elements. The group has an average of 26 patents. Top assignees vary in the group depending on the subtopic term. Companies such as BOE and LG have considerable presence in the hardware level touch screen technology. Examples of inventions in this group are the Korea Research Institute of Standards and Science's patenting in the elastic tactile sensors and Samsung's physical button display module. The software group contains patents consisting of information, data, and computer programs. The group has an average of 37 patents. The Advanced Telecommunication Research Institute International's patent on brain information processing software, Apple's programmable tactile touch for interfacing, Baidu on line network technology patent on transaction information systems, and Guangdong Coagent Electronics gesture and voice control systems are some grants in this group.

The interaction group contains patents relating to user's communicating with a system or other users. The group has an average of 30 patents. BOE Technology patents are in the wearable interaction technologies, Commissariat's patents are in neural control, and Ethicon Enco Surgery Inc.'s patent targets eye glance guidance. General Motor, Huawei Device, and Guangdong's patents cover head mounted display interaction technology. Hyundai Motor Company's

Table 8: IIT patent topic dictionary.

Reduced term	Average number of patents	LDA topic
Optics	36	3D, angle, beam, camera, capture, color, concave, crystal, curved, diffraction, direction, display, disposition, film, frame, glass, grating, guide, haptic, laser, layer, lens, light, medium, mirror, panel, photoresist, picture, piezoelectric, plate, portion, position, projection, reflect, region, scene, screen, section, state, stereoscopic, surface, transparent, video, visual, wave, waveguide
Hardware	26	Actuator, array, board, circuit, compute, connected, controller, EEG, electrode, EMG, feedback, gate, infrared, network, platform, processing, robot, sensing, sensor, transmission, wireless
Software	37	Access, activity, character, cloud, communication, configuration, content, data, detection, driver, environment, filter, frequency, GPS, indication, information, key, mode, navigation, operation, pattern, process, recognition, security, unlocking
Interaction	30	Biometric, biosignal, brainwave, button, capacitive, command, elastic, electroencephalogram, gaze, gesture, glove, haptic, headup, helmet, HMD, holographic, HUD, interface, menu, mobile, notification, phone, stimulus, tactile, terminal, touch, wearable
Anatomy	23	Action, arm, biological, blood, body, brain, eye, face, finger, hand, head, neural, person, physical, sensory, skin, stimulation, surgical
Industrial	17	Apparatus, assembly, component, coordinate, current, customization, dimension, driving, effect, electric, fluid, force, grid, harness, housing, instrument, insulating, intelligent, lighting, line, location, machine, management, manufacturing, marker, mass, material, metric, motion, mounting, movement, operator, plane, portable, presentation, product, safety, shell, shopping, simulation, structure, subsystem, support, temperature, tool, training, vehicle, vibration, welding

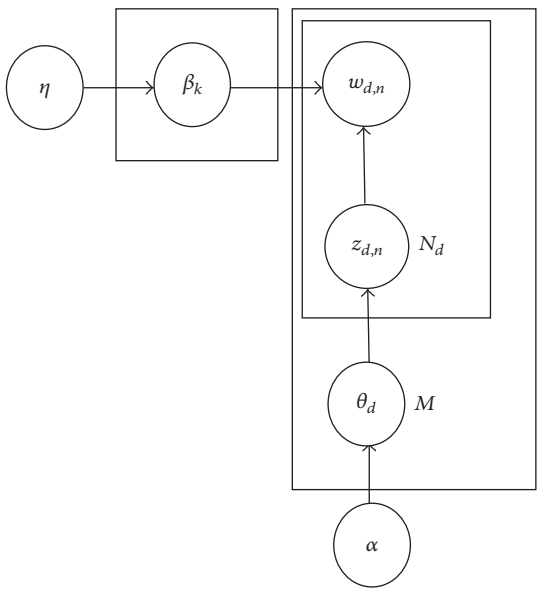

Figure 7: LDA algorithm process model.

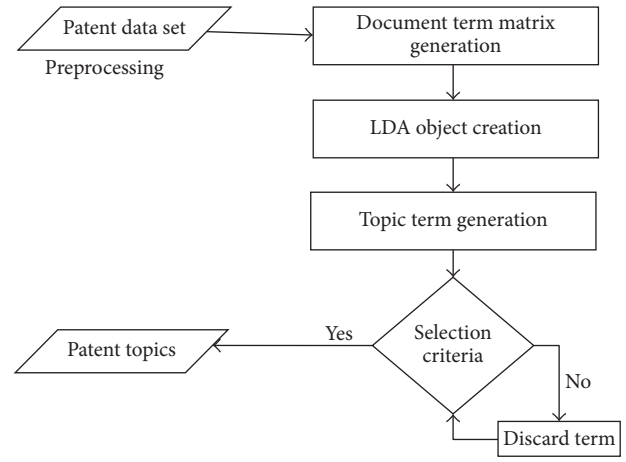

Figure 8: Flowchart for applying LDA algorithm in patent topic generation.

patents present examples of patenting under the topic group. The anatomy group contains patents related to the structure, characteristics, and functions of human anatomy roles and implication in IIT. Sensory feedback patents of AliphCom and BOE Technology face motion-capturing method for the head mounted display systems, the center of Human-Centered Interaction for Coexistence patents related to mobile terminal and training method for a person, and finger operation of a vehicle by Hyundai Motor Company. The industrial group represents patents applied in the context of industrial engineering including assembly, manufacturing, welding, automobile, and tools. The group has an average of 17 patents. The group contains patents related to self-adaptive interaction systems by Anhui Agricultural University, three-dimensional GIS system by Beijing Huadian Tianyi, intelligent lens rotation by Beijing Yunshi, and VR welding education systems by Lincoln Global.

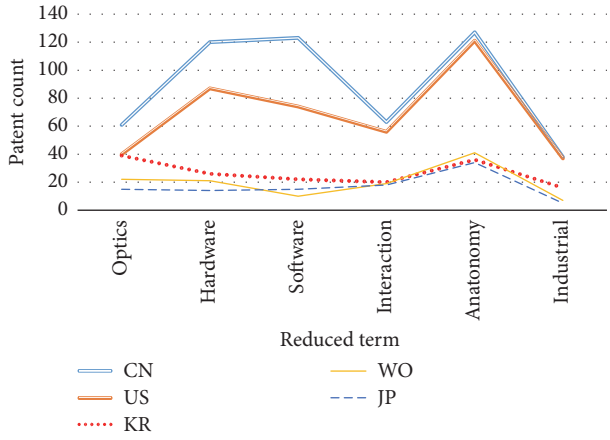

Figure 9: IIT patent topic distribution of top countries.

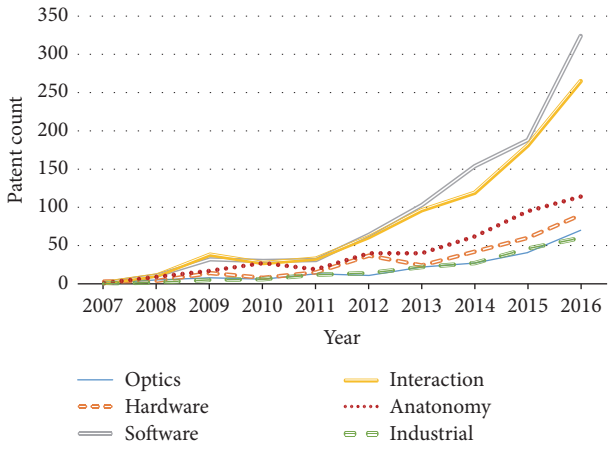

Figure 10: Evolutionary trends in IIT topics.

The leading country reduced term analysis can be analyzed using LDA. The results are represented graphically in Figure 9. China has good topic coverage in the IIT domain with an average distribution of 7 patents per topic, followed by the USA, Korea, WIPO, and Japan with 6, 2, and 1 patents per topic. These findings are in line with Lexinnova's prior VR patent landscape analysis reports for geographical coverage [22]. A comparative reduced term graph is shown in Figure 7 and shows that the market leaders in IIT patent representations have uniformly high patents followed by followed by groups dealing with hardware, software, and interactive optics.

Further evolutionary trends of topics over a period of years from 2007 are calculated. Figure 10 demonstrates a graphical layout of a topic trend across the reduced topic spectrum. The evolution graph shows that patents related to IIT software and interaction have dynamic progressive trends since 2007. These reduced term groups show exponential growth since the year 2011 with patent grants doubling yearly. The topic evolution graph identifies the direction of promising patents for frequent transfer transactions for future industrial use. Technology transfer and licensing are mechanisms for industrial collaboration and helps secure advances in technology.

LDA as modeling technique achieves a platform for a host of patent analytics functions. LDA is a probabilistic, generative model, with patents grouped on top of LDA semantics. Patent groups identified in this section promote technological opportunity and identify areas of risk, opportunity within a given technology area.

9. Standardization Outline and Future Research Scope

Standardization is a systematic approach to propagate innovation, interoperability, and knowledge [64]. The lack of clarity in generic immersive technology standards limits the rate of adaptation for designers and engineers [35]. Virtual reality markup language (VRML) is one such standard. The University of Kiel has created a tool for Volkswagen that produces point clouds in VRML 2.0 format [39]. A report on Devices and Radiological Health workshop in brain-computer interfacing summarize the need for regulations, privacy, and patient protection. Regulation deals with the development of new tools, standards, and approaches to assess the safety, efficiency, quality, and performance. The need for creation of standards in engineering adhering to established medical standards ensures consistency in product development and clinical trial design. The need for medical device standards organizations, such as Association for the Advancement of Medical Instrumentation in collaboration with engineering associations such as Institute of Electrical and Electronics Engineers (IEEE) and International Organization for Standardization (ISO), are needed to develop BMI/BCI standards [65]. Patent data citation analytics play an important role in standards outline mapping. Forward citations (patents that cite a given patent), backward citations (patents that a given patent cites), and nonpatent citation analytics help determine essential patents via a citation map. A preliminary forward citation analysis in the IIT patent dataset reveals that USPTO patent in the BMI area with patent ID US20090312817A1 published in the year 2009 by Wicab has the highest count of citing patents with 136 citations. Wicab's patent deals with systems and methods for altering brain and body functions and for treatment. Patent ID US20100238161A1 in the VR area refers to a computer-aided system for 360° heads-up display published in the year 2010 with 127 citations. Patent ID US20090273563A1 on programmable tactile touch screens has 115 citations. An average citation analysis shows that industrial VR and AR technology Japan's semiconductor energy lab (SEL) has the highest average citation. The companies' 14 patents have been cited 135 times giving it an average citation value of 9.64. BMI's InteraXon has key patents in the area of brainwave-controlled computing technology and applications has 9 patents cited 58 times giving it an average citation value of 6.44. Since the immersive technology adoption pace in the area of manufacturing depends on the creation of standards and a broader range of licensable IPs, standardization outline is an urgent requirement.

Research findings show that immersive technologies in manufacturing are reaching an inflection point. Industries today approach new products by simulations and analysis instead of assumptions or conjecture [38]. Technology research firm Superdata predict VR reality will grow in areas other than gaming. This report predicts that the initial growth wave in VR related to the gaming the market share will shrink and social media, entertainment, automobile, aerospace, and manufacturing will see exponential growth [41, 66]. According to latest WIPO IP Facts and Figures, 2016 consolidation report that trademarks are the fastest growing segment with 27% growth in the past one year [59]. This research shows that the volume of patents in each competitor segment has grown exponentially in the past 12 to 18 months. This growth curve shows similar characteristic as the smartphone growth curve. Historically, such growth curves lead to litigation. Thus, standardization for litigation avoidance and mitigation along with trademarking is required.

10. Conclusions

This paper presents a systematic study of IIT for improving manufacturing systems using collective intelligence. The idea of "smart" factories is no longer a futuristic vision but a commercial necessity. Independent publication, reports, and white papers from leading manufacturers report a planning reliability increase, higher shop floor utilization, and testing outsourcing benefits achieved using immersive component's application such as VR and AR [37–39, 58]. Manufacturing industries, however, lack confidence in new immersive investments to upgrade their existing infrastructure due to concerns of underlying market fragmentation and costs involved. This research presented a novel review to the problem of immersive inclusion using exploratory discovery over a large corpus of unstructured technical literature and patents. A collection of 179 publications and 2,672 patents between years 2007 to 2016 is subjected to statistical, text mining and probabilistic analysis. The key contributions are outlined as an ontology for IIT and technology review specifications presented in Sections 4 and 5. An organized patent query generation method and preliminary statistical analysis representing top assignees in each category, IPC classes, the time evolution of patent publications, and geographical indicators are presented in Section 6. Section 7 presents word frequencies mined technology function matrix that allowed visualization of the technofunctional direction and current industry trend. A probabilistic topic modeled patent grouping is presented in Section 8 identifying topics terms in underlying IIT spectrum. The results are validated using subject matter expertise and cross-referencing with external sources to further find associations and evolution across geography and time. The algorithmic discussion and simplification presented in this paper towards analytic ensure transparency for IP professionals and industry practitioners who usually find it hard to accept results of black-box engines in generic landscape reports. An introduction to future standards research using standard essential patents and patent citation analytics is presented in Section 9. These research maps and benchmarks prove the market potential and growth benefits for embedding immersive technologies in advanced manufacturing. Industry 4.0 promises an increase in efficiency, flexible resource management, and the individualization of mass customization. The resulting intelligent collaboration of all technical components presented involved in immersive technology spectrum has high potential in advanced manufacturing technologies and smart factories for the realization of Industry 4.0 [22, 47, 67, 68].

Conflicts of Interest

The authors declare that there are no conflicts of interest regarding the publication of this paper.

Acknowledgments

This research is partially supported by the Taiwan Ministry of Science and Technology (Grant no. MOST 106-2218-E-007-012 -MY2).

References

[1] Intelligent Technical Systems OstWestfalenLippe, On the road to Industry 4.0: Solutions from the Leading-Edge Cluster It's OWL, 2017, https://www.its-owl.com/fileadmin/PDF/Informationsmaterialien/2015-On_the_road_to_Industry_4.0_-_Solutions_from_the_Leading-Edge_Cluster_it_s_OWL.pdf.

[2] H. Kagermann, "Change through digitizationvalue creation in the age of Industry 4.0," in *Proceedings of the Management of Permanent Change*, pp. 23–45, Springer Fachmedien Wiesbaden, 2015.

[3] Forschungs-Gemeinschaft, Deutsche, *The impact of control technology*, IEEE Control Systems Magazine, 2011.

[4] E. A. Lee, "Cyber-physical systems-are computing foundations adequate," *Position paper for NSF Workshop on Cyber-Physical Systems: Research Motivation, Techniques and Roadmap*, vol. 2, 2006.

[5] A. Bhave, B. H. Krogh, D. Garlan, and B. Schmerl, "View consistency in architectures for cyber-physical systems," in *Proceedings of the 2011 IEEE/ACM 2nd International Conference on Cyber-Physical Systems, ICCPS 2011*, pp. 151–160, USA, April 2011.

[6] L. Sha, S. Gopalakrishnan, X. Liu, and Q. Wang, "In machine learning in cyber trust," in *Proceedings of the Cyber-Physical Systems: A new frontier*, pp. 3–13, Taichung, Taiwan, 2009.

[7] L. Hu, N. Xie, Z. Kuang, and K. Zhao, "Review of cyber-physical system architecture," in *Proceedings of the IEEE 15th International Symposium on Object Component Service-Oriented Real-Time Distributed Computing Workshops*, pp. 25–30, Guangdong, China, 2012.

[8] K. T. V. Grattan and T. Sun, "Optical fiber sensor systems for monitoring a variety of engineering structures," in *Proceedings of the 2013 IEEE 6th International Conference on Advanced Infocomm Technology, ICAIT 2013*, pp. 1-2, Hsinchu, Taiwan, July 2013.

[9] Industrie 4.0 Working Group, *Securing the future of German manufacturing industry—Recommendations for implementing the strategic initiative*, Acatech, Munich, Germany, 2016.

[10] F. Hu, Q. Hao, Q. Sun et al., "Cyberphysical System with Virtual Reality for Intelligent Motion Recognition and Training," *IEEE*

Transactions on Systems, Man, and Cybernetics: Systems, vol. 47, no. 2, pp. 347–363, 2017.

[11] N. Fujii, *VR, AR, BMI, and IoA Approach and relationship between the brain and digital*, 2016, http://dentsu-ho.com/articles/3805.

[12] P. Rajesh Desai, P. Nikhil Desai, K. Deepak Ajmera, and K. Mehta, "A Review Paper on Oculus Rift-A Virtual Reality Headset," *International Journal of Engineering Trends and Technology*, vol. 13, no. 4, pp. 175–179, 2014.

[13] P. Halarnkar, S. Shah, H. Shah, and A. Shah, "A review on virtual reality," *International Journal of Computer Science*, vol. 9, no. 6, pp. 325–330, 2012.

[14] A. J. C. Trappey, C. V. Trappey, U. H. Govindarajan, J. J. Sun, and A. C. Chuang, "A Review of Technology Standards and Patent Portfolios for Enabling Cyber-Physical Systems in Advanced Manufacturing," *IEEE Access*, vol. 4, pp. 7356–7382, 2016.

[15] A. C. Chuang, J. J. Sun, A. J. C. Trappey, C. V. Trappey, and U. H. Govindarajan, "Computer supported technology function matrix construction for patent data analytics," in *Proceedings of theIEEE 21st International Conference on Computer Supported Cooperative Work in Design*, pp. 26–28, Wellington, New Zealand, 2017.

[16] A. J. C. Trappey, C. V. Trappey, U. Hareesh Govindarajan, A. C. Chuang, and J. J. Sun, "A review of essential standards and patent landscapes for the Internet of Things: A key enabler for Industry 4.0," *Advanced Engineering Informatics*, vol. 33, pp. 208–229, 2017.

[17] K. J. Panoulas, L. J. Hadjileontiadis, and S. M. Panas, "Brain-computer interface (BCI): Types, processing perspectives and applications," *Smart Innovation, Systems and Technologies*, vol. 3, pp. 299–321, 2010.

[18] A. Lécuyer, F. Lotte, R. B. Reilly, R. Leeb, M. Hirose, and M. Slater, "Brain-computer interfaces, virtual reality, and videogames," *The Computer Journal*, vol. 41, no. 10, pp. 66–72, 2008.

[19] J. D. Bayliss and D. H. Ballard, "A virtual reality testbed for brain-computer interface research," *IEEE Transactions on Neural Systems and Rehabilitation Engineering*, vol. 8, no. 2, pp. 188–190, 2000.

[20] D. Huang, K. Qian, D.-Y. Fei, W. Jia, X. Chen, and O. Bai, "Electroencephalography (EEG)-based brain-computer interface (BCI): a 2-D virtual wheelchair control based on event-related desynchronization/synchronization and state control," *IEEE Transactions on Neural Systems and Rehabilitation Engineering*, vol. 20, no. 3, pp. 379–388, 2012.

[21] P. Milgram and F. Kishino, "A taxonomy of mixed reality visual displays," *IEICE Transactions on Information and Systems D*, vol. 77, pp. 1321–1329, 1994.

[22] LexInnova, "Virtual reality: patent landscape analysis – WIPO," 2017, http://www.wipo.int/edocs/plrdocs/en/lexinnova_plr_virtual_reality.pdf.

[23] N. K. Ahmed, "The Hololens Revolutions," in *Mechanical Engineering Magazine*, vol. 138, pp. 30–35, New York, NY, USA, 2016.

[24] X. Zhao, Y. Chu, J. Han, and Z. Zhang, "SSVEP-Based Brain-Computer Interface Controlled Functional Electrical Stimulation System for Upper Extremity Rehabilitation," *IEEE Transactions on Systems, Man, and Cybernetics: Systems*, vol. 46, no. 7, pp. 947–956, 2016.

[25] D. M. Blei, A. Y. Ng, and M. I. Jordan, "Latent Dirichlet allocation," *Journal of Machine Learning Research*, vol. 3, no. 4-5, pp. 993–1022, 2003.

[26] D. J. Hu, *Latent Dirichlet Allocation for text, images, and music*, University of California, San Diego, Calif, USA, 2013.

[27] M. Liénou, H. Maître, and M. Datcu, "Semantic annotation of satellite images using latent dirichlet allocation," *IEEE Geoscience and Remote Sensing Letters*, vol. 7, no. 1, pp. 28–32, 2010.

[28] R. Krestel, P. Fankhauser, and W. Nejdl, "Latent Dirichlet allocation for tag recommendation," in *Proceedings of the 3rd ACM Conference on Recommender Systems*, pp. 61–68, October 2009.

[29] J. C. Niebles, H. Wang, and L. Fei-Fei, "Unsupervised learning of human action categories using spatial-temporal words," *International Journal of Computer Vision*, vol. 79, no. 3, pp. 299–318, 2008.

[30] S. K. Lukins, N. A. Kraft, and L. H. Etzkorn, "Source code retrieval for bug localization using latent Dirichlet allocation," in *Proceedings of the 15th Working Conference on Reverse Engineering, WCRE 2008*, pp. 155–164, Antwerp, Belgium, October 2008.

[31] L. Cao and L. Fei-Fei, "Spatially coherent latent topic model for concurrent segmentation and classification of objects and scenes," in *Proceedings of the 2007 IEEE 11th International Conference on Computer Vision, ICCV*, pp. 1–8, Rio de Janeiro, Brazil, October 2007.

[32] F.-F. Li and P. Perona, "A bayesian hierarchical model for learning natural scene categories," in *Proceedings of the IEEE Computer Society Conference on Computer Vision and Pattern Recognition (CVPR '05)*, vol. 2, pp. 524–531, San Diego, CA, USA, June 2005.

[33] N. F. Noy and D. L. McGuinness, *Ontology Development 101: A Guide to Creating Your first Ontology*, 2017.

[34] J. Moar, "Virtual reality markets hardware, Content and accessories 2017-2022," in *Crabtree, Whitepaper*, 2016.

[35] J. Thilmany, "The More," *The American Society of Mechanical Engineers Magazine*, pp. 36–41, 2016.

[36] A.-H. G. Abulrub, A. N. Attridge, and M. A. Williams, "Virtual reality in engineering education: The future of creative learning," in *Proceedings of the 2011 IEEE Global Engineering Education Conference, EDUCON 2011*, pp. 751–757, Amman, Jordan, April 2011.

[37] N. S. S. Hamid, F. A. Aziz, and A. Azizi, "Virtual reality applications in manufacturing system," in *Proceedings of the 2014 Science and Information Conference, SAI 2014*, pp. 1034–1037, London, UK, August 2014.

[38] V. Fecova, L. Novakova-Marcincinova, M. Janak, J. Novak-Marcincin, J. Barna, and J. Torok, "Devices and software possibilities for using of motion tracking systems in the virtual reality system," in *Proceedings of the 2012 IEEE 10th International Symposium on Applied Machine Intelligence and Informatics (SAMI)*, pp. 165–168, Herl'any, Slovakia, January 2012.

[39] K. Pentenrieder, C. Bade, F. Doil, and P. Meier, "Augmented reality-based factory planning - An application tailored to industrial needs," in *Proceedings of the 2007 6th IEEE and ACM International Symposium on Mixed and Augmented Reality, ISMAR*, Nara, Japan, November 2007.

[40] E. Richard, V. Billaudeau, P. Richard, and G. Gaudin, "Augmented reality for rehabilitation of cognitive disabled children: A preliminary study," in *Proceedings of the 2007 Virtual Rehabilitation, IWVR*, pp. 102–108, Venice, Italy, September 2007.

[41] M. Hincapié, A. Caponio, H. Rios, and E. González Mendívil, "An introduction to Augmented Reality with applications in

aeronautical maintenance," in *Proceedings of the 2011 13th International Conference on Transparent Optical Networks, ICTON 2011*, pp. 1–4, Stockholm, Sweden, June 2011.

[42] R. Schoenfelder and D. Schmalstieg, "Augmented reality for industrial building acceptance," in *Proceedings of the IEEE Virtual Reality 2008, VR*, pp. 83–90, Reno, NE, USA, March 2008.

[43] S. M. Abbas, S. Hassan, and J. Yun, "Augmented reality based teaching pendant for industrial robot," in *Proceedings of the 12th International Conference on Control, Automation and Systems*, pp. 2210–2213, JeJu Island, South Korea, 2012.

[44] Y. Huang, Y. Liu, and Y. Wang, "AR-view: An augmented reality device for digital reconstruction of Yuangmingyuan," in *Proceedings of the IEEE 2009 International Symposium on Mixed and Augmented Reality - Arts, Media and Humanities*, pp. 3–7, Orlando, FL, USA, October 2009.

[45] M. Kitagawa and T. Yamamoto, "3D puzzle guidance in augmented reality environment using a 3D desk surface projection," in *Proceedings of the IEEE Symposium on 3D User Interfaces 2011, 3DUI 2011*, pp. 133-134, March 2011.

[46] B. Luo and S. Ge, "Augmented reality for material processing within shielded radioactive environment," in *Proceedings of the 8th International Congress on Image and Signal Processing, CISP 2015*, pp. 92–97, Shenyang, China, October 2015.

[47] Markets and Markets, *Augmented reality market by component (sensor, display, and software), display type (head mounted, head-up, handheld, and spatial), application (aerospace and defense, consumer, commercial), and geography - global forecast to 2020*, 2016.

[48] S. Bhattacharyya, S. Shimoda, and M. Hayashibe, "A Synergetic Brain-Machine Interfacing Paradigm for Multi-DOF Robot Control," *IEEE Transactions on Systems, Man, and Cybernetics: Systems*, vol. 46, no. 7, pp. 957–968, 2016.

[49] C.-T. Lin, I.-F. Chung, L.-W. Ko, Y.-C. Chen, S.-F. Liang, and J.-R. Duann, "EEG-based assessment of driver cognitive responses in a dynamic virtual-reality driving environment," *IEEE Transactions on Biomedical Engineering*, vol. 54, no. 7, pp. 1349–1352, 2007.

[50] S. Bermúdez I Badia, A. García Morgade, H. Samaha, and P. F. M. J. Verschure, "Using a hybrid brain computer interface and virtual reality system to monitor and promote cortical reorganization through motor activity and motor imagery training," *IEEE Transactions on Neural Systems and Rehabilitation Engineering*, vol. 21, no. 2, pp. 174–181, 2013.

[51] K. August, J. A. Lewis, G. Chandar, A. Merians, B. Biswal, and S. Adamovich, "fMRI analysis of neural mechanisms underlying rehabilitation in virtual reality: Activating secondary motor areas," in *Proceedings of the 28th Annual International Conference of the IEEE Engineering in Medicine and Biology Society, EMBS'06*, pp. 3692–3695, New York, NY, USA, September 2006.

[52] L. M. Di Diodato, R. Mraz, S. N. Baker, and S. J. Graham, "A haptic force feedback device for virtual reality-fMRI experiments," *IEEE Transactions on Neural Systems and Rehabilitation Engineering*, vol. 15, no. 4, pp. 570–576, 2007.

[53] T. R. Gruber, "A translation approach to portable ontology specifications," *Knowledge Acquisition*, vol. 5, no. 2, pp. 199–220, 1993.

[54] B. Edwards, *Unraveling the Enigma of Nintendo's Virtual Boy*, 2017.

[55] L. Daghestani, R. D. Ward, Z. Xu, and H. Al-Nuaim, "The design, development and evaluation of virtual reality learning environment for numeracy concepts using 3D virtual manipulatives," in *Proceedings of the 5th International Conference on Computer Graphics, Imaging and Visualisation (CGIV '08)*, M. Sarfraz, E. Banissi, and W. C. Jeng, Eds., pp. 93–100, IEEE Computer Society, Penang, Malaysia, August 2008.

[56] L. Xiaoliang, Y. Yuwen, Y. Tianyu, H. Yebo, Y. Tianbiao, and W. Wanshan, "Development and research of simulation system of vitrified bond CBN grinding wheel based on virtual reality technology," in *Proceedings of the International Conference on Management and Service Science, MASS 2009*, pp. 1–4, Wuhan, China, September 2009.

[57] N. Marion, C. Septseault, A. Boudinot, and R. Querrec, "GASPAR: Aviation management on an aircraft carrier using virtual reality," in *Proceedings of the 2007 International Conference on Cyberworlds, CW'07*, pp. 15–22, Hannover, Germany, October 2007.

[58] M. Lorenz, M. Busch, L. Rentzos, M. Tscheligi, P. Klimant, and P. Frohlich, "I'm There! the influence of virtual reality and mixed reality environments combined with two different navigation methods on presence," in *Proceedings of the IEEE Virtual Reality Conference, VR 2015*, pp. 223-224, Arles, France, March 2015.

[59] WIPO, *WIPO IP Facts and Figures*, 2016.

[60] Y. Mo, G. Kontonatsios, and S. Ananiadou, "Supporting systematic reviews using LDA-based document representations," *Systematic Reviews*, vol. 4, no. 1, article no. 172, 2015.

[61] M. Hoffman, R. B. Francis, and D. M. Blei, "Online learning for latent Dirichlet allocation," in *Proceedings of the Advances in Neural Information Processing Systems*, pp. 856–864, Shanghai, China, 2010.

[62] R. Rehurek, *Scalability of semantic analysis in natural language processing, [Doctoral, thesis]*, Masaryk University, Brno, Czech Republic, 2011.

[63] J. Yuan, Y. Zheng, and X. Xie, "Discovering regions of different functions in a city using human mobility and POIs," in *Proceedings of the 18th ACM SIGKDD International Conference on Knowledge Discovery and Data Mining (KDD '12)*, pp. 186–194, Beijing, China, August 2012.

[64] German Institute for Standardization, "German Standardization Roadmap – Industry 4.0, 2016".

[65] K. Bowsher, E. F. Civillico, J. Coburn et al., "Brain-computer interface devices for patients with paralysis and amputation: A meeting report," *Journal of Neural Engineering*, vol. 13, no. 2, article 023001, 2016.

[66] Super Data Research, Superdata VR report, 2017.

[67] Relecura, *Augmented Reality: IP Landscape Report, 2017*.

[68] Relecura, *Virtual Reality (VR) IP Assets Commercialization Viability Analysis, 2017*.

Hindawi
Complexity
Volume 2018, Article ID 8701219, 8 pages
https://doi.org/10.1155/2018/8701219

Research Article

Input-to-State Stability of Nonlinear Switched Systems via Lyapunov Method Involving Indefinite Derivative

Peng Li,[1] Xiaodi Li ,[1,2] and Jinde Cao [1,3]

[1] *School of Mathematics and Statistics, Shandong Normal University, Jinan 250014, China*
[2] *Institute of Data Science and Technology and Shandong Province Key Laboratory of Medical Physics and Image Processing Technology, Shandong Normal University, Jinan 250014, China*
[3] *School of Mathematics and Research Center for Complex Systems and Network Sciences, Southeast University, Nanjing 210 096, China*

Correspondence should be addressed to Xiaodi Li; lxd@sdnu.edu.cn

Received 30 July 2017; Revised 24 November 2017; Accepted 28 December 2017; Published 24 January 2018

Academic Editor: Peter Galambos

This paper studies the input-to-state stability (ISS) of nonlinear switched systems. By using Lyapunov method involving indefinite derivative and average dwell-time (ADT) method, some sufficient conditions for ISS are obtained. In our approach, the time-derivative of the Lyapunov function is not necessarily negative definite and that allows wider applications than existing results in the literature. Examples are provided to illustrate the applications and advantages of our general results and the proposed approach.

1. Introduction

Switched systems are a special subclass of hybrid systems which consist of two components: a family of systems and a switching signal. The systems in the family are described by a collection of indexed differential or difference equations. The switching signal selects an active mode at every instant of time, that is, the system from the family that is currently being followed. As a special class of hybrid systems, switched systems arise in a variety of applications, such as biological systems [1], automobiles and locomotives with different gears [2], DC-DC converters [3], manufacturing processes [4], and shrimp harvesting mode [5]. Many interesting results for switched systems have been reported in the literature [6–9]. Qualitative behaviour of switched systems depends not only on the behaviour of individual subsystems in the family, but also on the switching signal. For instance, divergent trajectories can be generated by switching appropriately among stable subsystems, while a proper switching signal may ensure stability of a switched system even when all the subsystems are unstable. Due to such interesting features, stability of switched systems has attracted considerable research attention over the past few decades; see [10–15].

When investigating stability of a system, it is important to characterize the effects of external inputs. The concepts of input-to-state stability (ISS) introduced by Sontag et al. in [16, 17] have been proved useful in this regard. Roughly speaking, the ISS property means that no matter what the size of the initial state is, the state will eventually approach a neighborhood of the origin whose size is proportional to the magnitude of the input. Many interesting results on ISS properties of various systems such as discrete systems, switched systems, and hybrid systems have been reported; see [18–29]. For example, [19] presented converse Lyapunov theorems for input-to-state stability and integral input-to-state stability (iISS) of switched nonlinear systems; [22, 23] studied the ISS of nonlinear systems subject to delayed impulses; [29] dealt with the ISS of discrete-time nonlinear systems. However, one may observe that most of them, such as those in [18–31], require the derivative of Lyapunov functions to be negative definite in order to derive the desired ISS property. Recently, [32] proposed a new approach for ISS property of nonlinear systems. It presents a new comparison principle for estimating an upper bound on the state of the system in which the derivative of the Lyapunov function may be indefinite, rather than negative definite, which improves the previous work on this topic greatly. The authors of [33] developed the idea to delayed systems and established a class of continuously differentiable Lyapunov-Krasovskii

functionals involving indefinite derivative, which generalizes the classic Lyapunov-Krasovskii functional method. However, the approach used there only applies for systems without switched structures. Moreover, to the best of our knowledge, there are few results on ISS of switched systems based on Lyapunov method involving indefinite derivative.

Motivated by the above discussions, in this paper, we shall study the ISS property for switched systems via Lyapunov method involving indefinite derivative. Some sufficient conditions based on ADT method are derived. It is worth mentioning that, although the method used in this paper is based on [32], the results in this paper are more general than [32], even for the case of systems without switched structures. The rest of this paper is organized as follows. In Section 2 the problem is formulated and some notations and definitions are given. In Section 3, we present some new characterizations of ISS based on Lyapunov method involving indefinite derivative. Examples are given in Section 4. Finally, the paper is concluded in Section 5.

2. Preliminaries

Notations. Let $\mathbb{Z}_+$ denote the set of positive integer numbers, $\mathbb{R}$ the set of real numbers, $\mathbb{R}_+$ the set of all nonnegative real numbers, and $\mathbb{R}^n$ and $\mathbb{R}^{m\times n}$ the n-dimensional and $m\times n$-dimensional real spaces equipped with the Euclidean norm $|\cdot|$, respectively. $a\wedge b$ and $a\vee b$ are the minimum and maximum of a and b, respectively. $P=\{1,2,\ldots,m\}$, $m\in\mathbb{Z}_+$, is an index set, $C(J,S)=\{\varphi\colon J\to S \text{ is continuous}\}$, $\mathcal{F}=\{\varphi\colon [t_0,\infty)\to P, \text{ is a piecewise constant function}\}$. The notations $\mathcal{A}^T$ and $\mathcal{A}^{-1}$ denote the transpose and the inverse of $\mathcal{A}$, respectively. I denotes the identity matrix with appropriate dimensions.

Consider the following switched system:

$$\dot{x}=f_{\sigma(t)}(t,x,u), \tag{1}$$

where $x\in\mathbb{R}^n$ is the system state, $u\in\mathbb{R}^m$ is a measurable locally bounded disturbance input, $\dot{x}$ denotes the right-hand derivative of x, and $\sigma\in\mathcal{F}$ denotes the switching function, which is assumed to be a piecewise constant function continuous from the right. When $\sigma(t)=i$, $1\le i\le m$, we say that the mode $\dot{x}=f_i$ is activated. A sequence of discrete times $\{t_n\}$, $n\in\mathbb{Z}_+$, called the switching times, determines when the switching occurs. Throughout this paper, we assume that it satisfies $0\le t_0<t_1<\cdots<t_k\to+\infty$ as $k\to+\infty$ (t_1 is the first switching time). In particular, we exclude the possibility of the $\{t_k\}$ having a finite accumulation point, often referred to as chattering. It indicates that a switching signal $(\{t_n\},\sigma)$ has at most finite switching times over a finite time interval. $f_{\sigma(t)}\in C(\mathbb{R}_+\times\mathbb{R}^n\times\mathbb{R}^m,\mathbb{R}^n)$ with local Lipschitz, and $f_{\sigma(t)}(t,0,0)\equiv 0$, $t\in\mathbb{R}_+$. In order to study the ISS, in the following we assume that the solution of system (1) with an initial condition $x(t_0)=x_0$ exists on $[t_0,+\infty)$ uniquely.

By the ideas proposed by Hespanha and Morse [34] for switched systems, we say that a switching signal $(\{t_n\},\sigma)$ has average dwell-time (ADT) τ if there exist numbers $N_0\ge 0$ and $\tau>0$ such that

$$N_\sigma(T,t)\le N_0+\frac{T-t}{\tau},\quad \forall T\ge t\ge t_0, \tag{2}$$

where N_0 is called the "chatter bound" and $N_\sigma(T,t)$ is the number of switches occurring in the interval $[t,T)$. We denote such kind of switching signals by set $\mathcal{F}_\tau$. Denote the switching times in the interval $(t,T]$ by $t_1,t_2,\ldots,t_{N_\sigma(t,t_0)}$ and the index of the system that is active in the interval $[t_n,t_{n+1})$ by p_n.

A function $\alpha:[0,\infty)\to[0,\infty)$ is of class $\mathcal{K}$ if α is continuous and strictly increasing and $\alpha(0)=0$. If α is also unbounded, it is of class $\mathcal{K}_\infty$. A function $\beta:[0,\infty)\times[0,\infty)\to[0,\infty)$ is of class $\mathcal{KL}$ if $\beta(\cdot,t)$ is of class $\mathcal{K}$ for each fixed $t\ge 0$, and $\beta(r,t)$ decreases to 0 as $t\to\infty$ for each fixed $r\ge 0$.

Definition 1 (see [16]). Suppose that a switching signal $(\{t_n\},\sigma)$ is given. The system (1) is said to be ISS if there exist functions $\gamma\in\mathcal{K}_\infty$ and $\beta\in\mathcal{KL}$ such that for each $t_0\ge 0$, $x_0\in\mathbb{R}^n$ and for each input u, the solution satisfies

$$|x(t)|\le\beta\left(|x_0|,t-t_0\right)+\gamma\left(|u|_{[t_0,t]}\right), \tag{3}$$

for all $t\ge t_0$, where $|\cdot|_J$ denotes the supremum norm on the interval J. This definition depends on the choice of the switching signal; however, it is often of interest to characterize ISS over classes of switching signals. We say that system (1) is uniformly input-to-state stable (UISS) over the class $\mathcal{F}_\tau$ (of switching signal) if for any $(\{t_n\},\sigma)\in\mathcal{F}_\tau$ condition (3) is satisfied with the same γ and β for every $(\{t_n\},\sigma)\in\mathcal{F}_\tau$.

3. ISS Theorems

In this section, we shall present some ADT results for ISS of switched system (1) based on Lyapunov method involving indefinite derivative.

Theorem 2. *Assume that there exist functions $\alpha_1,\alpha_2\in\mathcal{K}_\infty$, $\rho\in\mathcal{K}$, a continuous function $\phi:\mathbb{R}_+\to\mathbb{R}$, continuous differentiable functions $V_p:\mathbb{R}_+\times\mathbb{R}^n\to\mathbb{R}_+$, and constants $\eta>0$, $\mu\ge 1$ such that, for all $t\in\mathbb{R}_+$, $x\in\mathbb{R}^n$, and all $p,q\in P$,*

$$\alpha_1(|x|)\le V_p(t,x)\le\alpha_2(|x|); \tag{4}$$

$$\frac{\partial V_p}{\partial x}f_p(t,x,u)+\frac{\partial V_p}{\partial t}\le\phi(t)V_p(t,x) \quad \text{whenever } V_p\ge\rho(|u|)\exp\left(\int_{t_0}^{t}\phi(s)\,ds\right); \tag{5}$$

$$V_p(t,x)\le\mu V_q(t,x); \tag{6}$$

$$\int_{t_0}^{t}(\phi(s)+\eta)\,ds\le 0. \tag{7}$$

Then the switched system (1) is UISS over the class $\mathcal{F}_\tau$, where ADT constant $\tau>0$ satisfies

$$\tau>\frac{\ln\mu}{\eta}. \tag{8}$$

Proof. Let $x(t)$ be a solution of system (1). Define $V_{\sigma(t)}(t)=V_{\sigma(t)}(t,x(t))$. If

$$V_p(t)\ge\rho(|u|)\exp\left(\int_{t_0}^{t}\phi(s)\,ds\right), \tag{9}$$

during some interval $[t', t'')$, in this case, suppose that there exists switching signal $\{t_n\}$ such that $t' < t_n < t_{n+1} < \cdots < t_{n+m} < t''$. For $t \in [t', t_n)$, it follows from (5) that

$$V_{p_{n-1}}(t) \le V_{p_{n-1}}(t') \exp\left(\int_{t'}^{t} \phi(s)\, ds\right). \tag{10}$$

For $t \in [t_n, t_{n+1})$, it follows from (5), (6), and (10) that

$$\begin{aligned} V_{p_n}(t) &\le V_{p_n}(t_n) \exp\left(\int_{t_n}^{t} \phi(s)\, ds\right) \\ &\le \mu V_{p_{n-1}}(t') \exp\left(\int_{t'}^{t} \phi(s)\, ds\right). \end{aligned} \tag{11}$$

Then it can be deduced that

$$\begin{aligned} V_{\sigma(t)}(t) \le \mu^{N_\sigma(t',t)} \exp\left(\int_{t'}^{t} \phi(s)\, ds\right) V_{\sigma(t')}(t'), \\ \forall t \in [t', t''). \end{aligned} \tag{12}$$

Since $\mu \ge 1$, it follows from the ADT condition (2) that

$$\begin{aligned} V_{\sigma(t)}(t) &\le \mu^{N_0 + (t-t')/\tau} \exp\left(\int_{t'}^{t} \phi(s)\, ds\right) V_{\sigma(t')}(t') \\ &= \mu^{N_0} \exp\left(\int_{t'}^{t} \frac{\ln \mu}{\tau} + \phi(s)\, ds\right) V_{\sigma(t')}(t'). \end{aligned} \tag{13}$$

We denote the first time when

$$V_{\sigma(t)}(t) \le \rho(|u|) \exp\left(\int_{t_0}^{t} \phi(s)\, ds\right) \tag{14}$$

by $\check{t}$; that is,

$$\begin{aligned} &\check{t}_1 \\ &= \inf\left\{t \ge t_0 \colon V_{\sigma(t)}(t) \le \rho(|u|) \exp\left(\int_{t_0}^{t} \phi(s)\, ds\right)\right\}. \end{aligned} \tag{15}$$

If $\check{t}_1 = \infty$, then it holds that

$$\begin{aligned} V_{\sigma(t)}(t) \le \mu^{N_0} \exp\left(\int_{t_0}^{t} \frac{\ln \mu}{\tau} + \phi(s)\, ds\right) V_{\sigma(t_0)}(t_0), \\ \forall t \ge t_0. \end{aligned} \tag{16}$$

It follows from (8) that there exists $\varepsilon > 0$ small enough such that

$$\frac{\ln \mu}{\tau} + \varepsilon \le \eta, \tag{17}$$

which together with (7) yields that

$$V_{\sigma(t)}(t) \le \mu^{N_0} \exp\left(-\varepsilon (t - t_0)\right) V_{\sigma(t_0)}(t_0), \quad \forall t \ge t_0. \tag{18}$$

It then follows from (4) that

$$|x(t)| \le \alpha_1^{-1}\left(\mu^{N_0} \exp\left(-\varepsilon (t - t_0)\right) \alpha_2(x(t_0))\right). \tag{19}$$

Thus $x(t)$ is bounded by a $\mathcal{KL}$-class function, which implies that system (1) is ISS. Hence we only need to consider the case that $\check{t}_1 < \infty$. It follows from (18) that

$$\begin{aligned} V_{\sigma(t)}(t) \le \mu^{N_0} \exp\left(-\varepsilon (t - t_0)\right) V_{\sigma(t_0)}(t_0), \\ t \in \left[t_0, \check{t}_1\right). \end{aligned} \tag{20}$$

For $t \ge \check{t}_1$, we denote the first time when

$$V_{\sigma(t)}(t) > \rho(|u|) \exp\left(\int_{t_0}^{t} \phi(s)\, ds\right) \tag{21}$$

by $\hat{t}_1$; that is,

$$\begin{aligned} &\hat{t}_1 \\ &= \inf\left\{t \ge \check{t}_1 \colon V_{\sigma(t)}(t) > \rho(|u|) \exp\left(\int_{t_0}^{t} \phi(s)\, ds\right)\right\}. \end{aligned} \tag{22}$$

If $\hat{t}_1 = \infty$, then it is obvious that system (1) is ISS. Assuming that $\hat{t}_1 < \infty$, then

$$\begin{aligned} V_{\sigma(t)}(t) &\le \rho(|u|) \exp\left(\int_{t_0}^{t} \phi(s)\, ds\right) \\ &\le \mu^{N_0} \rho\left(|u|_{[t_0,t]}\right) \exp\left(\int_{t_0}^{t} \phi(s)\, ds\right), \\ &\qquad t \in \left[\check{t}_1, \hat{t}_1\right). \end{aligned} \tag{23}$$

Then we further denote the second time when

$$V_{\sigma(t)}(t) \le \rho(|u|) \exp\left(\int_{t_0}^{t} \phi(s)\, ds\right) \tag{24}$$

by $\check{t}_2$; that is,

$$\begin{aligned} &\check{t}_2 \\ &= \inf\left\{t \ge \hat{t}_1 \colon V_{\sigma(t)}(t) \le \rho(|u|) \exp\left(\int_{t_0}^{t} \phi(s)\, ds\right)\right\}. \end{aligned} \tag{25}$$

Due to the continuity of $V_{\sigma(t)}(t)$ and the monotonicity of $\rho(|u(t)|)$, when $\check{t}_2 < \infty$, it holds that

$$\begin{aligned} &V_{\sigma(\hat{t}_1)}(\hat{t}_1) = \rho\left(|u(\hat{t}_1)|\right) \exp\left(\int_{t_0}^{\hat{t}_1} \phi(s)\, ds\right), \\ &V_{\sigma(t)}(t) \le \mu^{N_0} \exp\left(\int_{\hat{t}_1}^{t} \left(\frac{\ln \mu}{\tau} + \phi(s)\right) ds\right) V_{\sigma(\hat{t}_1)}(\hat{t}_1) \\ &\le \mu^{N_0} \exp\left(\int_{\hat{t}_1}^{t} \left(\frac{\ln \mu}{\tau} + \phi(s)\right) ds\right) \rho\left(|u(\hat{t}_1)|\right) \\ &\cdot \exp\left(\int_{t_0}^{\hat{t}_1} \phi(s)\, ds\right) \le \mu^{N_0} \exp\left(\int_{\hat{t}_1}^{t} \frac{\ln \mu}{\tau} ds\right) \\ &\cdot \rho\left(|u|_{[\hat{t}_1,t]}\right) \exp\left(\int_{t_0}^{t} \phi(s)\, ds\right) \le \mu^{N_0} \end{aligned}$$

$$\cdot \exp\left(\int_{t_0}^{t}\left(\frac{\ln\mu}{\tau}+\phi(s)\right)ds\right)\rho\left(|u|_{[t_0,t]}\right)\le \mu^{N_0}$$
$$\cdot \exp\left(-\varepsilon(t-t_0)\right)\rho\left(|u|_{[t_0,t]}\right)\le \mu^{N_0}\rho\left(|u|_{[t_0,t]}\right),$$
$$\forall t\in\left[\widehat{t}_1,\check{t}_2\right). \tag{26}$$

By this way, it can be deduced that, for every $t\ge\check{t}_1$, it holds that

$$V_{\sigma(t)}(t)\le\mu^{N_0}\lambda\rho\left(|u|_{[t_0,t]}\right), \tag{27}$$

where

$$\lambda=\exp\left(\int_{t_0}^{t}\phi(s)\,ds\right)\vee 1. \tag{28}$$

It follows from (20) and (27) that

$$V_{\sigma(t)}(t)\le\mu^{N_0}\exp\left(-\varepsilon(t-t_0)\right)V_{\sigma(t_0)}(t_0)+\mu^{N_0}\lambda\rho\left(|u|_{[t_0,t]}\right), \tag{29}$$

for all $t\ge t_0$, which together with (4) yields that

$$\begin{aligned}|x(t)|&\le\alpha_1^{-1}\left(2\mu^{N_0}\exp\left(-\varepsilon(t-t_0)\right)\alpha_2\left(|x(t_0)|\right)\right)\\&\quad+\alpha_1^{-1}\left(2\mu^{N_0}\lambda\rho\left(|u|_{[t_0,t]}\right)\right)\\&:=\beta\left(|x(t_0)|,t-t_0\right)+\gamma\left(|u|_{[t,t_0]}\right),\end{aligned} \tag{30}$$

for all $t\ge t_0$. This indicates that system (1) is UISS over the class $\mathscr{F}_\tau$. The proof is completed. □

In particular, if system (1) is given in the form of

$$\dot{x}=f(t,x,u), \tag{31}$$

which is a general case without switched structure, by Theorem 2, one may derive the following corollary.

Corollary 3. *Assume that there exist functions $\alpha_1,\alpha_2\in\mathscr{K}_\infty$, $\rho\in\mathscr{K}$, a continuous function $\phi:\mathbb{R}_+\to\mathbb{R}$, a continuous differentiable function $V:\mathbb{R}_+\times\mathbb{R}^n\to\mathbb{R}_+$, and a constant $\eta>0$ such that, for all $t\in\mathbb{R}_+$, $x\in\mathbb{R}^n$, (7) and the following conditions hold:*

$$\alpha_1(|x|)\le V(t,x)\le\alpha_2(|x|);$$
$$\frac{\partial V}{\partial x}f(t,x,u)+\frac{\partial V}{\partial t}\le\phi(t)V(t,x) \quad \text{whenever } V\ge\rho(|u|)\exp\left(\int_{t_0}^{t}\phi(s)\,ds\right). \tag{32}$$

Then system (31) is ISS.

Remark 4. Recently, [32] has presented some sufficient conditions for ISS property of system (31) based on Lyapunov method involving indefinite derivative under the assumption that

$$\int_{t_0}^{\infty}\phi^+(s)\,ds<\infty,\qquad \int_{t_0}^{t}\phi^-(s)\,ds\ge\epsilon(t-t_0), \tag{33}$$

where $\phi^+(s)=\phi(s)\vee 0$, $\phi^-(s)=[-\phi(s)]\vee 0$, and $\epsilon>0$ is a constant, while our ISS result in Corollary 3 only requires that (7) holds, which has wider applications. For example, $\phi=\sin t-0.9$ and $t_0=0$, and it is easy to see that ϕ is a sign reversal function. In this case, one may choose $\eta=0.1$ such that

$$\int_{t_0}^{t}(\phi(s)+\eta)\,ds=\int_0^t(\sin s-0.8)\,ds<0,\quad\forall t>0, \tag{34}$$

which implies that (7) holds. However, it is easy to see that

$$\int_0^{\infty}\phi^+(s)\,ds=\infty. \tag{35}$$

Next we consider the time-varying linear switched system in the form of

$$\dot{x}=A_{\sigma(t)}(t)x(t)+B_{\sigma(t)}(t)u(t),\quad t\ge 0, \tag{36}$$

where $x(t)\in\mathbb{R}^n$ is the system state, $u\in\mathbb{R}^m$ is locally bounded input, and $A_{\sigma(t)}(t)\in\mathbb{R}^{n\times n}$ and $B_{\sigma(t)}(t)\in\mathbb{R}^{m\times n}$ are time-varying functions. To ensure the ISS property of (36), we present the following result.

Theorem 5. *Assume that there exist constants $\eta>0,\mu\ge 1$, $\omega_p>0$, and continuous functions $\phi:\mathbb{R}_+\to\mathbb{R}$ and $\overline{\phi}:\mathbb{R}_+\to\mathbb{R}$ such that, for all $t\in\mathbb{R}_+$ and all $p,q\in P$, $\omega_p\le\mu\omega_q$, (7), and the following hold:*

$$\begin{aligned}&A_p(t)+A_p^T(t)+B_p(t)B_p^T(t)\exp\left(-\int_0^t\overline{\phi}(s)\,ds\right)\\&\quad+\omega_p\exp\left(\int_0^t\overline{\phi}(s)-\phi(s)\,ds\right)\cdot I_{n\times n}\\&\le\phi(t)\cdot I_{n\times n}.\end{aligned} \tag{37}$$

Then system (36) is UISS over the class $\mathscr{F}_\tau$, where ADT constant $\tau>0$ satisfies (8).

Proof. Let $x(t)$ be a solution of system (36) and define $V_p(t)=V_p(t,x(t))$. Then the proof of Theorem 5 is similar to Theorem 2. We only need to notice that the following are chosen: $V_p(t)=\omega_p x(t)^Tx(t)$ and $\rho(|u|)=u^T(t)u(t)$. It then follows from Theorem 2 that when $V_p(t)\ge\rho(|u|)\exp(\int_0^t\phi(s)ds)$, it holds that $\omega_p x^T(t)x(t)\ge u^T(t)u(t)\exp(\int_0^t\phi(s)ds)$, which, together with (37), leads to the following:

$$\begin{aligned}\dot{V}_p(t)&=2\omega_p x^T(t)\dot{x}(t)=2\omega_p x^T(t)\left(A_p(t)x(t)\right.\\&\quad\left.+B_p(t)u(t)\right)=2\omega_p x^T(t)A_p(t)x(t)\\&\quad+2\omega_p x^T(t)B_p(t)u(t)\le 2\omega_p x^T(t)A_p(t)x(t)\end{aligned}$$

$$
\begin{aligned}
&+ \exp\left(-\int_0^t \overline{\phi}(s)\,ds\right)\omega_p x^T(t)\times B_p(t)\,B_p^T(t)\,x(t)\\
&+ \omega_p u^T(t)\,u(t)\exp\left(\int_0^t \overline{\phi}(s)\,ds\right)\le \omega_p x^T(t)\\
&\cdot\left[A_p(t)+A_p^T(t)+B_p(t)\,B_p^T(t)\right.\\
&\times\exp\left(-\int_0^t \overline{\phi}(s)\,ds\right)\\
&\left.+\omega_p\exp\left(\int_0^t \overline{\phi}(s)-\phi(s)\,ds\right)\cdot I_{n\times n}\right]x(t)\le\phi(t)\\
&\cdot V_p(t),
\end{aligned}
\tag{38}
$$

which implies that condition (5) holds. Then it is easy to check that all conditions in Theorem 2 hold and thus Theorem 5 can be derived. The proof is completed. □

In particular, if we choose $\overline{\phi}(t)=\phi(t)$, then the following corollary can be derived directly.

Corollary 6. *Assume that there exist constants $\eta>0$, $\mu\ge 1$, $\omega_p>0$, and continuous function $\phi:\mathbb{R}_+\to\mathbb{R}$ such that, for all $t\in\mathbb{R}_+$ and all $p,q\in P$, $\omega_p\le\mu\omega_q$, (7), and the following hold:*

$$
\begin{aligned}
&A_p(t)+A_p^T(t)+B_p(t)\,B_p^T(t)\exp\left(-\int_0^t\phi(s)\,ds\right)\\
&\quad\le\left(\phi(t)-\omega_p\right)\cdot I_{n\times n}.
\end{aligned}
\tag{39}
$$

Then the system (36) is UISS over the class $\mathcal{F}_\tau$, where ADT constant $\tau>0$ satisfies (8).

In addition, note that the ISS property guarantees the uniform asymptotic stability (UAS) of a system with a zero input. Consider the nonlinear switched system

$$
\dot{x}=f_{\sigma(t)}(t,x),
\tag{40}
$$

where $\sigma\in\mathcal{F}$ is the switching function, $f_\sigma\in C(\mathbb{R}_+\times\mathbb{R}^n,\mathbb{R}^n)$ is local Lipschitz and $f_\sigma(t,0)=0$, $x(t,t_0,x(t_0))$ is the solution for system (40) with the initial value $x(t_0)\in\mathbb{R}^n$ and an initial time $t_0\ge 0$. Then we have the following result for system (40).

Corollary 7. *Assume that there exist functions $\alpha_1,\alpha_2\in\mathcal{K}_\infty$, a continuous function $\phi:\mathbb{R}_+\to\mathbb{R}$, continuous differentiable functions $V_p:\mathbb{R}_+\times\mathbb{R}^n\to\mathbb{R}_+$, and constants $\eta\in\mathbb{R}_+$, $\mu\ge 1$ such that, for all $t\in\mathbb{R}_+$, $x\in\mathbb{R}^n$, and all $p,q\in P$, (4), (6), (7), and the following condition hold:*

$$
\frac{\partial V_p}{\partial x}f_p(t,x)+\frac{\partial V_p}{\partial t}\le\phi(t)\,V_p(t,x).
\tag{41}
$$

Then system (40) is UAS in Lyapunov sense, where ADT constant τ satisfies (8).

4. Applications

In this section, we present two examples to illustrate our main results.

Example 8. Consider the switched system (1) with $P=\{1,2\}$, $t_0=0$, and

$$
\begin{aligned}
f_1(t,x,u)&=a(t)\,x+b(t)\,u,\\
f_2(t,x,u)&=c(t)\,x+d(t)\,u,
\end{aligned}
\tag{42}
$$

where $a(t)=-\cos t-5/6$, $b(t)=(1/6)\exp(-\sin t-(2/3)t)$, $c(t)=-\cos t-(1/2)\exp(\cos t-2/3)$, and $d(t)=\exp(\cos t-\sin t-(2/3)t)$.

Note that $a(t)$ and $c(t)$ are sign reversal functions. Most of existing results, such as those in [18–23, 26–29], are inapplicable to switched system (1). Choose $V_1(t,x,u)=|x|$ and $V_2(t,x,u)=(1/2)|x|$ as ISS-Lyapunov functions. It is easy to see that condition (6) holds with $\mu=2$. Let $\rho(t)=t$ and $\phi(t)=-\cos t-2/3$, and then when

$$
V_1(t,x,u)\ge\rho(|u|)\exp\left(\int_0^t\phi(s)\,ds\right),
\tag{43}
$$

that is,

$$
|x|\ge|u|\exp\left(-\sin t-\frac{2}{3}t\right),
\tag{44}
$$

it leads to

$$
\begin{aligned}
\dot{V}_1(t,x,u)&\le\left(-\cos t-\frac{5}{6}\right)|x|+\frac{1}{6}|x|\\
&\le\left(-\cos t-\frac{2}{3}\right)V_1(t,x,u)\\
&=\phi(t)\,V_1(t,x,u).
\end{aligned}
\tag{45}
$$

Similarly, it can be deduced that $\dot{V}_2(t,x,u)\le(-\cos t-2/3)V_2(t,x,u)$ when $V_2(t,x,u)\ge\rho(|u|)\exp(\int_0^t\phi(s)ds)$. Thus condition (5) is satisfied. Choose $\eta=0.45$ such that

$$
\begin{aligned}
\int_{t_0}^t\left(\phi(v)+\eta\right)dv&=\int_0^t(-\cos v-0.2167)\,dv<-0.02\\
&<0,\quad\forall t>0,
\end{aligned}
\tag{46}
$$

which implies that (7) holds. Note that $\ln\mu/\eta\approx 1.5403$. Hence, the switched system (1) is UISS over the class $\mathcal{F}_\tau$ with $\tau>1.5403$. In particular, if we choose the switching sequence $t_{2n-1}=6n-4$, $t_{2n}=6n$, $n\in\mathbb{Z}_+$ and let $x(0)=5$, $\tau=3$, $u=\mathrm{sat}(x)$, then Figures 1(a) and 1(b) illustrate the switching signal and the state trajectory of system (1), respectively.

Remark 9. Note that, if we choose $V_2=|x|$ in the above example, then it can be deduced that $\dot{V}_2\le(-\cos t+(1/2)\exp(\cos t)-2/3)V_2$, which goes against condition (5). It indicates that sometimes it is necessary and important to consider multiple Lyapunov functions for switched systems. In addition, it is easy to check that the ISS Theorems in [32] are invalid for the above example due to the stronger restriction on ϕ^+.

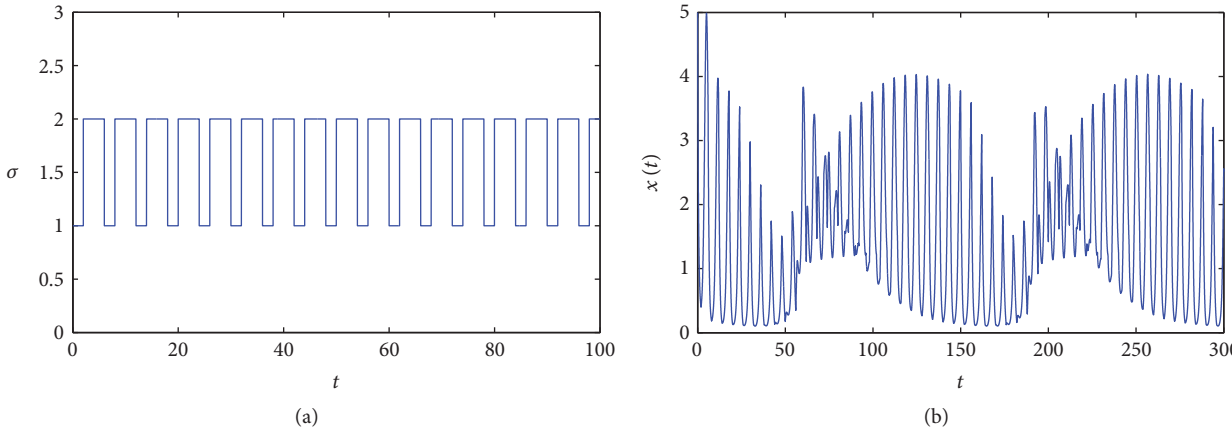

(a) (b)

Figure 1: Simulation results for Example 8.

Example 10. Consider the time-varying switched system (36) with $P = \{1, 2\}$ and

$$\begin{aligned} \dot{x}(t) &= [A_1 + \Delta A_1(t)]\, x(t) + [B_1 + \Delta B_1(t)]\, u_1(t), \\ \dot{x}(t) &= [A_2 + \Delta A_2(t)]\, x(t) + [B_2 + \Delta B_2(t)]\, u_2(t), \end{aligned} \tag{47}$$

where

$$\begin{aligned} A_1 &= \begin{pmatrix} -0.105 & 0 \\ 0 & -0.11 \end{pmatrix}, \\ \Delta A_1(t) &= \begin{pmatrix} a_1 & 0 \\ 0 & a_2 \end{pmatrix}, \\ A_2 &= \begin{pmatrix} -0.115 & -0.005 \\ -0.005 & -0.115 \end{pmatrix}, \\ \Delta A_2(t) &= \begin{pmatrix} b_1 & 0 \\ 0 & b_2 \end{pmatrix}, \\ B_1 &= B_2 = \begin{pmatrix} 0 \\ 0 \end{pmatrix}, \\ \Delta B_1(t) &= \begin{pmatrix} 0 \\ c \end{pmatrix}, \\ \Delta B_2(t) &= \begin{pmatrix} c \\ c \end{pmatrix}, \\ a_1 &= a_2 = b_1 = -\frac{1}{2}\sin t, \\ b_2 &= \frac{1}{2}\left(-\sin t - \exp(-2t)\right), \\ c &= \frac{1}{10}\exp\left(\frac{1}{2}\left(\cos t - \frac{1}{5}t - 1\right)\right). \end{aligned} \tag{48}$$

In this case, choose $\omega_1 = 0.01$, $\omega_2 = 0.02$, $\eta = 0.1$, $\mu = 2$, and $\phi(t) = -\sin t - 0.2$. Then it is easy to see that

$$\int_0^t (\phi(s) + \eta)\, ds = \int_0^t (-\sin s - 0.1)\, ds < 0, \quad \forall t > 0, \tag{49}$$

which implies that (7) holds. Moreover, note that

$$\begin{aligned} &A_1(t) + A_1^T(t) + B_1(t) B_1^T(t) \exp\left(-\int_0^t \phi(s)\, ds\right) \\ &\quad = \begin{pmatrix} -\sin t - 0.21 & 0 \\ 0 & -\sin t - 0.21 \end{pmatrix}, \\ &A_2(t) + A_2^T(t) + B_2(t) B_2^T(t) \exp\left(-\int_0^t \phi(s)\, ds\right) \\ &\quad = \begin{pmatrix} -\sin t - 0.22 & 0 \\ 0 & -\sin t - \exp(-2t) - 0.22 \end{pmatrix}. \end{aligned} \tag{50}$$

Note that $\ln \mu/\eta \approx 6.931$. Thus it follows from Corollary 6 that the switched system (36) is UISS over the class $\mathscr{F}_\tau$ with $\tau > 6.931$. In particular, if we choose the switching sequence $t_{2n-1} = 14n - 1$, $t_{2n} = 14n$, $n \in \mathbb{Z}_+$ and let $x^T(0) = (3, 3)$, $\tau = 7$, $u_1 = \sin x$, $u_2 = \mathrm{sat}(x)$, then Figures 2(a) and 2(b) illustrate the switching signal and the 2-norm of the state trajectory of system (36), respectively.

5. Conclusion

In this paper, we presented some new ADT-based sufficient conditions for ISS of switched systems via Lyapunov method involving indefinite derivative. The ISS property of the switched system can be guaranteed under the designed ADT scheme. Our results improved some recent work in the literature. Two examples were given to show the effectiveness and advantage of the obtained results. It should be pointed out that the main results of this paper are based on multiple Lyapunov functions, which are more general than existing results in some cases. Since complex factors such as nonlinearities, impulsive perturbations, and delays exist widely in

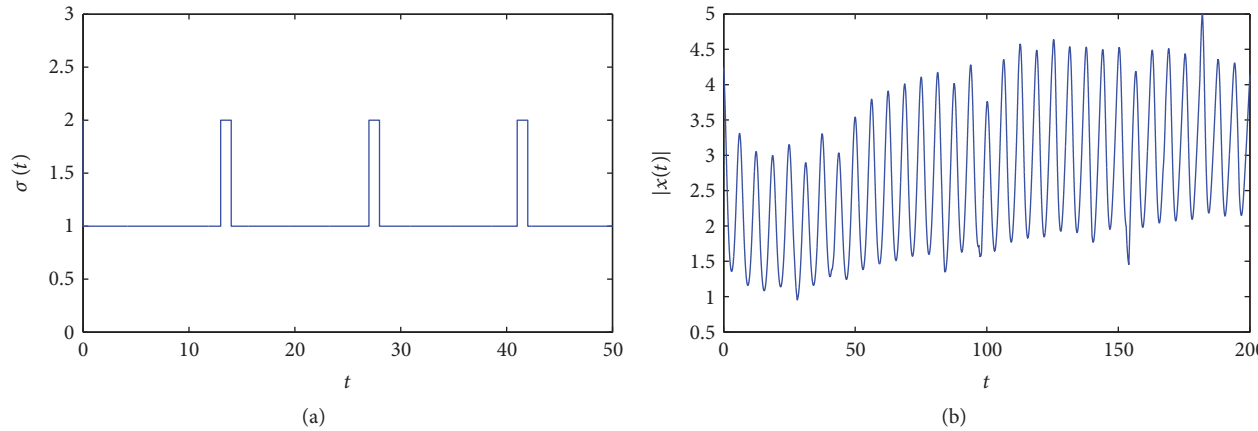

Figure 2: Simulation results for Example 10.

various engineering systems [35], future work can be done to develop the Lyapunov method involving indefinite derivative to switched systems subject to complex factors.

Conflicts of Interest

The authors declare that they have no conflicts of interest.

Acknowledgments

This work was supported by National Natural Science Foundation of China (11301308, 61673247) and the Research Fund for Excellent Youth Scholars of Shandong Province (ZR2016JL024, JQ201719).

References

[1] C. Liu, Z. Gong, E. Feng, and H. Yin, "Optimal switching control of a fed-batch fermentation process," *Journal of Global Optimization*, vol. 52, no. 2, pp. 265–280, 2012.

[2] P. G. Howlett, P. J. Pudney, and X. Vu, "Local energy minimization in optimal train control," *Automatica*, vol. 45, no. 11, pp. 2692–2698, 2009.

[3] R. C. Loxton, K. L. Teo, V. Rehbock, and W. K. Ling, "Optimal switching instants for a switched-capacitor DC/DC power converter," *Automatica*, vol. 45, no. 4, pp. 973–980, 2009.

[4] C. G. Cassandras, D. L. Pepyne, and Y. Wardi, "Optimal control of a class of hybrid systems," *IEEE Transactions on Automatic Control*, vol. 46, no. 3, pp. 398–415, 2001.

[5] Q. Lin, R. Loxton, K. l. Teo, and Y. H. Wu, "A new computational method for optimizing nonlinear impulsive systems," *Dynamics of Continuous, Discrete and Impulsive Systems Series B: Applications & Algorithms*, vol. 18, pp. 59–76, 2011.

[6] W. Yu, J. Cao, and K. Yuan, "Synchronization of switched system and application in communication," *Physics Letters A*, vol. 372, no. 24, pp. 4438–4445, 2008.

[7] G. J. Huang and W. H. Chen, "A revisit to the design of switched observers for switched linear systems with unknown inputs," *International Journal of Control, Automation, and Systems*, vol. 12, no. 5, pp. 954–962, 2014.

[8] R. a. Zawiski, "Stabilizability of nonlinear infinite dimensional switched systems by measures of noncompactness in the space c_0," *Nonlinear Analysis: Hybrid Systems*, vol. 25, pp. 79–89, 2017.

[9] L. V. Hien and H. Trinh, "Switching design for suboptimal guaranteed cost control of 2-D nonlinear switched systems in the Roesser model," *Nonlinear Analysis: Hybrid Systems*, vol. 24, pp. 45–57, 2017.

[10] Q. Wang, H. Sun, and G. Zong, "Stability analysis of switched delay systems with all subsystems unstable," *International Journal of Control, Automation, and Systems*, vol. 14, no. 5, pp. 1262–1269, 2016.

[11] G. Zong, X. Wang, and H. Zhao, "Robust finite-time guaranteed cost control for impulsive switched systems with time-varying delay," *International Journal of Control, Automation, and Systems*, vol. 15, no. 1, pp. 113–121, 2017.

[12] R. Shorten, F. Wirth, O. Mason, K. Wulff, and C. King, "Stability criteria for switched and hybrid systems," *SIAM Review*, vol. 49, no. 4, pp. 545–592, 2007.

[13] C. Huang, J. Cao, and J. Cao, "Stability analysis of switched cellular neural networks: A mode-dependent average dwell time approach," *Neural Networks*, vol. 82, pp. 84–99, 2016.

[14] X. Li and J. Cao, "An impulsive delay inequality involving unbounded time-varying delay and applications," *IEEE Transactions on Automatic Control*, vol. 62, pp. 3618–3625, 2017.

[15] X. Yang, C. Huang, and Q. Zhu, "Synchronization of switched neural networks with mixed delays via impulsive control," *Chaos Solitons & Fractals*, vol. 44, pp. 817–826, 2011.

[16] E. D. Sontag, "Comments on integral variants of ISS," *Systems Control Letters*, vol. 34, no. 1-2, pp. 93–100, 1998.

[17] M. Krichman, E. D. Sontag, and Y. Wang, "Input-output-to-state stability," *SIAM Journal on Control and Optimization*, vol. 39, no. 6, pp. 1874–1928, 2001.

[18] C. Cai and A. R. Teel, "Results on input-to-state stability for hybrid systems," in *Proceedings of the 44th IEEE Conference on Decision & Control*, pp. 5403–5408, 2005.

[19] J. L. Mancilla-Aguilar and R. A. Garcia, "On converse Lyapunov theorems for ISS and iISS switched nonlinear systems," *Systems & Control Letters*, vol. 42, pp. 47–53, 2001.

[20] D. Nešić and A. R. Teel, "Input-output stability properties of networked control systems," *IEEE Transactions on Automatic Control*, vol. 49, no. 10, pp. 1650–1667, 2004.

[21] P. Pepe and Z. P. Jiang, "A Lyapunov-Krasovskii methodology for ISS and iISS of time-delay systems," *Systems & Control Letters*, vol. 55, pp. 1006–1014, 2006.

[22] X. Li, X. Zhang, and S. Song, "Effect of delayed impulses on input-to-state stability of nonlinear systems," *Automatica*, vol. 76, pp. 378–382, 2017.

[23] X. Zhang and X. Li, "Input-to-state stability of non-linear systems with distributed-delayed impulses," *IET Control Theory & Applications*, vol. 11, pp. 81–89, 2017.

[24] L. Liu, R.-W. Guo, and S.-P. Ma, "Input/output-to-state stability of switched nonlinear systems with an improved average dwell time approach," *International Journal of Control, Automation, and Systems*, vol. 14, no. 2, pp. 461–468, 2016.

[25] Y. Ji, Q. Zong, B. Tian, and H. Liu, "Input-to-state-stability modular command filtered back-stepping attitude control of a generic reentry vehicle," *International Journal of Control, Automation, and Systems*, vol. 11, no. 4, pp. 734–741, 2013.

[26] W.-H. Chen and W. X. Zheng, "Input-to-state stability and integral input-to-state stability of nonlinear impulsive systems with delays," *Automatica*, vol. 45, no. 6, pp. 1481–1488, 2009.

[27] S. N. Dashkovskiy, B. S. Rüffer, and F. R. Wirth, "Small gain theorems for large scale systems and construction of ISS Lyapunov functions," *SIAM Journal on Control and Optimization*, vol. 48, no. 6, pp. 4089–4118, 2010.

[28] X. Wu, Y. Tang, and W. Zhang, "Input-to-state stability of impulsive stochastic delayed systems under linear assumptions," *Automatica*, vol. 66, pp. 195–204, 2016.

[29] Z.-P. Jiang and Y. Wang, "Input-to-state stability for discrete-time nonlinear systems," *Automatica*, vol. 37, no. 6, pp. 857–869, 2001.

[30] J. Cheng, J. H. Park, L. Zhang, and Y. Zhu, "An asynchronous operation approach to event-triggered control for fuzzy Markovian jump systems with general switching policies," *IEEE Transactions on Fuzzy Systems*, vol. 99, pp. 1-1, 2016.

[31] J. Cheng, J. H. Park, Y. Liu, Z. Liu, and L. Tang, "Finite-time H1 fuzzy control of nonlinear Markovian jump delayed systems with partly uncertain transition descriptions," *Fuzzy Sets and Systems*, vol. 314, pp. 99–115, 2017.

[32] C. Ning, Y. He, M. Wu, Q. Liu, and J. She, "Input-to-state stability of nonlinear systems based on an indefinite Lyapunov function," *Systems & Control Letters*, vol. 61, pp. 1254–1259, 2012.

[33] C. Ning, Y. He, M. Wu, and S. Zhou, "Indefinite derivative Lyapunov-Krasovskii functional method for input to state stability of nonlinear systems with time-delay," *Applied Mathematics and Computation*, vol. 270, Article ID 21587, pp. 534–542, 2015.

[34] J. P. Hespanha and A. S. Morse, "Stability of switched systems with average dwell-time," in *Proceedings of the 38th IEEE Conference on Decision & Control*, pp. 2655–2660, 1999.

[35] X. Li and S. Song, "Stabilization of Delay Systems: delay-dependent Impulsive Control," *IEEE Transactions on Automatic Control*, vol. 62, no. 1, pp. 406–411, 2017.